VOLTAGE STABILITY AND CONTINGENCY SELECTION STUDIES IN ELECTRIC POWER SYSTEMS

By

Satish Joshi

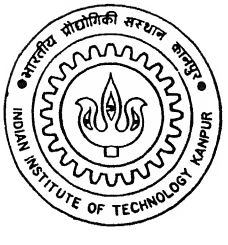

DEPARTMENT OF ELECTRICAL ENGINEERING

INDIAN INSTITUTE OF TECHNOLOGY KANPUR

DECEMBER, 1995

VOLTAGE STABILITY AND CONTINGENCY SELECTION STUDIE IN ELECTRIC POWER SYSTEMS

A Thesis Submitted
in Partial Fulfillment of the Requirements
for the Degree of

DOCTOR OF PHILOSOPHY

By

Satish Joshi

to the

DEPARTMENT OF ELECTRICAL ENGINEERING

INDIAN INSTITUTE OF TECHNOLOGY KANPUR

DECEMBER, 1995

THESIS SUPERVISORS

During the initial period from July 28, 1992 to April 30, 1994, this work for the award of the Ph.D. degree submitted by Mr. Satishkumar Kantilal Joshi was carried out under the co-supervision of Prof. S.C. Srivastava and Prof. P.K. Kalra. Thereafter, Prof. S.C. Srivastava served as the sole supervisor.

Dean of Academic Affairs

Certificate

It is certified that the work contained in the thesis entitled **VOLTAGE STABILITY AND CONTINGENCY SELECTION STUDIES IN ELECTRIC POWER SYSTEMS** by *Satishkumar Kantilal Joshi* has been carried out under my supervision and that this work has not been submitted elsewhere for a degree.

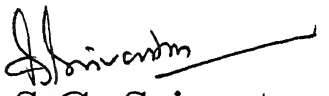

(Dr S.C. Srivastava)
Professor
Department of Electrical Engineering
Indian Institute of Technology
Kanpur-208016 India

December, 1995.

dedicated to my Parents

Synopsis

Name of Student: Satishkumar Kantilal Joshi Roll no.: 9210468
Degree for which submitted: Ph.D. Department: Electrical Engineering

Thesis Title: **VOLTAGE STABILITY AND CONTINGENCY SELECTION STUDIES IN ELECTRIC POWER SYSTEMS**

Name of thesis supervisor: Professor S. C. Srivastava

Month and year of thesis submission: December 1995.

The present day power utilities are facing the problem of maintaining the required bus voltages due to stressed operation of the network. The power systems which used to be transient (angle) stability limited have now become voltage stability limited. Hence the focus of the research in the power system area is being more concentrated on voltage security and voltage stability studies.

Voltage security has been defined [1] as the ability of a system not only to operate stably but also remain stable (as far as maintenance of system voltage is concerned) following any reasonably credible contingency or adverse system change. Voltage stability [1] is the ability of the system to maintain voltage so that when load admittance is increased load power will increase and so that both power and voltage are controllable.

The security assessment involves contingency analysis which can be performed by AC load flow for various outage cases. However, in a practical system, number of contingencies are so large that they can not be analyzed online by the AC load flow methods. Hence the contingencies are first ranked in rough order of their relative severity employing contingency selection algorithms. Then full AC load flow is run for only severe contingency cases.

Existing contingency selection algorithms employ approximate methods such as local solution method [2], one iteration of AC load flow [3], the linearized load flow methods [4], and distribution factor methods [5]. These methods are either quite inaccurate or

requires large computational time. Artificial neural network are being popularly used in in power system and other engineering applications due to their capability to map nonlinear functions accurately and the fast computational speed.

Voltage security has been conventionally assessed with respect to operating limits of bus voltage and/or reactive power output of the sources. However, the secure operation of present day system requires ensuring a minimum margin of voltage stability. With the increased use of compensating devices such static VAR compensators, which raises the critical voltage to normal operating range, makes the bus voltage itself a poor indicator of voltage stability.

For contingency ranking required to assess the relative severity of contingencies, scalar performance indices have been used. The performance indices suffer from two typical problems of misranking and masking effects. One of the attempts to overcome these problems was suggested by Hsu et al. [6] by using Fuzzy Logic.

In most of the research works the voltage stability have been considered as static phenomena due to slow variation of voltage over a long time until it reaches near to maximum loadability or collapse point. Extensive works on prediction of voltage stability exist which can be classified into Direct and Indirect methods. In *Direct method* stability margin is defined in terms of additional demand that will take the system to stability boundary. It uses methods such as optimization method [7], multiple load flow solution [8] etc. *Indirect methods* utilize some indices such as singularity of load flow Jacobian [9], minimum singular value or condition number of load flow Jacobian [10] etc. However, these methods, in general require large computing time and may not be suitable for certain applications such as the voltage contingency selection.

From literature survey it has been observed that even some simplified power system models exhibit oscillatory type unstable response due to Hopf bifurcation much before the saddle node bifurcation [11] i.e. maximum loadability limit. Dobson et al. [12] derived the first order sensitivity factor of system parameters with respect to Hopf bifurcation. However, no proper method has been suggested to predict the numerical values of stability margin with respect to Hopf bifurcation required for the secure operation of power system.

Weakness of transmission boundary around the group of buses are the structural weakness that causes voltage collapse. These group of buses are called as *voltage control areas.* To determine voltage control areas Schlueter et al. [13] developed an algorithm based on load flow Jacobian sensitivity. However, with this method, the control areas have to be

recomputed with slight change in system loading conditions.

One of the recent operating concerns in the power system network is to ensure a minimum margin of voltage stability. This can be achieved by installing compensating devices in the system and taking appropriate control actions. An optimal generation rescheduling scheme with respect to maximization of minimum singular value has been presented in ref. [14] for enhancing the voltage stability margin. Flexible A.C. transmission system (FACTS) devices are being popularly used in the power systems for improvement of system stability. From the literature survey it appears that the effect of optimal setting of FACTS devices on voltage stability margin has not yet been explored.

Therefore the motivation behind the work presented in this thesis are:

(i) To develop a new method for contingency selection combining an Artificial Neural Network (ANN) for post outage voltage prediction and a fuzzy logic based ranking method considering both the bus voltage deviations and system voltage stability margin.

(ii) To develop a fast method for prediction of nearest saddle-node bifurcation point in the system using simulation based Artificial Neural Network [15]

(iii) To present a new method based on optimization technique for determining the distance to closest Hopf bifurcation.

(iv) To explore a new method to determine voltage control area which remain valid for wide range of operating conditions

(v) To study the effectiveness of optimal adjustment of generators and FACTS devices' output in voltage stability enhancement.

A brief description of the work reported in the thesis is given below:

Chapter 1 introduces the voltage security and stability problems, presents a brief survey of research work carried out in the areas of voltage contingency selection and the voltage stability studies.

In Chapter 2 , a fast method based on Artificial Neural Network (ANN) has been developed for post outage bus voltage prediction. Contingency ranking has been performed considering both voltage stability margin as well as bus voltage deviation and employing a Fuzzy Logic based method.

Chapter 3 presents the development of a new method employing an analog simulation based neural network to determine the nearest saddle node bifurcation point in loading parameter space.

Chapter 4 reports the development of a method for prediction of minimum distance to Hopf bifurcation in terms of system loading parameters. The estimation of closet Hopf bifurcation has been formulated as an optimization problem.

Chapter 5 describes a new method based on entropy concept to determine voltage control area and explores its validity for wide operating range.

In chapter 6, a simple approach for siting the FACTS devices has been developed based on identification of weakest bus and the knowledge of voltage control areas. An optimal power flow formulation has been suggested to determine the optimal adjustment of output of generators and FACTS devices. Their impact on enhancement of the voltage stability margin has been studied.

Chapter 7 concludes the main findings and significant contributions of the thesis and provides a few suggestions for further research work in this area.

References

[1] IEEE system dynamic performance subcommittee, *Voltage Stability of Power Systems: Concepts, Analytical Tools and Industry Experience*, IEEE document 90TH0358-2-PWR-1990.

[2] J. Zaborsky, K.W. Whang and K. Prasad, *Fast Contingency Evaluation Using Concentric Relaxation*. IEEE Trans. on Power Apparatus and Systems, Vol-PAS-99. No.1, January/February 1980, pp. 28-36.

[3] F. Albuyeh, A. Bose and B. Heath, *Reactive Power Consideration in Automatic Contingency Selection,* IEEE Trans. on Power Apparatus and Systems, Vol-PAS-101, No.1, January 1982, pp. 107-112.

[4] A.K. Jana, P.B. Duttagupta and G.D. Prasad, *An Improved Linearized Method for Evaluation of Bus Voltage for Line Outage Contingency,* Int. Journal of Electric Power and Energy Systems, Vol-15, No.5, 1993 ,pp. 301-305.

[5] C. Lee and N. Chen, *Distribution Factors of Reactive Power Flow in Transmission Line and Transformer Outage Studies,* IEEE Trans. on Power Systems, Vol-PWRS-7, No.1, February 1992, pp. 194-200.

[6] Yoan-Yih Hsu and Han-Ching Kuo,*Fuzzy set based contingency ranking,* IEEE Trans. on Power Systems, Vol.7, No.3, pp. 1189-1196, Aug 1992.

[7] T. Van Cutsem, *A Method to Compute Reactive Power Margins with respect to Voltage Collapse*, IEEE Trans. on Power Systems, Vol. 6, No. 1, Feb. 1991, pp. 145-156.

[8] Y. Tamura, K. Iba and S. Iwamoto, *Relationship between Instability and Multiple Load Flow Solutions in Electric Power Systems*, IEEE Trans. on Power Systems, Vol. 102, No. 2, May 1983, pp. 1115-1125.

[9] P.W. Sauer and M.A. Pai, *Power System Steady-State Stability and the Load Flow Jacobian*, IEEE Trans. on Power Systems, Vol. 5, No. 4, Nov. 1990, pp. 1374-1383.

[10] P.A. Lof, T. Smed, G. Anderson and D.J. Hill, *Fast Calculation of a Voltage Stability Index*, IEEE Trans. on Power Systems, Vol. 7, No. 1, Feb. 1992, pp 54-64.

[11] V. Ajjarapu and B. Lee, *Bifurcation Theory and its Application to Nonlinear Dynamical Phenomena in an Electric Power System*, IEEE Trans. on Power Systems, Vol. 7, No. 1, Feb. 1992, pp. 424-431.

[12] I. Dobson, F. Alvarado and C.L. DeMarco, *Sensitivity of Hopf Bifurcations to Power System Parameters*, Proc. 31st IEEE Conference on Decision and Control, Tucson, AZ, December 1992, pp. 2928-2933.

[13] R.A. Schlueter, I. Hu, M.W. Chang, J.C. Lo and A. Costi, *Methods for Determining Proximity to Voltage Collapse*, IEEE Trans. on Power Systems, Vol. 6, No. 1, Feb. 1991, pp. 285-292.

[14] A. Tiranuchit and R.J. Thomas, *A Posturing Strategy against Voltage Instabilities in Electric Power Systems*, IEEE Trans. on Power Systems, Vol. 3, No. 1, Feb. 1988, pp. 87-93.

[15] M.P. Kennedy and L.O. Chua, *Neural Networks for Nonlinear Programming,* IEEE Trans. on Circuits and Systems, Vol.35, No.5, May 1988, pp. 554-562.

Acknowledgements

I am most fortunate to have had professor Suresh Chandra Srivastava as my thesis supervisor. There are many reasons for arriving at this conclusion, but most important one is the patience that he exhibited over the last three-and-a-half years in dealing with "fundamental philosophical" issues that kept coming up from time to time. In addition to direct technical contributions, he has also had a strong impact on my thinking, and I am beginning to realize that I am going to continue to appreciate the doctoral thesis experience more and more as the years go by. On the completion of this work, it is my proud privilege to express my deep sense of gratitude and indebtedness towards him for his skilled guidance, unfailing support, stimulating discussions and constant encouragement not only during this dissertation work but also over entire period of my association with him. I can only offer my most humble and profound indebtedness to him for deep concern both for my academics and for my personal welfare.

I am extremely grateful to Professors L.P. Singh, S.S. Prabhu, Arindam Ghosh, Sachchidanand, R.K. Verma and R. Arora for their sincere advice and encouragement through out the course of this work. I thankfully acknowledge to all faculty members of I.I.T. Kanpur who have taught me various courses during my academic program. I am truly indebted to Dr. P.K. Kalra for his inspiration during the early phase of my work while he was my co-supervisor.

My senior colleagues Sri Niwas Singh and Kailash Nath Srivastava were constant sources of inspiration and encouragement. I warmly acknowledge and express my special thanks for the inspiring discussion and infallible suggestions extended to me, without whose unfailing support and untiring help it would have been hard for me to bring out this thesis in the form it appears today.

I Thank my colleagues Biswarup Das, D.M. Vinodkumar, R.P. Gupta and R.K.Singh for creating a stimulating research atmosphere. My association with research associates

Shesha, Shobhit, Mishra, Nagoree, Kannan, Awdhesh and Shankar will be memorable. Special thanks to Alok, Deshraj and Shyamsundar for creating hilarious atmosphere during tense situation.

I thank the authorities of the Maharaja Sayajirao University of Baroda, for deputing me to pursue Ph.D. degree under Quality Improvement Program.

The financial support received from the Central Board of Irrigation and Power, New Delhi vide project no.CBIP/EE/93038 is gratefully acknowledged.

Nimisha and myself will always cherish the affection and attention received from professor S.C. Srivastava, Professor Y.R. Waghmare and members of their family during our stay .

I also want to express my affection and high regards for a small set of people who had provided Gujrati environment at IITK. My heartfelt thanks goes to Bhavesh ,Bhushit, Dinesh, Kamlesh, Kaushik, Manish, Manoj, Ruta, Sanjay, uncle and Angli auntie.

Finally, no words are adequate to express my indebtedness to my parents for all their pains and sufferings, they have undergone to bring me up to this stage. To them all I bow in the deepest reverence. I acknowledge with utmost warmth the unending support, love and affection received from my wife Nimisha.

Satish Joshi

Contents

List of Figures

List of Tables

Chapter 1

Introduction

1.1 General

With ever-increasing interconnections and loadings in the modern power system networks all over the world, power utilities are facing a major challenge in maintaining desired quality and security of power supply. Power system security and analysis forms an integral part of modern energy management system. The economic recession coupled with environmental and ecological pressures have compelled the electric utilities, all over the world, to serve the increase in load demand without corresponding increase in generation and transmission facilities. This has forced the utilities to operate their generators and transmission systems to their maximum capabilities. With the developments of improved protective devices, static VAR compensators, generator speed governing systems and voltage regulators, transient stability limits of the system have increased, thereby allowing more real power to be transferred over longer distances and systems which used to be transient stability limited are now facing the problem of maintaining the required bus voltages and has become voltage stability limited [130, 172, 191].

The terms reliability, security and stability are related to each other and can be defined as given in reference [16]. *Reliability* is referred to the probability of satisfactory system performance over a long run. This is a function of time-average performance of system and should be studied at system planning stage. *Security* is considered to be an instantaneous time varying condition that is a function of the robustness of the system relative to imminent disturbances. It reflects ability of power system to meet its load without unduly stressing its apparatus or allowing network variables to stray from prescribed range. The

power system stability is broadly defined as the property of the system that enables it to remain in state of operating equilibrium under normal operating conditions and to regain an acceptable state of equilibrium after being subjected to a disturbance [220, 233].

1.1.1 Voltage Security, Voltage Stability and Voltage Collapse

Voltage security, Voltage stability and Voltage collapse have been formally defined in IEEE report [111] and by Concordia [119] as follows:

- Voltage security is the ability of a system, not only to operate stably, but also remain stable (as far as the maintenance of the system voltage is concerned) following any reasonably credible contingency or adverse system change.
- Voltage stability is the ability of a system to maintain voltage so that when load admittance is increased, load power will increase and so that both power and voltage are controllable.
- Voltage collapse is the process by which voltage instability leads to very low voltage profile in a significant part of the system.

However, definition of voltage stability conditions are not (directly) compatible with the general IEEE definitions for stability concept. Hence, a new set of definitions were given in Cigre report [170]. They are

Voltage Stability: A power system, at a given operating state and subject to a given disturbancae, is voltage stable if voltages near loads approach post-disturbance equilibrium values. The disturbed state is within the region of attraction of the stable post-disturbance equilibrium.

Voltage instability: Voltage instability is the absence of voltage stability, and results in progressive voltage decrease(or increase). Destabilizing controls reaching limits, or other control actions (e.g., load disconnection), however, may establish global stability.

Voltage Collapse: Following voltage instability, a power system undergoes voltage collapse if the post-disturbance equilibrium voltages near loads are below acceptable limits. Voltage collapse in the system may be either total(blackout) or partial.

Voltage stability has been considered as *fast* as well as *slow* phenomena depending on the dynamics of the components responsible for the system instability. Most of the

researchers have considered it as static phenomenon and have linked it to the maximum loadability of the system. This is due to the fact that in many incidents of voltage collapse, it has been characterized as slow variation of voltage over a long time until it reaches close to the collapse point. Recently it has also been studied as dynamic phenomenon. Bifurcation and chaos theory has been applied to understand the dynamic voltage stability in power systems.

Security assessment is normally performed into three distinct stages: Contingency definition, Contingency selection and Contingency evaluation.

Contingency definition gives the list of contingencies to be processed whose probability of occurrence is high. *Contingency selection* employs an adaptive scheme to select a set of important and critical contingencies. It invariably uses an approximate power system model with appropriate computational techniques, to give relatively fast results but with limited accuracy. On the basis of these results, the contingencies are ranked in rough order of their relative severities. *Contingency evaluation* using AC power flow is then performed on the contingency cases in decreasing order of severity. The process is continued up to the point where no post-contingency violations are encountered. In some cases, contingency selection and evaluation are merged into one process.

1.2 State-of-the-Art

The problem of security emerged in the wake of the 1965 northeast black-out in U.S. The most significant paper in the literature of security is that of DyLiacco on adaptive reliability [1] which discusses three state system model of the system. Further, detailed classification of power system states has been suggested by Fink and Carlson [16] and Stott et al. [67]. In these papers, the system security was defined with respect to the operating states. The problem of security monitoring has been introduced as that of monitoring the conditional transition of the system into an emergency state through contingency analysis.

On-line contingency analysis becomes difficult due to the conflict between the accuracy with which the power system is to be solved and the speed required to simulate all the contingencies. In order to speed up the contingency analysis process, contingency selection is performed. The methods for contingency selection can be divided into two major groups

Direct methods and *Indirect methods.*

The *direct methods* assemble the appropriate severity indices using the individual monitored quantities (bus voltage, branch flows, reactive generation). This suggests that these quantities have to be determined first [30, 52, 104]. While the indirect methods rely on explicit calculation of severity indices without evaluating the monitored quantities [18,89]. The *indirect methods* are less accurate, but faster and selective than the *direct methods.*

Most of the developments on contingency selection has been performed for active power problems using DC power flow or some other linearized models. A review of real power ranking methods has been performed in reference [76]. For voltage contingency selection, a number of trends has emerged. Main aim of these methods is to reduce computational time either by localizing outage effect or speeding up the non-linear solution of entire system.

The concentric relaxation method of Zaborsky et al. [21] can be seen as the earliest localization attempt. The main idea behind the method is to solve a small portion of the system in the vicinity of the contingency while remainder of the network is considered as infinite expanse. The area to be solved is concentrically expanded until the incremental voltage changes along with the first solved tier of buses is not significantly affected by additional tier of buses. A modification of the original approach has used a fixed number of tires for AC contingency selection as suggested by Lauby et al. [38]. An alternative approach is based upon bounding of outage effects [87, 88] in which an attempt to find the solution, only in stressed area of the system, is made.

The use of single iteration of load flow approach [30] became well established. The main idea behind the method was to take advantage of the speed and reasonably fast convergence of the fast decoupled power flow by limiting the number of iterations to one. The single iteration approach has been combined with other techniques like use of the reduced network representation [68] to improve numerical efficiency. Khu et al. [33] have reported non-iterative linearization method devised to evaluate the effect of single or multiple-circuit contingencies upon the system load bus voltages. Jana et al. [183] have presented an improved linearized method to evaluate load bus voltage following line outage. However, this method also involved some unrealistic assumptions such as the lines are assumed to be purely inductive. Also the P-V and Q-δ decoupling assumption has been suggested which may not be valid, specially in heavily stressed conditions of

the network [233]. Leonidopololous [125] has retained P-V and Q-δ coupling in linearized load flow model but uses an iterative procedure, which is time consuming. Singh [249] developed linearized load flow for voltage security analysis around complete operating range based on integral square error minimization and least square error minimization principles. Tripathi et al. [82] used a system's theory approach to predict post-outage quantities.

Lee and Chen [156] have presented a method to calculate distribution factors. defined in terms of only pre-outage reactive power flows. For transmission line and transformer outage studies, the distribution factors were computed utilizing the fast decoupled load flow equations. Sensitivity property of Newton-Raphson load flow Jacobian has been exploited in [161] to derive the distribution factors for both voltage and reactive power calculations. A more exact set of new distribution factors were developed by Singh [249].

Artificial Neural Networks (ANN) are being used these days for their ability to map non-linear functions and to provide extremely fast results. Hsu and Yang [181] used an ANN and entropy based model to predict bus voltages . However, this method requires development of as many neural networks as the product of the number of buses and the number of contingencies. Review of various contingency selection methods are reported in references [85, 142, 222].

Schlueter et al. [162] suggested a multiple contingency selection method for transmission system reliability and transfer capability studies. The use of a pattern recognition technique has been reported in references [103, 248] for contingency screening. The application of expert system in contingency selection has been reported in referencers [73, 81]. Lo et al. [93] have shown effectiveness of various existing voltage ranking methods. Shafer et al. [115] extended the definition of the PI based on vector norm formulation and utilized exponent of performance index as high as to avoid the masking effect. Hsu and Kuo [154] used fuzzy set for voltage ranking to avoid masking and misranking effects.

The voltage stability has become an increasingly important limit in practical systems [58, 130] for ensuring system security. However, it is also more difficult to characterize the voltage stability limit mathematically as compared to the thermal or generation limits. Furthermore, voltage itself is a poor indicator of voltage collapse as increased use of compensating devices such as static VAR compensators and shunt capacitors raise the

critical voltage into normal voltage range.

With the increase in real power transmission capabilities, the problem of voltage stability has become a serious operating concern. The voltage stability studies have been carried out with static as well as dynamic considerations. Though the voltage stability studies have been reported on AC as well as AC-DC systems, a representative survey on only AC systems is being presented below:

Mercede et al. [77] and Chow et al. [106] have presented frame work for analysis and prediction of voltage stability problems. Depending upon the nature of disturbance and the subsystem dynamics, the voltage stability may be regarded as slow or fast phenomenon [168]. A special issue on the subject [171] contains some of the state-of-art papers.

The static or steady state voltage stability has often been regarded as viability problem suitable for static load flow. The ability to transfer reactive power from production sources to consumption nodes during steady state operating conditions is a significant aspect of voltage stability. A CIGRE report [63] recommends analysis methods and power system planning approach based on static models.

The singularity of load flow Jacobian has been linked to steady state stability [9,57,114] and its positive definiteness has been proved to be the sufficient condition for an operating point to be small disturbance stable [62,91]. Various indices for prediction of steady state voltage stability margin has been presented in CIGRE report [212].

It has been observed that when the operating point reaches the nose point of P-V or Q-V curve, the sensitivity of bus voltage to the load power becomes alarmingly high and at the nose of P-V or Q-V curve, dV/dP or dV/dQ becomes infinity [13]. The concept of load flow Jacobian sensitivity has been used by Flatabo et al. [108,176] and has been applied on the Norwegian system for maintaining required security level. The sensitivity of total reactive power generation to the variation in real and reactive load, has also been proposed as security index by Carpentier [45] and Begovic et al. [143]. Carpentier has termed this index as Voltage Collapse Proximity Indicator (VCPI). Another sensitivity based indirect criterion which relates the change in generator voltage E with corresponding change in load bus voltage V (dE/dV), has been proposed by Venikov [13] and used by Borremans et al. [44] for voltage stability studies. At the point of voltage instability, dE/dV becomes zero, meaning thereby the load voltage can not be controlled by generators, a fact which

has been mathematically proved by Hiskens et al. [91,121]. The deficit of reactive power has been cited as one of the important reasons responsible for voltage instability by Lachs [50]. Tamura et al. [40] observed that voltage instability is closely related to multiple load flow solutions which are caused by the non-linear nature of load flow equations. A heavily loaded system has two very close power flow solutions. One is the higher voltage power flow solution which is usually obtained by the conventional power flow calculations and the other is the lower voltage solution which is obtained by the methods proposed in reference [20]. When these two solutions coalesce, a saddle node bifurcation occurs. The proximity of these two solutions have been used by many researchers as an index for voltage stability margin. Use of energy based measures has been suggested to determine the closeness of multiple solution [107,128,129,200]. Jeyasurya used ANN to predict proximity to voltage collapse based on energy function [219]. Use of P-V and Q-V curves have also been made to assess the vulnerability of an operating point to voltage collapse [78,86,113,132,137,144,163,169,224]. Near the nose point, the Newton - Raphson algorithm may diverge. To overcome this difficulty, the continuation power flow method has been introduced by Ajjarapu et al. [139], Canizares et al. [211] and Iba et al. [123].

The divergence of load flow solution has been used as one of the indicators for assessing voltage instability [109]. However, the divergence of load flow may also be due to the load flow Jacobian being ill-conditioned. The proximity of load flow Jacobian to singularity can be better measured in terms of its minimum singular value [83,84,94,157,186–188,201, 245]. A fast algorithm based on parallel processing for computation of minimum singular value has been suggested by Tiranuchit et al. [84]. A minimum singular value based security index for scheduling real and reactive power outputs of sources has also been suggested by Tiranuchit et al. [83]. Lof et al. [157,186] presented a fast algorithm based on inverse iteration method to compute minimum singular value and tested it on a large system. Prediction of static voltage stability has also been made by Lof et al. [187,245] using minimum singular value of power flow Jacobian and considering voltage dependent reactive power capability of generators. Pai et al. [94] have considered an exponential type voltage dependent load model and considered a new index called condition number for static voltage stability prediction. Begovic et al. [118] demonstrated that by minimizing the weighted sum of the absolute values of control actions subject to equality constraints (real and reactive power balance equations) and inequality constraints (limits on the state

variables, real and reactive power generations) voltage stability could be improved.

Eigenvalue analysis has been used to assess static voltage stability. Sensitivity analysis has been carried out to determine critical group of buses responsible for voltage collapse [100,131,152,193,218]. Participation analysis has also been carried out to determine participation of various states in different modes of power system model by Hamdan [177] and Rajagopalan et al. [97]. The concept of coherency among load buses with respect to voltage dynamics was introduced by Begovic et al. [101] and Vargas et al. [204]. An algorithm for approximate assessment of minimum singular value [101] and eigenvalue [204] of Jacobian was presented based on partial state information about network obtained from coherent clusters of load buses. Ajjarapu et al. [207] have presented a scheme to improve voltage stability margin by use of fixed capacitors at appropriate locations. However, the use of fixed capacitors may prove detrimental to voltage stability in some operating conditions (example 11.3 of reference [13] and example 14.1 of reference [220]).

The prevailing approach for real time control of voltage collapse (as opposed to system planning) consists of security monitoring coupled with algorithms for allocation of resources for minimizing risk of voltage collapse [143, 185, 197]. A related problem is that of maintaining maximum distance (in parameter space) to the set of parameter values at which bifurcation from the nominal operating point occurs. The development of voltage stability indices is essential studies of this kind [106, 148, 174, 175, 198, 208, 246]. Dobson [147] has studied the geometry of saddle node bifurcation and presented a method to avoid saddle node bifurcation [148]. Overbye [225, 247] has also presented a method to restore power flow solvability.

On dynamic considerations, the problem of voltage instability has been studied by solving set of non-linear differential algebraic equations [99, 155, 173, 188]. It has been shown that when the Jacobian associated with the algebraic system becomes singular, the system model breaks down and the load bus voltages can no longer be controlled [99,121,165,216]. The eigenvalue analysis has also been carried out using dynamic models of power systems for analysis of voltage instability [97, 124, 160, 189, 205, 228, 235].

With developments and increased understanding of the dynamic system theory along with availability of inexpensive computing facility, it is being increasingly used to study the power system behavior [206]. Varaiya et al. [164] presented a survey of non-linear dynamical phenomena covering bifurcation and chaos. They demonstrated that even the

simplest representation of a power system can exhibit both local and global bifurcations. Saddle node bifurcation was hypothesised by some researchers as the only cause of voltage collapse [57,90,105,140]. However, later work demonstrated the possible role of other bifurcations, such as Hopf bifurcation, in power system voltage instability leading to voltage collapse [96,126,184,199,236]. Abed et al. [206] demonstrated the effect of variable damping, frequency dependence of electrical torque, transmission line resistance and excitation control on the classical swing equation dynamics and observed the emergence of periodic orbit through Hopf bifurcation. Alexander [54] demonstrated the existence of sub critical and super critical Hopf bifurcations for different values of resistance to reactance (R/X) ratio of transmission lines. A fourth order generator model along with excitation system has been considered by Rajagopalan et al. [96] and it has been shown that a complex pair of eigenvalues associated with the excitation system results in to Hopf bifurcation. Ajjarapu et al. [140] have considered a dynamic load model as suggested by Walve [61] along with generator swing dynamics and demonstrated multiple Hopf bifurcations in a sample 3-bus system. Hopf bifurcation has been demonstrated in synchronous motor dynamics [120]. Chen et al. [72] demonstrated degenerate Hopf bifurcation in power system. Frequency domain approach has been adopted by Kwatny et al. [112] to study Hopf bifurcation in power system. Srivastava [231] suggested a method to compute critical values of load parameters and generator controls at Hopf bifurcations.

Voltage stability has also been called to be load stability [13] as the load characteristics have profound effect on the system dynamics [227]. Dynamics of induction motor, especially large induction motors, have been reported to be crucial for voltage stability studies [227]. Effect of various load characteristics including synchronous and induction motor loads on voltage stability have been studied [91,94,116,124,159,195,205,213,215,226,230]. Canizares [239] have demonstrated the effect of load model on the bifurcation characteristic of the system model.

The classical stability simulation of Swedish blackout on 27th December 1983 could not explain the system behavior that led to cascade tripping. This prompted the researchers to develop new load models for voltage stability studies such as by Hill [178] Walve [61], Xu et al. [237] and Hill et al. [217]. Probabilistic load models have also been considered in references [64,194,238]. IEEE task force on load representation for dynamic performance presented a bibliography in reference [242] and suggested standard load models for power

flow and dynamic performance simulation [243].

The effect of on load tap changer (OLTC) is to restore the load. However, it has been found to aggravate the voltage instability [29, 51, 92, 127, 166]. Instability due to OLTC controls may lead to the possibility of either hunting or voltage collapse [66]. The behavior of SVC has been studied by Hiskens et al. [153] under voltage collapse.

Recently the system stability has also been linked to the structural weakness of the system [227]. The structural weakness of the power system is due to weak transmission boundaries, that isolate or decouple particular group of buses. The voltage changes at these buses are coherent for any disturbances that occur out side this group of buses. These group of buses are called *voltage control areas*. To determine the voltage control areas, Schlueter et al. [131] have proposed the use of power flow Jacobian sensitivity.

With the advancements in high voltage power electronics, recently new devices, known as FACTS (Flexible AC transmission system) devices for controlling the bus voltage and power flow in transmission lines, have been developed [149, 179, 180]. The most prominent among them are controllable series capacitors (CSC), static phase angle regulators (PAR) and static VAR compensators (SVC). The effect of these devices have been studied to eliminate dynamic bifurcation such as Hopf Bifurcation [231] in power system networks.

1.3 Motivation

From the literature survey it appears that most of the voltage contingency selection algorithms have utilized non-iterative methods such as local solution methods [21], one iteration of AC load flow methods [30], linearized load models [183] and distribution factors methods [249]. These methods, in general, are either quite inaccurate or require more computation time. Many of the methods are based on decoupling principle and some other unrealistic assumptions, which may not be valid during stressed operating condition of the system.

In order to assess the relative severity of the contingencies, scalar performance indices have been used. Two typical problems with the performance indices are the misranking and masking effects. Misranking of contingencies are mainly due to the inaccuracies in the model used for computing the performance indices. It is characterized by errors in the computed order of relative severities of various contingencies. Masking effect can be

described as the lack of discrimination in which the performance index for a case with one huge violation is ranked lower as compared to a case having many small violations. By most of the operational standards former case is much more severe. Masking effect to some extent can be avoided by using higher order performance indices. However, to avoid the misranking, proper selection of weights for performance indices is required.

Today's power system operates near to voltage stability limits and with the increased use of compensating devices such as shunt capacitors, voltage alone is a poor indicator of voltage stability. Hence, voltage stability margin or distance to voltage instability point should be considered along with the bus voltage deviation values for contingency selection.

There exists several direct as well as indirect methods to predict static voltage stability point and to determine the corresponding voltage stability margin [175, 208]. These methods, in general, require large computing time. In some of the applications such as for contingency selection, where stability margin is required to be computed fast, the above existing methods may not be suitable and new methods such as one based on Artificial Neural Network, that can predict the voltage stability margin fast, is required. Jayant Kumar et al. [244] have used analog simulation based neural network for real time economic load dispatch and found it to provide extremely fast results.

From the literature survey on dynamic bifurcation in power systems, it is observed that Hopf bifurcation may occur much before saddle node bifurcation in several system networks under parameter variation. Most of the work have defined the voltage stability margin with respect to the saddle node bifurcation. However, the stable operation of the power system networks may require defining the stability margin with respect to the Hopf bifurcation. Practically no attempt has yet been made to define the margin with respect to the Hopf bifurcation except a work by Dobson et al. [145] who have suggested a method to find sensitivity of parameters with respect to the Hopf bifurcation.

An existing method to determine voltage control areas is based on power flow Jacobian sensitivity [131]. However, control areas determined by this method do not remain valid at different operating (loading) point.

The operation of a power system requires maintaining a minimum level of stability margin for secure operation of the system. In order to enhance the stability margin, the

effect of generation rescheduling was studied in reference [83, 231]. FACTs devices are being popularly used to improve the dynamic stability of the system. However, the effect of their optimal settings along with the outputs of generators on enhancement of voltage stability margin has not yet been established.

Hence, the motivation behind the work reported in this thesis was

(i) To develop a new method for contingency selection consisting of a fast model based on Artificial Neural Network (ANN) for post-outage voltage prediction and a fuzzy logic based ranking method considering the bus voltage deviations as well as system voltage stability margin.

(ii) To develop a fast method for prediction of nearest saddle node bifurcation point in the system using an analog simulation based neural network [74].

(iii) To present a new method based on optimization technique for determining the distance to closest Hopf bifurcation.

(iv) To explore new method to determine voltage control area based on entropy concept which remain valid for wide range of operating conditions.

(v) To study the effectiveness of optimal adjustment of generators and FACTS devices output in voltage stability enhancement.

1.4 Thesis Organization

The present *chapter 1* introduces the voltage security and stability problems, presents a brief state-of-art survey of voltage contingency selection and the voltage stability problems and lays down the motivation behind the research work carried out in this thesis.

In *chapter 2*, a fast method based on Artificial Neural Network (ANN), has been developed for post-outage bus voltage prediction. Functional link model of the ANN has been utilized. Contingency ranking has been performed considering both voltage stability margin as well as voltage deviation. A fuzzy logic approach has been used for the contingency ranking.

Chapter 3 presents the development of a new method employing an analog simulation based neural network to determine the nearest saddle node bifurcation point. This has

been formulated as an optimization problem which has been realized through analog circuitry [74].

Chapter 4 reports the development of a method for prediction of minimum distance to Hopf bifurcation. The estimation of closest Hopf bifurcation has been formulated as an optimization problem and has been solved using sequential quadratic programming.

Chapter 5 describes a new method based on entropy concepts to determine voltage control areas valid for wide operating range. The validity of the control areas has been established by using the Q-V curve.

In *Chapter 6*, a simple approach based on identification of the weakest bus along with the knowledge of control area has been used for siting the FACTS devices. The effectiveness of optimal adjustment of generators and FACTS devices to enhance the voltage stability margin has also been studied. The optimal settings of these devices have been obtained by solving an optimal power flow problem which minimizes the system transmission losses.

Chapter 7 summarizes the main findings and significant contributions of the thesis and provides a few suggestions for further scope of research work in this area.

Chapter 2

Voltage Contingency Selection using ANN and Fuzzy Logic

2.1 Introduction

Power system security monitoring and anaiysis forms an integral part of modern energy management systems, but its real time impiementation is still a challenging task to power system engineers. Outage of a transmission unit (line or transformer) or a generator may lead to over loading of other healthy lines and generators and/or cause sudden changes in the system bus voltages. For secure operation of system, the operating personnel must know which branch or generator outage will cause line flows or bus voltages to fall out side the limit and thus force the system to enter the emergency state.

In real time environment it is hardly feasible to perform on line load flows for all the possible contingencies. Hence, contingency selection is performed before the analysis to reduce computational time. Contingency selection is carried out for quick identification of those contingencies which may cause out-of-limit violation so as to reduce the number of contingencies that need to be analyzed by full AC load flow while assessing the power system's security. Two popularly used methods for the contingency selection are ranking method and screening method.

The Ranking methods rank the contingencies in approximate order of severity. Contingencies are ranked based on value of scalar performance index (PI) which measures the system stress in some manner. For example, contingencies could be ranked for voltage problems using PI defined as the sum of the squared voltage deviations [18,27] from their

specified values. Several PI based methods have been suggested and tested for voltage security analysis [18,38,89,93]. In ranking methods, the performance indices are explicitly expressed in terms of network variables and are directly evaluated. It does not require computation of post-outage quantities which are evaluated in the screening methods by using some approximate solution approach.

Screening methods use approximate network solution to identify cases causing limit violations. The network monitored quantities are first calculated for all the contingencies. Ranking is done based on the results of the approximate solutions. Some of the solution methods utilized are the distribution factors [48, 161], DC load flow [75], linearized load flow, one iteration of AC load flow [32], local solution methods [21], etc. These methods, in general, are either quite inaccurate or require more computational time. Artificial Neural Networks are being used these days for their ability to map nonlinear functions and provide extremely fast results. Hence, in this chapter an attempt has been made to apply an ANN model for the post-outage voltage estimation required for the voltage contingency selection. The studies have been conducted on IEEE 14-bus, IEEE 30-bus and a 75-bus Indian systems and results have been compared with an exact AC load flow method.

Most of the works on voltage contingency selection utilize the second order performance indices based on bus voltage deviation which suffer from masking and misranking effects. Masking effect is generally overcome by using higher order performance indices. However, misranking is associated with wrong choice of weighing factors. To overcome this problem an approach based on fuzzy logic has been suggested in this chapter for obtaining the performance index and ranking of contingencies.

Due to the stressed operation of most of the power system networks today, the voltage stability has become one of the major concern. Hence, it was felt necessary to consider the voltage stability margin along with voltage deviation in defining the performance indices. The fuzzy logic approach has been extended in the present work to form the overall performance indices considering these two aspects and its effectiveness has been demonstrated on the three sample systems.

2.2 Artificial Neural Network Based Voltage Prediction

The current interest in Artificial Neural Networks (ANN) is largely due to their ability to mimic natural intelligence. ANN have been used in a broad range of applications. These include pattern classification, function approximation, optimization, prediction, and automatic control. ANN can achieve high computational speed by employing a massive number of simple processing elements arranged in parallel with high degree of connectivity called *neurons* which operate concurrently. There are large number of neural network paradigms [117]. Most of the Artificial Neural Networks perform essentially the function of vector or functional mapping. The ANN models accept a set of inputs (an input vector) and produce a corresponding set of outputs (an output vector).

Neural networks have also been applied to various fields of engineering including electrical power systems. Vankayala and Rao [203] carried out a survey of various artificial neural networks and their applications to power systems. Majority of the works in the power systems have used feed forward networks based on back propagation algorithm (BPA). However, it has been shown in [95] that higher order networks such as functional link networks have a superior functional mapping capability as compared to the BPA model. Hence in the present work a functional link network (FLN) has been used for prediction of bus voltages, which is briefly described below.

2.2.1 Functional Link Network

The functional link network, developed by Pao et al [95], not only increases learning rate but also has an unexpected effect of simplifying the learning algorithms. The functional link network is a single layer neural network that is able to handle linearly nonseparable tasks due to the enhanced input representation.

The key idea of the method is to find a suitably enhanced representation of the input data. Additional input data that are used in the scheme incorporate higher order effects and artificially increase the dimension of the input space. The expanded inputs are then used for training along with the actual input data as shown in Figure 2.1. These enhanced training set increases accuracy of mapping of input-output relations. Suppose the functional link contains the functions f_1, f_2,f_3 ..., f_n for enhancement of inputs, an

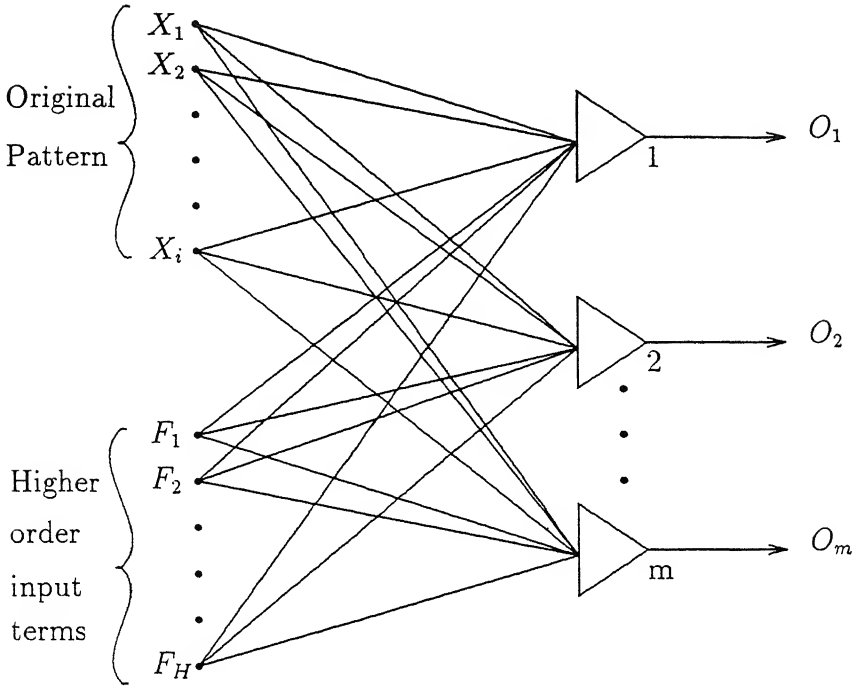

Figure 2.1: Functional Link Network

input x will be transformed first into $f_1(x)$, $f_2(x)$, ..., $f_n(x)$ which are then fed to the network for further processing.

There are two models of functional link network, the tensor (outer product) model and the functional expansion model. In the functional expansion model, the functional link acts on each node singly. Each component (x_i) of the input vector is acted on by the functional link to produce the enhanced inputs $f_1(x_i)$, $f_2(x_i)$, ... $f_n(x_i)$. These functions can be a subset or complete set of orthonormal basis functions such as

x, $\sin\pi x$, $\cos\pi x$, $\sin 2\pi x$, $\cos 2\pi x$, ...

In the tensor model, each component of input patterns multiplies the entire input pattern vector. The functional link in this case generates an entire vector from each of the individual components. In this model the pattern might undergo a sequence of transformations such as

$$\{x_i\} \Rightarrow \{x_i, x_i x_j\}_{j \geq i} \Rightarrow \{x_i, x_i x_j, x_i x_j x_k\}_{k \geq j \geq i}$$

In this model, no new information has been added but joint activation have been made explicitly available to the network. In the present work, tensor (outer product) model.

only upto the second order products of the inputs, have been used which was found to provide desired accuracy for voltage prediction problem. Thus, if x_1, ..., x_n are the original inputs the enhanced inputs contain (x_1x_2, x_2x_3 ..., $x_{n-1}x_n$) terms, which have been used as additional input vector to ANN.

2.2.2 Training of Functional Link Network

The Functional link network, consists of only two layers, the input layer and output layer. It does not have any hidden layer. Hence, simple Delta rule [98] can be used for training of the functional link network. The training algorithm is described below:

(i) Input pattern is enhanced by multiplying each of its component by the entire input pattern vector.

(ii) Output of node j, o_j is function of (net_j) i.e.,

$$o_j = f(net_j) \tag{2.1}$$

where

$net_j = \sum_{i=1}^{N} x_i w_{ij} \quad j = 1, ..., m$

x_i = inputs including enhanced terms

w_{ij} = weight between neuron i and neuron j

m = number of output nodes

N = number of enhanced inputs

(iii) Compare the actual output with the desired output and determine the measure of error δ_j at each output node j

δ_j = (desired output - actual output) at node j

(iv) Change in weight is determined by

$$\Delta w_{ij}(t) = \eta \delta_j f\prime(net_j) + \alpha \delta w_{ij}(t-1) \tag{2.2}$$

where, η is the learning rate and α is the momentum

(v) Weights are adjusted by

$$w_{ij_{new}} = w_{ij_{old}} + \Delta w_{ij} \tag{2.3}$$

(vi) Steps (ii) to (v) are repeated till the error reduces to a prespecified tolerance.

2.2.3 Implementation of Functional Link Network for Voltage Prediction

The artificial neural networks based on the functional link network model have been developed for the outage (contingency) analysis. The present study was limited to only voltage security analysis. Hence, the FLN model was trained and tested to predict voltage magnitudes at all the buses. Original inputs to the FLN are the real power injections, at all the buses except the reference bus, reactive power injections at only load (P-Q) buses and network topology number corresponding to the simulated outage. Topology number was in the form of a string of bipolar numbers (+1 or -1) whose length was decided based on the total number of contingencies simulated. The study was restricted to only single line outages. For IEEE 14-bus, 30 bus and 75 bus Indian systems, outages of total $20(< 2^5)$, $41(< 2^6)$ and $12(< 2^4)$ lines respectively, were considered. Hence, the topology numbers were represented as a string of 5, 6 and 4 bipolar digits in these three systems. The base case in each system was represented by a string of bipolar numbers all of them having (-1) values and other cases with different combinations of +1 and -1 digits. For example in IEEE 14-bus system the base case is represented by a bipolar string (-1 -1 -1 -1 -1) and different line outage cases as given in Table 2.1. Figure 2.2 shows a block diagram of the ANN for voltage prediction listing the original inputs and output variables for a system having total n buses (bus-n being the reference bus), buses 1 to m being the P-Q buses and rest being the P-V buses.

For the voltage prediction, training patterns were generated for the base case as well as different outage cases by varying the loads randomly at all the buses in the range of 80% to 130% of their base case values and utilizing the corresponding bus voltages obtained from the load flow.

Once the training was complete, the ANN was tested with novel patterns not included in the training set. The voltages predicted for each outage cases have been subsequently utilized to define performance indices (described in next section) indicating their relative severities.

2.2.3 Implementation of Functional Link Network for Voltage Prediction

The artificial neural networks based on the functional link network model have been developed for the outage (contingency) analysis. The present study was limited to only voltage security analysis. Hence, the FLN model was trained and tested to predict voltage magnitudes at all the buses. Original inputs to the FLN are the real power injections, at all the buses except the reference bus, reactive power injections at only load (P-Q) buses and network topology number corresponding to the simulated outage. Topology number was in the form of a string of bipolar numbers (+1 or -1) whose length was decided based on the total number of contingencies simulated. The study was restricted to only single line outages. For IEEE 14-bus, 30 bus and 75 bus Indian systems, outages of total $20(< 2^5)$, $41(< 2^6)$ and $12(< 2^4)$ lines respectively, were considered. Hence, the topology numbers were represented as a string of 5, 6 and 4 bipolar digits in these three systems. The base case in each system was represented by a string of bipolar numbers all of them having (-1) values and other cases with different combinations of +1 and -1 digits. For example in IEEE 14-bus system the base case is represented by a bipolar string (-1 -1 -1 -1 -1) and different line outage cases as given in Table 2.1. Figure 2.2 shows a block diagram of the ANN for voltage prediction listing the original inputs and output variables for a system having total n buses (bus-n being the reference bus), buses 1 to m being the P-Q buses and rest being the P-V buses.

For the voltage prediction, training patterns were generated for the base case as well as different outage cases by varying the loads randomly at all the buses in the range of 80% to 130% of their base case values and utilizing the corresponding bus voltages obtained from the load flow.

Once the training was complete, the ANN was tested with novel patterns not included in the training set. The voltages predicted for each outage cases have been subsequently utilized to define performance indices (described in next section) indicating their relative severities.

Table 2.1: Bipolar strings for outage representation (14-bus system)

Sr. No.	Line outage	Topology number				
1	1	-1	-1	-1	-1	+1
2	2	-1	-1	-1	+1	-1
3	3	-1	-1	-1	+1	+1
4	4	-1	-1	+1	-1	-1
5	5	-1	-1	+1	-1	+1
6	6	-1	-1	+1	+1	-1
7	7	-1	-1	+1	+1	+1
8	8	-1	+1	-1	-1	-1
9	9	-1	+1	-1	-1	+1
10	10	-1	+1	-1	+1	-1
11	11	-1	+1	-1	+1	+1
12	12	-1	+1	+1	-1	-1
13	13	-1	+1	+1	-1	+1
14	14	-1	+1	+1	+1	-1
15	15	-1	+1	+1	+1	+1
16	16	+1	-1	-1	-1	-1
17	17	+1	-1	-1	-1	+1
18	18	+1	-1	-1	+1	-1
19	19	+1	-1	-1	+1	+1
20	20	+1	-1	+1	-1	-1

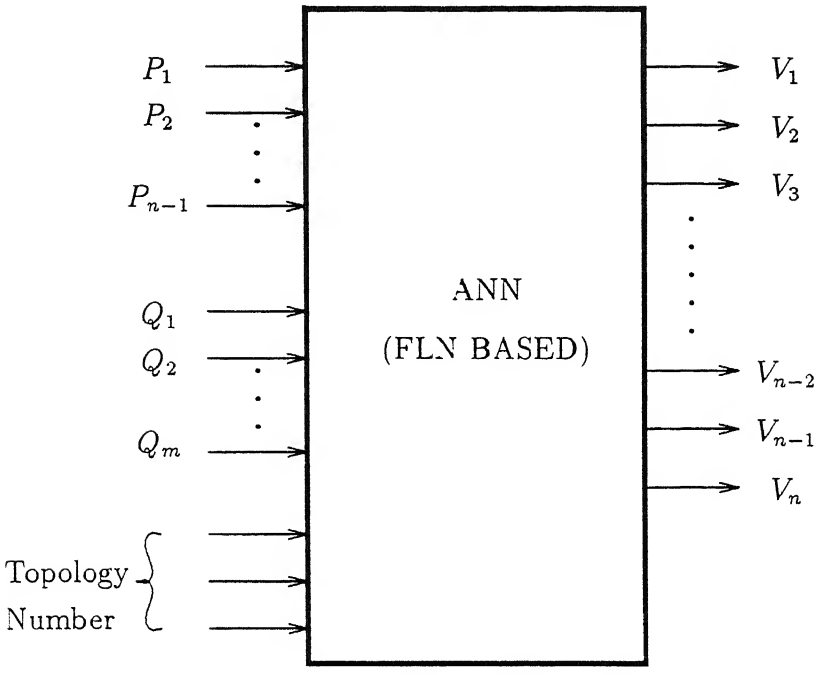

Figure 2.2: Block diagram of ANN based voltage predection

2.3 Contingency Ranking Using Fuzzy Logic

For ranking the contingencies according to their relative severities, performance indices [18, 115] have been popularly used. The performance indices, in a general form, can be written as

$$PI = \sum_i \frac{W_i}{2n} f_i(\underline{Z})^{2n} \tag{2.4}$$

where $f_i(\underline{Z})$ is a linear function of Z_i which denotes the changes in bus voltage magnitudes or generator bus reactive power injections with respect to their ratings. The order of the above performance index is 2n.

The conventional voltage ranking methods have been effectively used to determine severity with respect to the bus voltage security limit violation coded in terms of the performance index as given by equation (2.4) above. However, probably none have considered the voltage stability margin in the above performance index, which has become of great concern to utilities these days.

Moreover in conventional performance index approach, proper weighing factor in performance indices are selected to avoid misranking which may be based on optimization or heuristics and past experience of the human experts. High value of exponent is generally used to avoid masking effect. As heuristics and past experience in most cases are in linguistic form, it is more suitable to apply fuzzy logic in determining weights associated with the performance indices and contingency ranking [154]. In the present work the fuzzy logic approach has been used to determine the performance indices for each outage case considering the voltage stability margin along with the bus voltage deviations. The complete fuzzy reasoning process for the contingency ranking involves three major steps [154]

(i) Compiling the heuristic rules used by system operator in contingency ranking.

(ii) Using heuristic rules as guideline for the representation of post contingent quantities utilizing fuzzy logic notations.

(iii) Perform fuzzy reasoning to combine the evidence from each post contingent quantity and reach the desired ranking list.

However, for the application of fuzzy reasoning, the data sets should be represented into different class of memberships as given in subsequent subsections.

2.3.1 Fuzzy Representation of Bus Voltage Data

Post contingent voltage deviation at bus-i can be written as

$$|\Delta V_i| = \left|V_i - V_{i_{sp}}\right| \tag{2.5}$$

where V_i = calculated value of voltage magnitude at bus-i
$V_{i_{sp}}$ = specified or target value of voltage magnitude at bus-i.

This can be normalized with respect to maximum allowable voltage deviation as

$$DV_i = \frac{|\Delta V_i|}{\Delta V_{i_{max}}} \tag{2.6}$$

where $\Delta V_{i_{max}} = (V_{i_{max}} - V_{i_{min}})/2$

These normalized voltages are divided into five categories using fuzzy set notations. VS (very small), S (small), M (medium), L (large) and VL (very large).

The Table 2.2 shows correspondence between the normalized voltage deviation (DV) and the five linguistic variable (LV).

Table 2.2: Relation between DV and LV

LV	VS	S	M	L	VL
DV	0.0 - 0.4	0.4 - 0.8	0.8 - 1.2	1.2 - 1.6	1.6 - ∞

Table 2.3: Relation between MI andLV

LV	VS	S	M	L	VL
MI	0.0 - 0.1	0.1 - 0.2	0.2 - 0.3	0.3 - 0.5	0.5 - 1.0

2.3.2 Fuzzy Representation for Stability Margin Data

For each contingency the voltage stability margin with respect to the maximum reactive power loadability has been calculated employing a method suggested by Dobson et al. [174]. These margins were normalized with respect to the margin available at the base case, as described below in equation(2.7)

$$(NMA)_i = \frac{(ML)_i - Q_{TL}}{(ML)_B - Q_{TL}} \tag{2.7}$$

where
$(NMA)_i$ = Normalized reactive power margin available after i^{th} contingency.
$(ML)_i$ = Maximum loadability after i^{th} contingency.
$(ML)_B$ = Maximum loadability at given base condition.
Q_{TL} = Total reactive power load in the system.

In any contingency case the higher the NMA, the lesser will be the severity index. Hence a performance index to indicate relative severity (maximum loadability index) MI can be defined as

$$MI = 1 - NMA \tag{2.8}$$

This maximum loadability index is also divided into five linguistic variables (LV) for fuzzy representation. Table 2.3 describes the relation between them.

2.3.3 Fuzzy Reasoning Procedure

If any outage causes loss of load or negative margin, it is declared as the most severe without performing further analysis. In other cases the load patterns were given to FLN

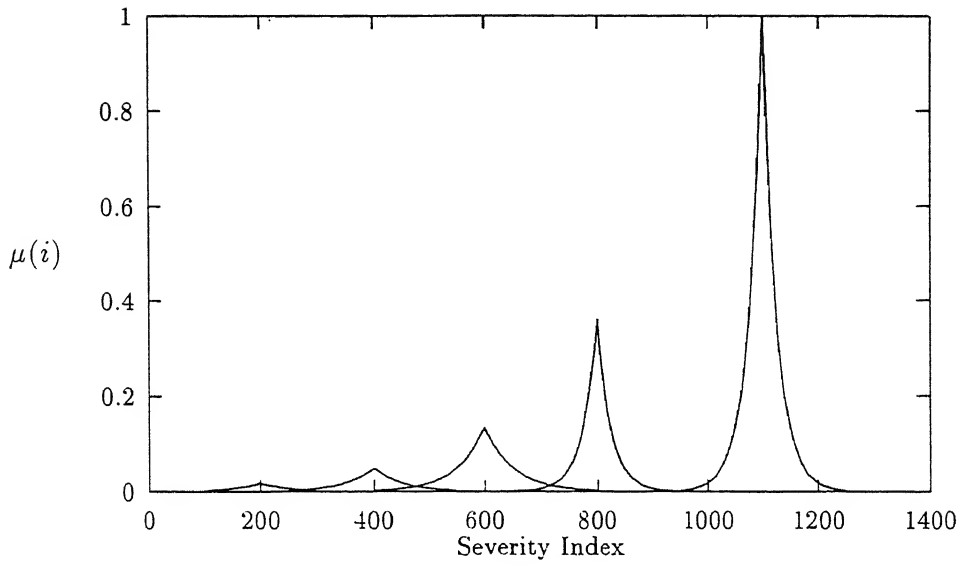

Figure 2.3: The membership function for the five linguistic variable

to predict the voltages. In the present work an exponential membership function (rather than conventional triangular function) for each linguistic variable has been utilized which covers a much wider range of variation. The exponential membership function can be expressed as given in equation(2.9)

$$\mu(SI) = \begin{cases} Pe^{(-A|SI-C|)} & if \quad |SI - C| < W \\ \\ 0 & \text{,otherwise.} \end{cases} \tag{2.9}$$

The values of C, W, P and A for different linguistic variables are given in Table 2.4. SI is the severity index. Figure 2.3 shows fuzzy representation of five linguistic variables. The values of C, W, P and A were decided heuristically for all the systems. For example voltages, most of the time, assume values in the medium range and for few cases in the VS or VL ranges. The value of W reflects this probability.

The membership function of each linguistic variable was enhanced by multiplying number of evidences described by that linguistic variable. In fuzzy reasoning, each post-contingent quantity was called as evidence. This modified membership function was used to find the performance index using center of gravity algorithm [12].

Table 2.4: The parameters of the membership functions

LV	VS	S	M	L	VL
C	200	400	600	800	1100
W	100	150	200	150	150
P	. 018	.049	.134	.360	1.000
A	.020	.020	.020	.040	.040

In center of gravity algorithm, we first define

$$A(x) = \int_{-\infty}^{x} [\mu'_{vs}(SI) + \mu'_{s}(SI) + \mu'_{M}(SI) + \mu'_{L}(SI) + \mu'_{VL}(SI)]dSI \tag{2.10}$$

The sum of total area covered by all membership functions is given by

$$A_{net} = A(\infty) \tag{2.11}$$

The performance index PI can be obtained by solving equation (2.12)

$$A(PI) = \int_{-\infty}^{PI} [\mu'_{vs}(SI) + \mu'_{s}(SI) + \mu'_{M}(SI) + \mu'_{L}(SI) + \mu'_{VL}(SI)]dSI = \frac{A_{net}}{2} \tag{2.12}$$

2.3.4 Overall Performance Index

To see the effect of reactive power margin on contingency ranking, three sets of performance indices have been defined along with fuzzy ranking. They are based on the voltage deviation (PI_V) based on the voltage stability/maximum loadability (PI_L) and the overall performance index combining the two (PI_A) as given below:

$$PI_V = \sum_{i=1}^{n} \frac{W_{V_i}}{2} \left(\frac{V_i - V_{spec_i}}{\Delta V_{i_{limit}}} \right)^2 \tag{2.13}$$

$$PI_L = MI \tag{2.14}$$

$$PI_A = PI_V + K \cdot PI_L \tag{2.15}$$

where K is a factor which assigns the relative weightage to the two criteria viz. the voltage deviation and stability margin. In the present work value of K has been selected as 1.

The overall performance index using fuzzy logic has been computed in this work by utilizing a membership function which has been obtained as the superposition of the two membership functions corresponding to voltage deviation and stability margin.

2.4 System Studies and Results

2.4.1 Voltage Prediction

To establish the effectiveness of the proposed voltage prediction method using functional link network, the artificial neural network was trained for IEEE 14-bus system, IEEE 30-bus system and practical 75-bus Indian system representing 132 KV, 220 KV and 400 KV network of U.P. State Electricity Board (UPSEB) as described in Appendices C, D and E respectively. An error criterion used for training was 0.005 p.u. A slightly higher value of criterion was selected to reduce the training time. Moreover, the exact voltages are not required for contingency ranking. During training, the learning rate (η) and momentum (α) were taken as 0.8 and 0.3 respectively for first 200 iterations and were changed to 0.6 and 0.35 respectively in subsequent iterations. It was found that this change helps in accelerating the convergence. Once the training was complete, it was tested with the patterns other than those used for the training. The predicted voltage values were compared with their exact values obtained from full AC Newton Raphson load flow method. The results of voltage prediction and outage analysis for the three systems are described below:

2.4.1.1 IEEE-14 bus system

For IEEE-14 bus system the ANN was trained for 200 training patterns corresponding to different loading conditions and line outages. After training, the ANN model was tested for 20 novel test patterns. For these test cases the absolute maximum error, the absolute minimum error and the absolute average error in the predicted voltages were found to be 0.017932 p.u., 0.000002 p.u. and 0.00419 p.u. respectively. Table 2.5 shows results of three typical contingency cases corresponding to the outage of lines (1-8), (3-10) and (13-14).

2.4.1.2 IEEE-30 Bus System

For the IEEE-30 bus system, artificial neural network was trained for 400 patterns corresponding to different loading conditions and line outages. The network was tested with 40 test patterns each corresponding to different line outages. These test patterns were not included in the training patterns. During testing, the absolute maximum error, absolute

Table 2.5: Post-outage voltages for 14-bus system

Bus No	Outage of					
	line (1-8)		line (7-10)		line (13-14)	
	Voltage by ANN	Voltage by NRLF	Voltage by ANN	Voltage by NRLF	Voltage by ANN	Voltage by NRLF
1	1.0600	1.0600	1.0600	1.0600	1.0600	1.0600
2	1.0443	1.0420	1.0473	1.0450	1.0450	1.0450
3	1.0701	1.0661	1.0723	1.0698	1.0700	1.0700
4	1.0145	1.0100	1.0058	1.0100	1.0099	1.0100
5	1.0907	1.0900	1.0912	1.0900	1.0900	1.0900
6	1.0641	1.0592	1.0709	1.0683	1.0617	1.0617
7	1.0498	1.0520	1.0590	1.0655	1.0529	1.0529
8	1.0227	1.0165	1.0296	1.0303	1.0293	1.0294
9	1.0229	1.0154	1.0257	1.0262	1.0238	1.0238
10	1.0474	1.0469	1.0307	1.0252	1.0479	1.0480
11	1.0556	1.0527	1.0493	1.0434	1.0547	1.0548
12	1.0564	1.0513	1.0523	1.0559	1.0571	1.0571
13	1.0473	1.0462	1.0526	1.0515	1.0551	1.0552
14	1.0331	1.0314	1.0367	1.0415	1.0206	1.0206

minimum error, and the absolute average error in the values of predicted voltages were found to be 0.032477 p.u., 0.000003 p.u. and 0.00587 p.u. respectively. The values of bus voltages predicted in p.u. with the neural network and NRLF method for outages of three lines (2-11), (18-19) and (29-30) have been given in Table 2.6.

2.4.1.3 75-bus UPSEB System

Total 150 training patterns were used to train the neural network for the 75-bus system, generated for the different loading conditions and for 12 different line outages. Once the neural network was trained, it was tested for 20 test patterns, other than those used for the training. The absolute maximum, minimum and average errors in bus voltages predicted by the ANN for this system were 0.0445 p.u., 0.000004 p.u. and 0.0061 p.u. respectively. Table 2.7 shows voltage values predicted in p.u. by the ANN and the NRLF methods for outages of lines (17-18), (54-63) and (35-36).

2.4.2 Contingency Ranking

The bus voltages predicted by the ANN model for all the three systems were first used for computing the voltage deviation based performance indices (PI_V) for each contingency cases. The ranking of few most severe contingencies and the associated PI_V values for the 14-bus, 30-bus and 75-bus systems are given in Tables 2.11, 2.14 and 2.15 respectively.

In order to compute the voltage stability margin performance index (PI_L) and the ranking of contingencies based on this criterion, the closest distance to the maximum loadability point (saddle node bifurcation) with respect to change in reactive power loads were computed for all contingency cases at the base case of the three systems by using an approach described in [90]. The reactive power margin were expressed as the first norm difference between the base case loading and the critical loading. These values for the base case and few contingency cases in the three systems are given in Tables 2.8, 2.9 and 2.10 respectively. Those contingency cases showing negative margin or resulting into loss of load were declared as most severe cases and were not included for calculation of performance index (PI_L). The performance indices PI_L for the remaining cases having positive margin were computed by the fuzzy logic approach and their values in the rank order for few cases are listed in Tables 2.12, 2.15 and 2.18 respectively for the three systems. It can be seen that the ranking of contingencies change in the present case as

Table 2.6: Post-outage voltages for 30-bus system

Bus No	Outage of					
	line (2-11)		line (18-19)		line (29-30)	
	Voltage by ANN	Voltage by NRLF	Voltage by ANN	Voltage by NRLF	Voltage by ANN	Voltage by NRLF
1	1.0601	1.0600	1.0601	1.0600	1.0601	1.0600
2	1.0445	1.0450	1.0444	1.0443	1.0457	1.0443
3	1.0079	1.0100	1.0098	1.0100	1.0088	1.0100
4	1.0819	1.0820	1.0828	1.0820	1.0825	1.0820
5	1.0071	1.0100	1.0120	1.0100	1.0097	1.0100
6	1.0701	1.0710	1.0705	1.0710	1.0677	1.0710
7	1.0377	1.0377	1.0399	1.0385	1.0410	1.0397
8	1.0234	1.0218	1.0239	1.0217	1.0229	1.0241
9	1.0417	1.0424	1.0472	1.0469	1.0425	1.0455
10	1.0817	1.0763	1.0849	1.0789	1.0744	1.0782
11	1.0046	1.0063	1.0164	1.0148	1.0141	1.0146
12	1.0002	1.0003	1.0044	1.0023	1.0051	1.0024
13	1.0050	1.0068	1.0102	1.0101	1.0091	1.0102
14	1.0269	1.0277	1.0347	1.0336	1.0274	1.0309
15	1.0242	1.0235	1.0322	1.0308	1.0255	1.0264
16	1.0272	1.0263	1.0292	1.0287	1.0248	1.0290
17	1.0183	1.0177	1.0186	1.0183	1.0154	1.0201
18	1.0115	1.0105	1.0249	1.0256	1.0136	1.0132
19	1.0080	1.0060	1.0032	.9962	1.0122	1.0086
20	1.0109	1.0092	1.0076	1.0018	1.0152	1.0117
21	1.0157	1.0128	1.0159	1.0130	1.0161	1.0150
22	1.0173	1.0144	1.0179	1.0149	1.0176	1.0167
23	1.0209	1.0175	1.0272	1.0229	1.0233	1.0203
24	1.0233	1.0181	1.0272	1.0208	1.0271	1.0205
25	1.0545	1.0489	1.0574	1.0515	1.0512	1.0511
26	1.0414	1.0318	1.0443	1.0345	1.0381	1.0340
27	1.0158	1.0158	1.0247	1.0232	1.0243	1.0231
28	1.0086	1.0091	1.0124	1.0117	1.0121	1.0118
29	1.0652	1.0575	1.0632	1.0602	1.0723	1.0698
30	1.0552	1.0467	1.0568	1.0493	1.0310	1.0328

Table 2.7: Post-outage voltages for 75-bus system

Bus No	Outage of					
	line (17-19)		line (54-63)		line (35-36)	
	Voltage by ANN	Voltage by NRLF	Voltage by ANN	Voltage by NRLF	Voltage by ANN	Voltage by NRLF
1	1.0300	1.0300	1.0300	1.0300	1.0300	1.0300
2	1.1513	1.1513	1.1377	1.1349	1.1636	1.1603
3	1.2407	1.2436	1.2051	1.2045	1.2596	1.2489
4	1.3721	1.3792	1.3145	1.3204	1.4141	1.3885
5	1.4228	1.4315	1.3648	1.3686	1.4684	1.4407
6	1.4224	1.4310	1.3641	1.3679	1.4680	1.4403
7	1.4237	1.4333	1.3696	1.3714	1.4692	1.4422
8	1.3049	1.3131	1.2428	1.2474	1.3484	1.3228
9	1.1515	1.1500	1.1406	1.1368	1.1613	1.1593
10	1.2578	1.2623	1.2196	1.2214	1.2829	1.2687
11	1.1958	1.1972	1.1466	1.1390	1.1746	1.1768
12	1.1648	1.1631	1.1519	1.1480	1.1742	1.1726
13	1.1342	1.1649	1.1236	1.1493	1.1961	1.1746
14	1.3819	1.3889	1.3232	1.3293	1.4238	1.3979
15	1.3532	1.3608	1.3116	1.3192	1.3962	1.3724
16	1.1499	1.1499	1.1363	1.1335	1.1622	1.1589
17	1.1297	1.1280	1.1230	1.1190	1.1401	1.1375
18	1.2413	1.2442	1.2058	1.2052	1.2602	1.2495
19	1.2065	1.2078	1.1611	1.1541	1.1870	1.1889
20	1.1964	1.1978	1.1484	1.1411	1.1758	1.1778
21	1.3902	1.3970	1.3312	1.3374	1.4330	1.4061
22	1.3879	1.3938	1.3325	1.3358	1.4239	1.4008
23	1.2493	1.2562	1.2194	1.2261	1.2866	1.2668
24	1.2566	1.2612	1.2185	1.2202	1.2818	1.2676
25	1.3850	1.3912	1.3276	1.3318	1.4234	1.3990
26	1.2452	1.2475	1.2048	1.2023	1.2542	1.2463
27	1.2459	1.2488	1.2067	1.2054	1.2601	1.2501
28	1.3707	1.3778	1.3131	1.3190	1.4126	1.3870
29	1.3949	1.4013	1.3394	1.3443	1.4365	1.4099
30	1.3914	1.3982	1.3325	1.3387	1.4341	1.4072
31	1.4211	1.4298	1.3632	1.3669	1.4667	1.4390
32	1.4207	1.4293	1.3626	1.3664	1.4662	1.4385
33	1.4223	1.4319	1.3681	1.3699	1.4677	1.4407
34	1.3052	1.3134	1.2431	1.2478	1.3487	1.3232
35	1.1526	1.1510	1.1417	1.1380	1.1623	1.1603
36	1.1637	1.1709	1.1372	1.1388	1.1624	1.1738
37	1.1409	1.1470	1.1176	1.1191	1.1432	1.1496

Contd

Table 2.7 (Contd.) ...

Bus No	Outage of					
	line (2-11)		line (18-19)		line (29-30)	
	Voltage by ANN	Voltage by NRLF	Voltage by ANN	Voltage by NRLF	Voltage by ANN	Voltage by NRLF
38	1.4140	1.4203	1.3576	1.3609	1.4540	1.4285
39	1.4142	1.4238	1.3602	1.3620	1.4595	1.4326
40	1.1896	1.1910	1.1401	1.1326	1.1684	1.1705
41	1.1656	1.1638	1.1527	1.1488	1.1749	1.1733
42	1.1354	1.1660	1.1249	1.1505	1.1970	1.1756
43	1.3823	1.3892	1.3235	1.3297	1.4240	1.3982
44	1.3601	1.3677	1.3189	1.3264	1.4028	1.3791
45	1.3603	1.3679	1.3195	1.3271	1.4033	1.3795
46	1.1236	1.1252	1.1078	1.1063	1.1345	1.1313
47	1.2337	1.2367	1.2004	1.2002	1.2546	1.2438
48	1.1775	1.1790	1.1270	1.1193	1.1558	1.1580
49	1.1694	1.1709	1.1185	1.1107	1.1475	1.1497
50	1.1751	1.1761	1.1528	1.1507	1.1928	1.1862
51	1.2476	1.2507	1.2066	1.2053	1.2624	1.2520
52	1.2504	1.2535	1.2090	1.2077	1.2653	1.2549
53	1.3942	1.4013	1.3349	1.3408	1.4376	1.4105
54	1.3272	1.3348	1.2695	1.2739	1.3677	1.3439
55	1.3463	1.3532	1.3019	1.3091	1.3871	1.3638
56	1.3796	1.3866	1.3211	1.3272	1.4219	1.3958
57	1.3863	1.3929	1.3223	1.3320	1.4294	1.4021
58	1.3826	1.3893	1.3199	1.3285	1.4255	1.3985
59	1.3927	1.3990	1.3245	1.3374	1.4358	1.4081
60	1.3794	1.3858	1.3211	1.3253	1.4184	1.3936
61	1.3983	1.4056	1.3388	1.3444	1.4422	1.4148
62	1.4112	1.4194	1.3519	1.3565	1.4564	1.4286
63	1.3390	1.3446	1.2989	1.3059	1.3754	1.3546
64	1.1864	1.1878	1.1372	1.1297	1.1653	1.1674
65	1.3899	1.3966	1.3308	1.3370	1.4326	1.4057
66	1.1893	1.1908	1.1407	1.1333	1.1685	1.1706
67	1.2526	1.2570	1.2152	1.2166	1.2771	1.2635
68	1.2390	1.2420	1.2026	1.2019	1.2571	1.2465
69	1.1220	1.1282	1.0980	1.0996	1.1243	1.1308
70	1.3830	1.3894	1.3240	1.3282	1.4224	1.3974
71	1.2421	1.2451	1.2035	1.2024	1.2574	1.2472
72	1.3830	1.3893	1.3241	1.3284	1.4223	1.3973
73	1.3490	1.3567	1.3095	1.3171	1.3919	1.3683
74	1.2482	1.2552	1.2189	1.2255	1.2857	1.2657
75	1.3968	1.4032	1.3414	1.3463	1.4385	1.4119

Table 2.8: Reactive power margin for IEEE 14-bus system

Sr. No.	Outage of line no.	from bus	to bus	Reactive power margin in p.u.
1	Base case	-	-	1.056600
2	1	8	3	0.432363
3	2	9	6	0.757790
4	3	9	7	0.886557
5	4	1	8	0.676244
6	5	2	8	0.931432
7	6	4	9	1.014365
8	7	9	8	0.961545
9	8	1	2	-0.366376
10	9	2	4	0.725048
11	11	2	9	0.879069
12	12	6	7	0.593989
13	15	3	12	0.830777
14	16	3	13	0755158
15	18	10	11	1.025420

compared to those obtained by using PI_V values given in Tables 2.11, 2.14 and 2.17. Thus, the contingencies which are most severe from voltage violation point of view may not remain the most severe one considering the voltage stability margin.

The overall performance index (PI_A) were also computed by using the fuzzy logic approach for various contingencies in the three systems. Tables 2.13, 2.16 and 2.19 respectively, list the rank of few contingencies along with the PI_A values for 14-bus, 30-bus and 75-bus systems.

2.5 Conclusions

In this chapter, a new method based on ANN using Functional Link Network (FLN) model was developed for post-outage bus voltage prediction. Fuzzy logic have been used to compute the performance indices of the contingencies required for ranking them in order of their relative severities. Voltage stability margin has been included, probably for the first time, for contingency selection. Results obtained on three systems reveal the following:

Table 2.9: Reactive power margin for IEEE 30-bus system

Sr. No.	Outage of line no.	from bus	to bus	Reactive power margin in p.u.
1	Base case	-	-	0.709849
2	1	13	7	0.464810
3	5	2	5	0.349252
4	6	2	13	0.612264
5	7	11	13	0.610965
6	7	11	13	0.610965
7	8	5	12	0.699412
8	9	13	12	0.708675
9	10	13	3	0.697366
10	12	1	27	0.413884
11	14	2	11	0.688404
12	18	14	15	0.709300
13	19	16	17	0.707198
14	25	8	21	0.705311
15	26	8	22	0.705920
16	27	21	22	0.704169
18	28	15	23	0.675625
19	30	23	24	0.670513
20	33	25	10	0.689757
21	34	27	11	0.420817
22	39	29	30	0.537596
23	40	3	28	0.689542
24	41	13	28	0.583216

Table 2.10: Reactive power margin for 75-bus system

Sr. No.	Outage of line no.	from bus	to bus	Reactive power margin in p.u .
1	Base case	-	-	1.8322
2	38	17	19	1.0991
3	39	17	23	0.7570
4	57	59	39	1.8210
5	58	54	63	1.8157
6	69	35	36	1.4293
7	66	19	36	1.8285
8	69	74	41	1.0644
9	78	41	42	0.5890
10	111	23	29	0.4839

Table 2.11: Contigency Ranking in 14-bus system based on voltage deviation

rank	line no.	from bus	to bus	PI_V
1	8	1	2	409.735
2	16	3	13	356.864
3	12	6	7	259.635
4	9	2	4	242.356
5	17	7	14	242.356

Table 2.12: Contigency Ranking in 14-bus system based on stability margin

rank	line no.	from bus	to bus	PI_L
1	1	8	3	59.079
2	12	6	7	43.782
3	4	1	8	35.998
4	9	2	4	31.379
5	16	3	13	28.719

Table 2.13: Contigency Ranking in 14-bus system based on overall index

rank	line no.	from bus	to bus	PI_A
1	4	1	8	497.370
2	1	8	3	330.164
3	2	9	6	277.222
4	9	2	4	237.812
5	12	6	7	237.812

Table 2.14: Contigency Ranking in 30-bus system based on voltage deviation

rank	line no.	from bus	to bus	PI_V
1	36	27	11	582.313
2	3	11	9	436.168
3	5	2	5	435.795
4	14	7	8	373.928
5	30	24	25	338.585
6	16	9	15	226.000
7	41	3	28	217.422

Table 2.15: Contigency Ranking in 30-bus system based on stability margin

rank	line no.	from bus	to bus	PI_L
1	5	2	5	50.799
2	13	1	27	41.694
3	36	27	11	40.717
4	1	13	7	34.519
5	39	29	30	24.266
6	41	13	28	17.839

Table 2.16: Contigency Ranking in 30-bus system based on overall index

rank	line no.	from bus	to bus	PI_A
1	36	27	11	582.313
2	5	2	5	453.658
3	39	29	30	436.168
4	13	1	27	221.342
5	1	13	7	214.229
6	41	13	28	204.636

Table 2.17: Contigency Ranking in 75-bus system based on voltage deviation

rank	line no.	from bus	to bus	PI_V
1	111	23	29	1098.740
2	69	74	41	1096.800
3	39	17	23	1093.640
4	64	35	36	806.989
5	78	41	42	791.662
6	38	17	19	788.417
7	56	54	63	782.442
8	57	59	39	394.424
9	66	19	36	201.830

Table 2.18: Contigency Ranking in 75-bus system based on stability margin

rank	line no.	from bus	to bus	PI_L
1	111	23	29	84.506
2	78	41	42	67.854
3	39	17	23	58.686
4	64	35	36	41.907
5	38	17	19	40.039
6	69	74	41	21.992

Table 2.19: Contigency Ranking in 75-bus system based on overall index

rank	line no.	from bus	to bus	PI_A
1	111	23	29	1682.320
2	69	74	41	1433.700
3	78	41	42	1096.650
4	39	17	23	1093.340
5	38	17	19	737.723
6	64	35	36	690.251
7	66	19	36	517.188

(i) Voltages predicted by the proposed FLN based ANN models were quite accurate and can be used for contingency selection. The average error in all the test cases were within 1%.

(ii) The ANN based voltage prediction method is extremely fast. The maximum CPU time in all the three systems was computed on HP9000/735 computer system. It was found to be 0.24 seconds.

(iii) Fuzzy logic can be effectively used for obtaining the performance indices (PIs) for various contingencies. It is free from misranking effect as it does not depend on the choice of weighting factors.

(iv) The contingency ranking changes when the PI is calculated based on the voltage stability margin as compared to those obtained by using only the bus voltage deviations.

Chapter 3

Estimation of Closest Saddle Node Bifurcation using ANN Based Analog Simulation

3.1 Introduction

In most of the research work the voltage stability has been considered as static phenomenon. This is due to slow variation of voltage over a long time observed in most of the incidents [220] until it reaches near to maximum loadability point where it decreases rapidly leading to the voltage collapse. This phenomenon can be described [90] as loss of stability when a stable equilibrium point disappears in saddle node bifurcation.

To predict the stability margin with respect to saddle node bifurcation, extensive works exist which can be broadly classified as *direct* or *indirect* methods. In *direct method*, stability margin is defined in term of the additional demand that will take the system to the stability boundary. This measure may correspond to the L_1 norm of the distance. The Euclidean distance or L_2 norm can also be used to measure the minimum distance to the boundary of the feasibility region as described in [137, 174].

In the *indirect methods*, some indices are generated which measure the stability margin such as reactive power sensitivity to bus voltage [108, 176], Voltage Collapse Proximity Indicator (VCPI) derived from the sensitivity of total reactive power generation to real or reactive load increase [45, 143], Voltage Instability Proximity Indicator (VIPI) based on multiple load flow solutions [40, 107], minimum singular value, minimum eigenvalue

or condition number of power flow Jacobian [83,84,94,157,187,245]. These methods, in general, require large computing time as they involve several power flow computations [250]. In some of the applications such as contingency selection and analysis as described in chapter-2, where voltage stability margin is required to be computed fast, the above existing methods may not be suitable.

To enhance the speed in determination of the stability margin with respect to the maximum loadability or the saddle node bifurcation point, a novel method employing analog simulation based Neural Network [74] has been suggested in this chapter. The problem of determining the saddle node bifurcation has been formulated as a nonlinear optimization problem and 'SPICE' program has been used to realize the analog circuitry of the ANN model. The proposed method has been tested on two sample systems.

3.2 Saddle Node Bifurcation

Bifurcation in a dynamical system refers to the onset of a qualitative change in its behavior. The qualitative change in the behavior of a dynamical system may take place when new fixed (equilibrium) points or periodic orbits are generated or existing ones disappear and/or there is change in their stability type. The bifurcation is said to be *local* when it emerges out of fixed point (equilibrium point). It can be determined by observing the behavior of the model in a small neighborhood of an equilibrium. The *global* bifurcation emerges out of periodic orbit and characterized by a qualitative change in the phase portrait not restricted to small neighborhood of an equilibrium. The global bifurcations are determined by nonlinear analysis.

Examples of local bifurcations are saddle node bifurcation (SNB) and Hopf bifurcation (HB). Period doubling bifurcation, cyclic fold bifurcation, are few examples of global bifurcation. In the above list saddle node bifurcation is a *static* bifurcation whereas all others are *dynamic* bifurcations.

To describe the saddle node bifurcation consider a simple dynamical equation [80].

$$\dot{x} = f(x, \mu) = \mu - x^2, \quad x \in R^1 \; \mu \in R^1 \tag{3.1}$$

The equilibrium points of this system can be obtained by equating the time derivative term to zero i.e.

$$0 = \mu - x^2 \tag{3.2}$$

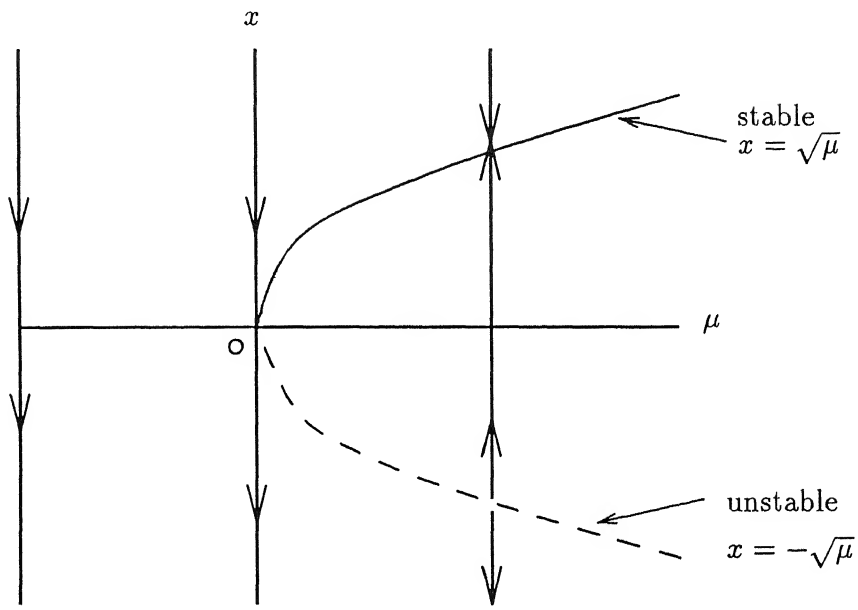

Figure 3.1: Saddle-node Bifurcation

This represents a parabola in $\mu - x$ plane as shown in Figure 3.1. For$\mu < 0$ equation (3.1) has no equilibrium point or equation (3.2) has no real solution. For $\mu > 0$, there exist two equilibrium points one of them being stable and the other is unstable. At $\mu = 0$, the associated matrix is singular. This particular type of bifurcation where on one side of a parameter value there is no equilibrium point and on the other side there exist two equilibrium points is referred to as a saddle node bifurcation.

In general at the saddle node bifurcation point (x^*, λ^*) of a dynamical system

$\dot{x} = g(x, \lambda) \qquad g : R^{n+p} \rightarrow R^n$

following conditions should be satisfied

- The Jacobian matrix $D_x g(x^*, \lambda^*)$ containing first partial derivative of g with respect to state variables x has a unique simple zero eigenvalue with right eigenvector v_* and left eigenvector w_* .
- $w_*.(D_\lambda g(X^*, \lambda^*)) \neq 0$
- $w_*.(D^2_{x^*} g(v_*, v_*)) \neq 0$, where $D^2_{x^*} g(v^*, v^*)$ denotes a Hessian Matrix.

3.3 Prediction of closest saddle node bifurcation

The saddle node bifurcation in power system (static) model occurs when the number of solutions to the load flow equations changes under loading parameter variation. The singularity of load flow Jacobian has been popularly used to identify saddle node bifurcation (SNB).

The static model of a power system can be described by equation (3.3)

$$0 = f(x, \lambda) \qquad g : R^{n+p} \rightarrow R^n \tag{3.3}$$

where $x \in R^n$ is the system state vector which includes bus voltage phasors and $\lambda \in R^p$ is a parameter vector of real and reactive power demand at buses. In the present study, voltage phasors have been considered in rectangular co-ordinates.

Consider an operating point λ_p^0 in R^p dimensional load parameter space which includes active and reactive power demand of the system. A set of critical loading at which the operating equilibrium of power system disappears in saddle node bifurcation [105] forms a hypersurface (say Σ) in parameter space. The dimension of the curved hypersurface Σ of critical loading is p-1. The closest bifurcation point λ_p^* on hypersurface of critical loading corresponds to maximum loadability or saddle node bifurcation. Stability margin with respect to saddle node bifurcation is the minimum distance between operating point λ_p^0 and λ_p^* on hypersurface Σ of critical loading. The point λ_p^* on Σ, closest to λ_p^0 in Euclidean sense, is called the closest saddle node bifurcation point.

The saddle node bifurcation will occur when stable equilibrium point coalesce with a nearby unstable equilibrium and disappears causing the system to loose stability. A saddle node bifurcation point of the power flow equation (3.3) can be defined at (x, λ) if the following conditions are satisfied.

- $g(x, \lambda) = 0.0$
- $\tilde{A} = D_x g(x, \lambda)$ is a rank (n-1) deficient matrix i.e. $\tilde{A}$ is singular and one of the eigenvalues is zero.

  where $\tilde{A}$ is the Jacobian containing derivatives of $g(x, \lambda)$ with respect to x.

A direct method computes saddle node bifurcation point (x, λ) by solving the following set of non-linear equations [246].

$$g(x, \lambda) = 0.0 \tag{3.4}$$

$$\tilde{A}v = 0 \ \ or \ \ w\tilde{A} = 0 \tag{3.5}$$

$$\|v\| \neq 0 \ \ or \ \ \|w\| \neq 0 \tag{3.6}$$

where $v(w)$ is the right(left) eigenvector associated with the zero eigenvalue of $\tilde{A}$.

The closest saddle node bifurcation point λ_p^* from an operating point λ_p^0 can be estimated by minimizing Euclidean norm of distance between λ_p^0 and λ_p^* (on hypersurface Σ). It can be formulated as an optimization problem to minimize an objective function

$$f \ = \ \|\lambda_p^0 - \lambda_p^*\|^2$$

subject to equality constraints given by equations (3.4) and (3.5) and inequality constraints given by equation (3.6). To solve this optimization problem, analog simulation based ANN, as described in subsequent section 3.4, has been used in the present work.

3.4 Non-linear programming using analog simulation

3.4.1 General

Non-linear programming is widely encountered in any engineering problem. The essence of any non-linear programming problem is to find the extremum of a non-linear objective function subject to certain constraints. There have been many numerical algorithms developed for solving non-linear programming using digital computers. The main disadvantage of the algorithmic methods is that they generally converge slowly, i.e., computational time could be excessive even for low-dimensional problems. Moreover, for certain non-linearities, they may offer convergence difficulty.

In solving non-linear programming problems one has the alternative of using a dedicated electrical circuit which simulates the objective and constraint functions. In 1984, Chua and Lin [47] developed a canonical non-linear programming circuit. This circuit description, at that time, was not based on artificial neural network. After Tank and Hopfield suggested an ANN based linear programming circuit [59], Kennedy and Chua [74] proved that the Tank and Hopfield linear programming ANN circuit was a special case of Chua and Lin's non-linear programming circuit [47]. Further, Kenedy and Chua [74] improved

the canonical circuit to make it suitable for Neural Network implementation. They utilized the fact that the solution of any non-linear programming problem is analogous to the operating point of reciprocal circuit with extremum of some potential function under certain constraints in non-linear circuit theory. Hence, if a reciprocal resistive non-linear circuit could be synthesised whose potential corresponds to a given objective function to be minimized and whose element constitute relations which impose the same equality and inequality constraints; the solution of this circuit is precisely the solution of the non-linear programming problem.

3.4.2 Non-linear Programming Circuit

Consider the following general non-linear programming problem which minimizes a scalar function

$$f(v_1, v_2, \ldots, v_p) \tag{3.7}$$

subject to the constraints

$$\begin{aligned} g_1(v_1, v_2, \ldots, v_p) &\geq 0 \\ g_2(v_1, v_2, \ldots, v_p) &\geq 0 \\ &\cdots \\ g_q(v_1, v_2, \ldots, v_p) &\geq 0 \end{aligned} \tag{3.8}$$

where p and q are two independent integers. Using La Grange multiplier approach to solve this problem is to define a La Grange function

$$L(v, \lambda) = f(v) + \sum_{j=1}^{q} \lambda_j g_j(v) \tag{3.9}$$

where the real constants $\lambda_1, \lambda_2, \ldots, \lambda_q$ are the La Grange multipliers. If the program has solution $v = v^*$ i.e.,

$$min\, f(v) = f(v^*)$$

and

$$g_i(v^*) \geq 0 \quad i = 1, ..., q$$

then the Kuhn-Tucker conditions defined by equations (3.11) to (3.13) must be satisfied.

$$\frac{\partial f(v^*)}{\partial v_i} + \sum_{j=1}^{q} \lambda_j^* \frac{\partial g_j(v^*)}{\partial v_i} = 0 \qquad i = 1, 2, \ldots, p \tag{3.10}$$

$$g_i(v^*) \geq 0 \qquad j = 1, 2, \ldots, q \tag{3.11}$$

$$\lambda_j \leq 0 \qquad j = 1, 2, \ldots, q \tag{3.12}$$

$$\lambda_j^* \cdot g_j(v^*) = 0 \qquad j = 1, 2, \ldots, q \tag{3.13}$$

It has been assumed that the non-linear programming problem has the following properties:

(1) At least one (and may be more) solution to the problem exists. Consequently, the optimization function described by equation (3.7) is bounded over which the constraints are to be satisfied.

(2) f(.) and g(.) are continuous and all first and second order partial derivatives of f(.) and g(.) exist and are continuous.

The corresponding equivalent *canonical non-linear programming circuit* is shown in the Figure 3.2. This figure implements the Kuhn-Tucker conditions mentioned above [36]. Here each variable v_i represents the node voltage V_i and each La Grange multiplier λ_j is represented by reversed diode current $i_j (j = 1, \ldots, q)$.

The circuit elements of the Figure 3.2 are represented in its equivalent form as follows:

Diode:

The diodes represented in the Figure 3.2 are the ideal diodes. However, it is difficult to simulate the ideal diode characteristics in some of the standard packages like SPICE . The equivalent circuit for diode which is represented in the canonical circuit corresponds to Figure 3.3. This contains a P-N diode connected in feed back with an ideal operational amplifier (OPAMP).

The v_d - i_d characteristics of an ideal diode is shown in Figure 3.4. This characteristics can be represented by following equations,

$$i_d = 0 \ , \ V_d \leq 0 \tag{3.14}$$

$$i_d \geq 0 \ , \ V_d = 0 \tag{3.15}$$

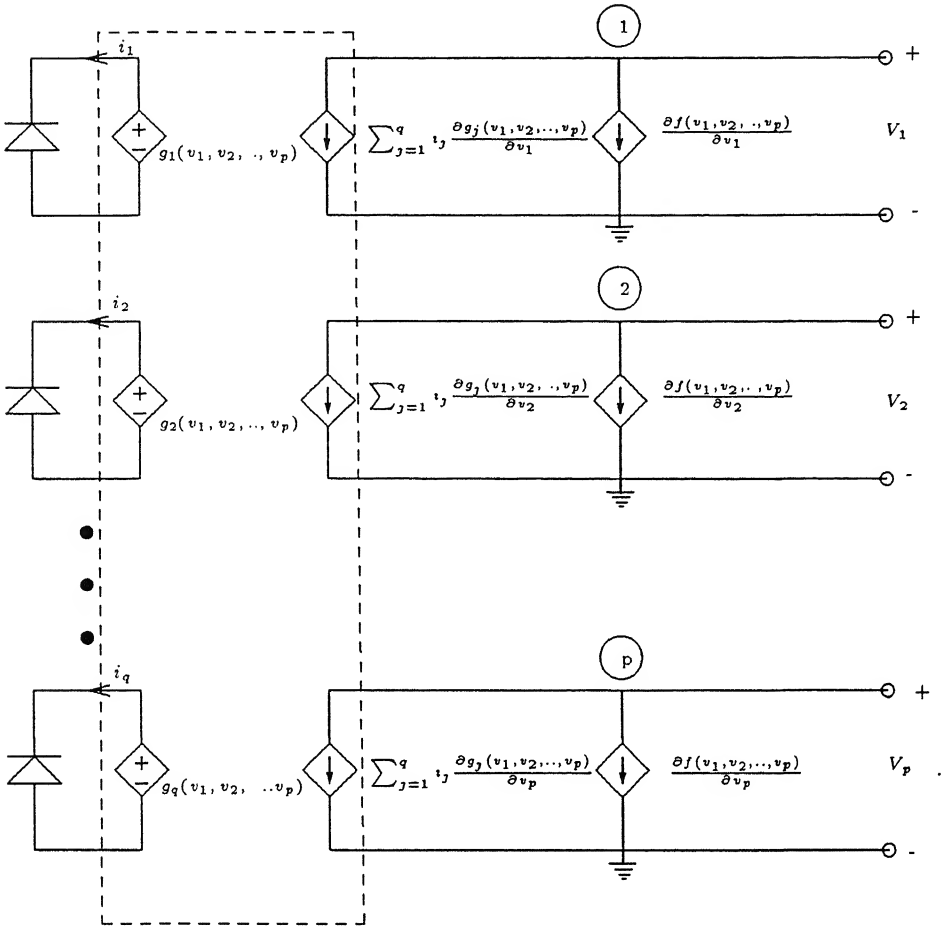

Figure 3.2: The ideal simulating circuit for general non-linear programming

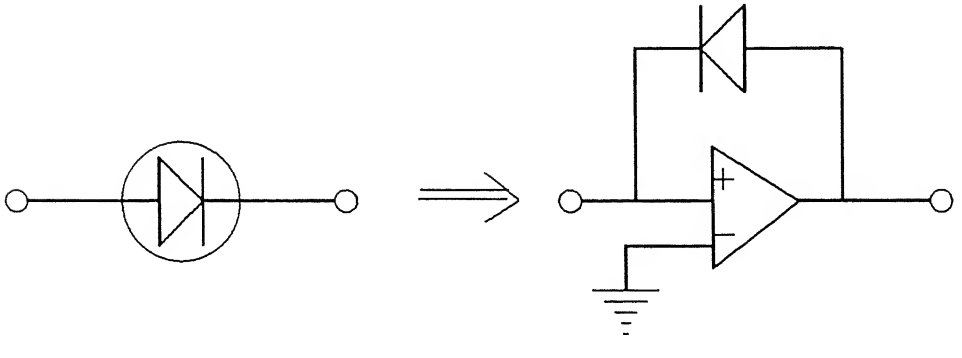

Figure 3.3: Diode equivalent circuit

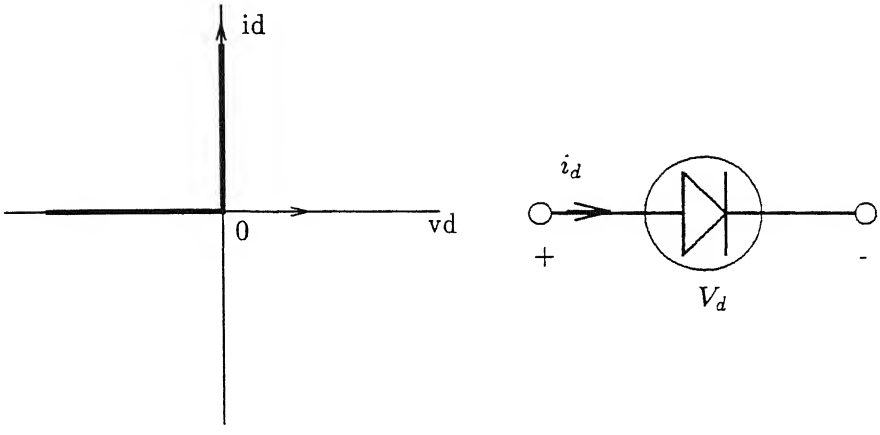

Figure 3.4: Ideal diode charateristics

$$V_i i_d = 0 \tag{3.16}$$

Voltage controlled voltage source: (VCVS)

Each diamond shaped symbol enclosing a + and - sign, represented in Figure 3.2, indicates non-linear voltage controlled source whose terminal voltage depends on the node voltages $V_1, V_2, \ldots, V_p$ in accordance with the prescribed non-linear constraint functions $g_i(v_1, v_2, \ldots, v_p)$.

Voltage controlled current source: (VCCS)

Each diamond shaped symbol (in the middle column of Figure 3.2) enclosing the arrowhead is a controlled current source whose terminal current depends on both reversed diode currents $i_1, i_2, \ldots, i_q$ and the node voltages $V_1, V_2, \ldots, V_p$ in accordance with the function,

$$\sum_{j=1}^{q} i_j \frac{\partial g_j(v_1, v_2, .., v_p)}{\partial v_i}$$

Each diamond shaped symbol (on the right in Figure 3.2) enclosing the arrowhead is a controlled current source whose terminal current depends on the node voltages $V_1, V_2, \ldots, V_p$ in accordance with the function

$$\frac{\partial f(v_1, v_2, .., v_p)}{\partial v_i}$$

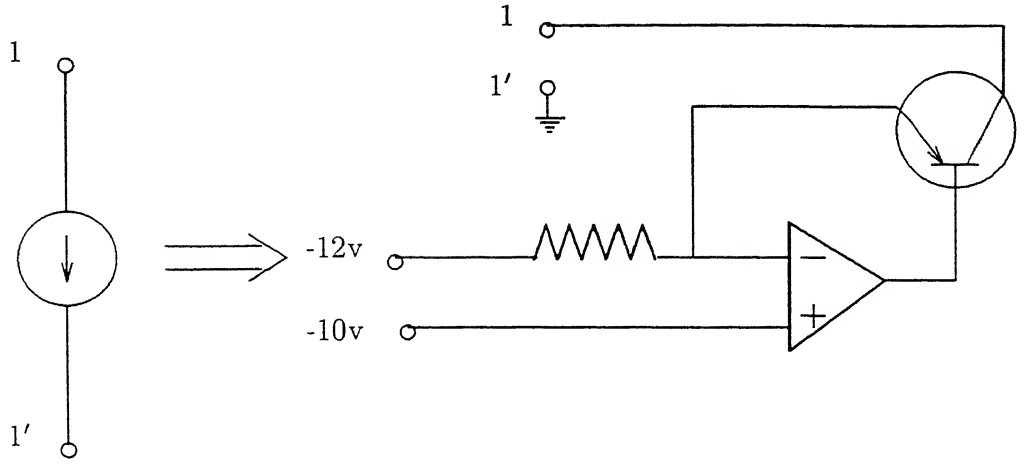

Figure 3.5: Independent current source

Independent Current Source

This is represented as a circle enclosing an arrowhead. This element simulates the corresponding constants in the objective function. Its equivalent circuit used in any circuit simulation program has been shown on right hand side of the Figure 3.5.

In order to satisfy the functional inequality constraints, multiport (p+q port) D.C. transformer [31] is required as shown within dotted lines in Figure 3.2.

3.4.3 Multiport D.C. Transformer

An $l+m$ port transformer is a multiport resistive element [31] described by the following relation.

$$\begin{bmatrix} e_i \\ i_j \end{bmatrix} = \begin{bmatrix} 0 & A^T \\ -A & 0 \end{bmatrix} \begin{bmatrix} i_i \\ e_j \end{bmatrix} \tag{3.17}$$

where

$e_i = [e_{i_1}, e_{i_2}, e_{i_3}, \ldots, e_{i_l}]$

$e_j = [e_{j_1}, e_{j_2}, e_{j_3}, \ldots, e_{j_m}]$

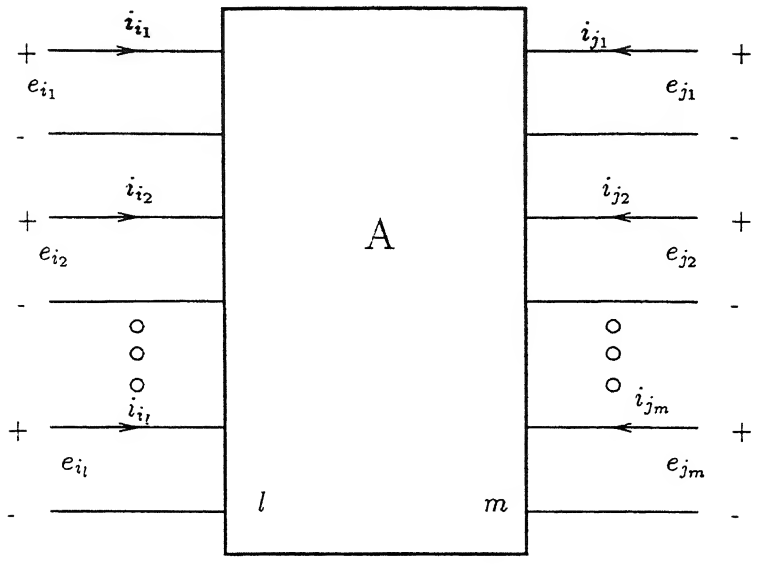

Figure 3.6: Simplified notation of (l+m) port transformer

$$i_i = [i_{i_1}, i_{i_2}, i_{i_3}, \ldots, e_{i_l}]$$

$$i_j = [i_{j_1}, i_{j_2}, i_{j_3}, \ldots, e_{j_m}]$$

$$A = \begin{bmatrix} a_{11} & a_{12} & \ldots & a_{1l} \\ a_{21} & a_{22} & \ldots & a_{2l} \\ \vdots & \vdots & & \\ a_{m1} & a_{m2} & \ldots & a_{ml} \end{bmatrix}_{m,l}$$

A is a real matrix called the *Turns Ratio Matrix.* Suffix i stands for input quantities of the transformer and j for the output quantities. Multiport transformers are built using operational amplifiers. A simplified notation of $(l + m)$ port transformer using equation (3.17) can be shown as in Figure 3.6 or in vector form as in Figure 3.7.

The multiport transformer circuit can be realized by two approaches:

(i) *Direct Approach* in which the equation (3.17) is realized directly.

(ii) *Scattering Matrix Approach* which realizes the scattering matrix of the equation (3.17) instead of realizing the equation directly.

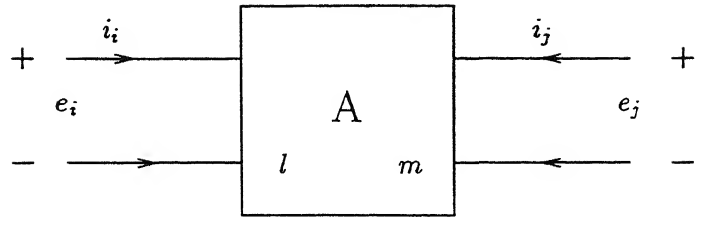

Figure 3.7: Vector notation of (1+m) port transformer

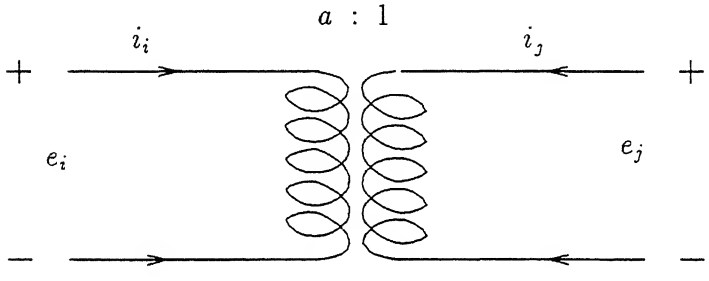

Figure 3.8: A (1+1)- port transformer

The direct approach has been used in realizing the multiport transformer in the present work as described below:

Consider a traditional (1+1) port transformer shown in Figure 3.8, whose constitutive relations are represented by equation (3.18),

$$\begin{bmatrix} e_i \\ i_j \end{bmatrix} = \begin{bmatrix} 0 & a \\ -a & 0 \end{bmatrix} \begin{bmatrix} i_i \\ e_j \end{bmatrix} \tag{3.18}$$

where a is real number.

The figure 3.9 realizes these relations for any $a \geq 0$. For the sake of analysis consider the circuit into two parts. The lower part of the circuit shown in Figure 3.9 satisfies the voltage constraint $e_i = ae_j$ and the upper part satisfies the current constraint $i_j = -ai_i$. To realize this the ideal model of the operational amplifier can be used which has been represented in figure 3.10.

The right portion of the Figure 3.10(b) is a norator, whose constitutive relation consists of every point in a v-i plane. The left portion is a nullator described by $e = 0$, $i = 0$.

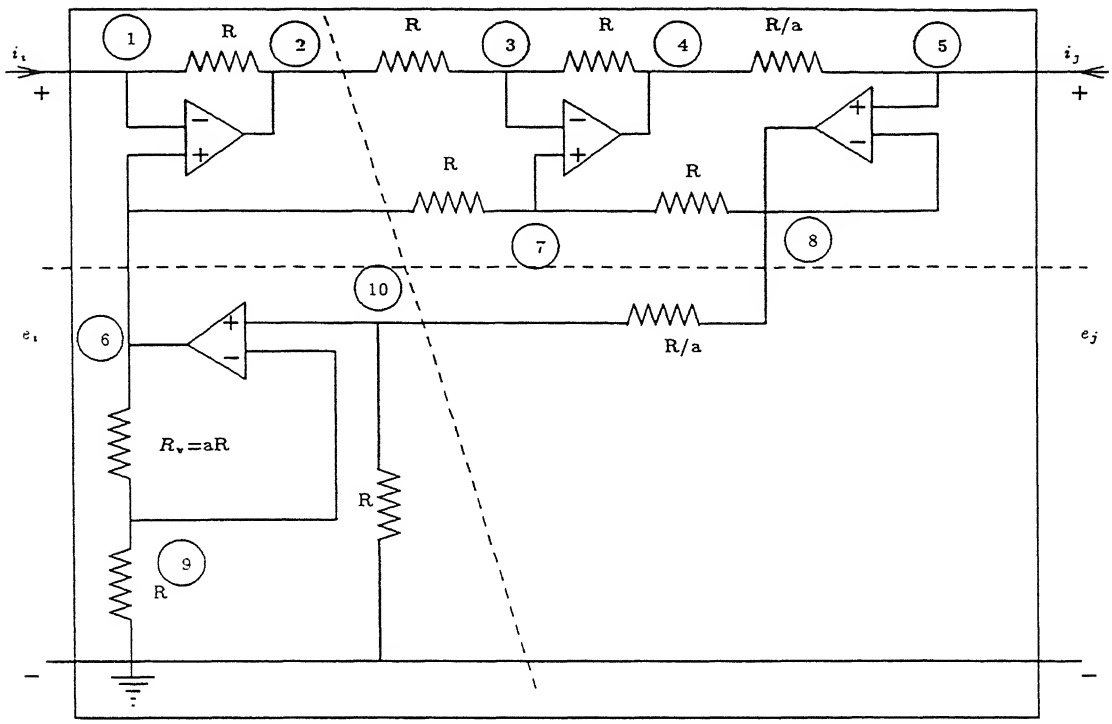

Figure 3.9: Circuit realizing (1 + 1)-port transformer

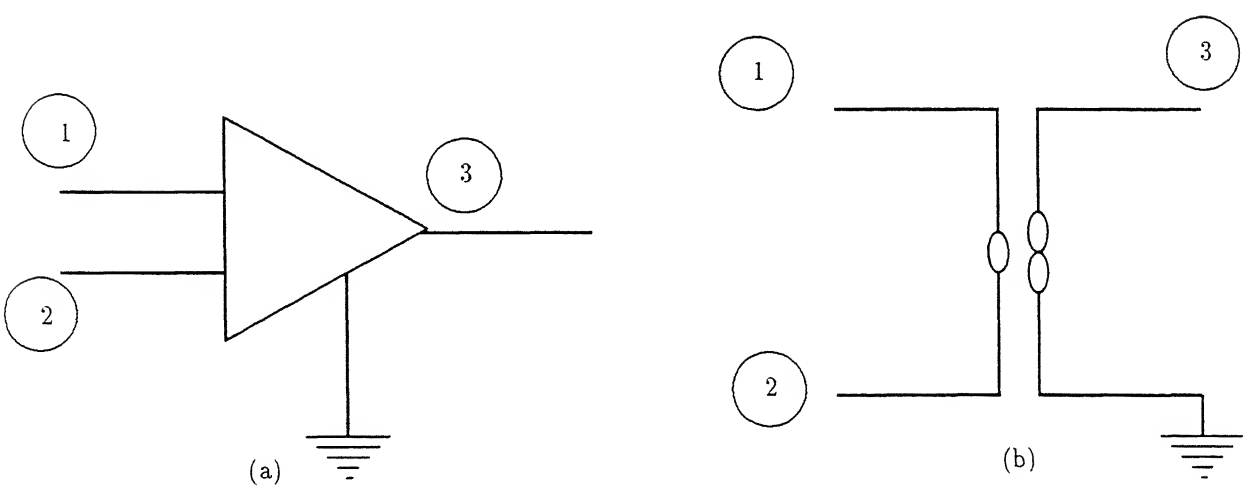

Figure 3.10: Operational amplifier with its ideal model

The equations corresponding to the lower part of the Figure 3.9 are

$$V_6 = e_i, \qquad V_8 = e_j, \qquad V_9 = V_{10}$$

$$V_9 = \frac{V_6}{a+1} \qquad V_{10} = \frac{aV_8}{a+1}$$

Therefore.

$$e_i = ae_j \tag{3.19}$$

The equations corresponding to upper part of the circuit shown in Figure 3.9 are

$$V_2 = e_i - R \cdot i_j, \qquad V_3 = V_7 \qquad V_3 = \frac{V_2 + V_4}{2}$$

$$V_4 = e_j - \frac{R_{ij}}{a}, \qquad V_7 = \frac{e_i + e_j}{2}$$

which is equivalent to

$$i_j = -ai, \tag{3.20}$$

On similar lines, $(1 + m)$-port transformer can be realized using the equation (3.21)

$$\begin{bmatrix} e_i \\ i_{j_1} \\ i_{j_2} \\ \vdots \\ i_{j_m} \end{bmatrix} = \begin{bmatrix} 0 & a_{11} & a_{21} & \dots & a_{m1} \\ -a_{11} & 0 & 0 & \dots & 0 \\ -a_{21} & 0 & 0 & \dots & 0 \\ \vdots & \vdots & \vdots & & \vdots \\ -a_{m1} & 0 & 0 & \dots & 0 \end{bmatrix} \begin{bmatrix} i_i \\ e_{j_1} \\ e_{j_2} \\ \vdots \\ e_{j_m} \end{bmatrix} \tag{3.21}$$

To form a $(l + m)$ port transformer, one should connect l $(1 + m)$ port transformers together. When they are connected in parallel across the m-port the whole network realizes equation (3.17).

3.4.4 An Example Problem

Consider an optimization problem to minimize a function

$$\phi(v_1, v_2, v_3) = v_1 + 5v_1^2 + 4v_2^2 + 4v_3^2 - 6v_1v_2 - 6v_2V_3 \tag{3.22}$$

subject to inequality constraints

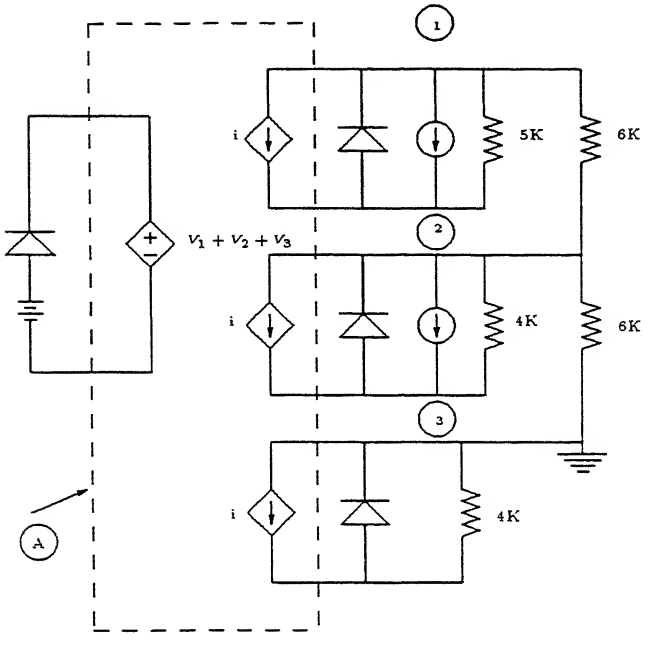

Figure 3.11: Cannonical circuit for the example problem

$$v_1 + v_2 + v_3 \geq 1 \tag{3.23}$$

$$v_1, v_2, v_3 \geq 0 \tag{3.24}$$

The Cannonical circuit representation for the above problem as explained in subsection 3.4.2 can be shown as in Figure 3.11. This optimization problem involves 3 variables v_1, v_2, & v_3 and one functional inequality constraint given by equation (3.23). Hence a (1+3) port dc transformer is required as shown by the dotted portion (A) in Figure 3.11.

The values of the variables v_1, v_2, & v_3 are obtained by applying KCL at nodes (1), (2) & (3) respectively in Figure 3.11.

The circuit implementation for the above mentioned problem using multiport transformer can be obtained as shown in Figure 3.12. The details of the multiport transformer is given in sub-section 3.4.3.

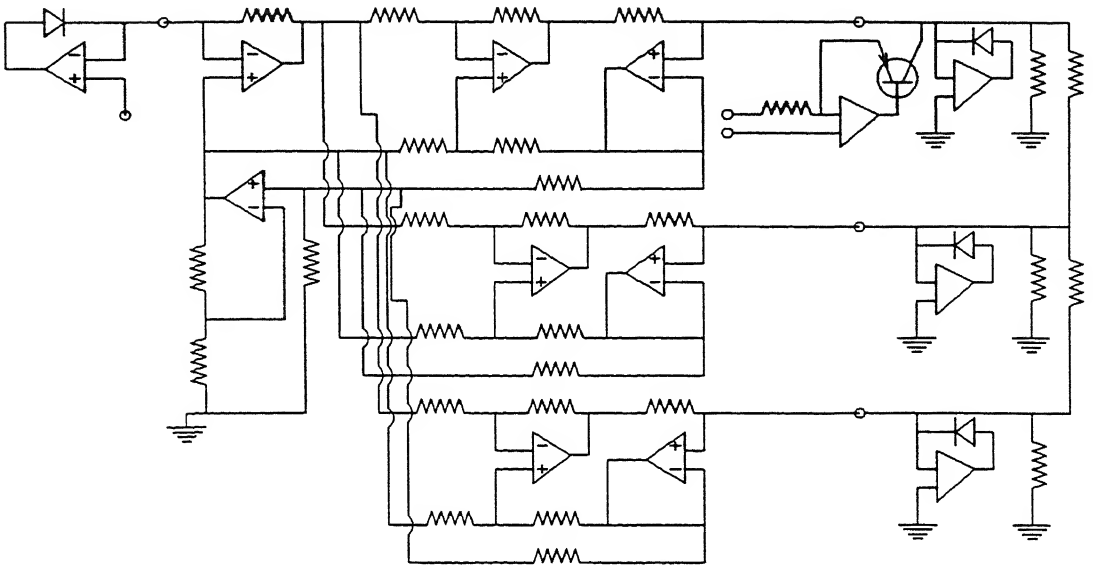

Figure 3.12: The circuit for the example problem

The circuit presented in Figure 3.12 was implemented using circuit simulation program SPICE version 3. The OPAMP's shown in the Figure 3.12 were represented as a voltage controlled current source with high gain (1 Mega ohm)

The values of v_1, v_2. & v_3 were obtained by carrying out dc analysis. The example problem described by equations (3.22) to (3.24) were also solved using a conventional method based on sequential quadratic programming. The values of variables v_1, v_2, & v_3 obtained using the proposed analog simulation method and the conventional optimization method, along with the CPU time taken by these methods are shown in Table 3.1.

3.5 Sample System Studies

The proposed method to estimate the closest saddle node bifurcation point in load parameter space using ANN based analog simulation has been tested on 3-bus and 9-bus systems. For simulation of the analog circuitry realizing the optimization based formulation described in sections 3.3 & 3.4 for estimating the closest saddle node bifurcation an available version-3 of SPICE package was utilized.

Appendix-A describes the data for the 3-bus system. The parameter considered as variables in this system were the loading at bus-2 ($P_L + Q_L$) and real power outputs of

Table 3.1: Results of the sample example

Method	Optimal seting of variable			Objective function	CPU time in msec
	v_1	v_2	v_3		
Analog simulation method	0.1908	0.4454	0.3635	0.4852	0.2
Conventional optimization method	0.1912	0.4453	0.3634	0.4853	3.8

Table 3.2: Parameters of 3-bus system (in p.u.)

Parameter	Initial	At saddle node Bifurcation	
		with S.Q.P.	Analog simulation
P_{G_1}	1.25	1.3361	1.3412
P_{G_2}	1.25	5.1210	5.1235
P_L	2.5	6.4571	6.4647
Q_L	1.0	1.5084	1.5103
Margin (M)	-	5.5363	5.5435

generators at buses 1 and 3. The values of these parameters obtained at closest saddle node bifurcation using sequential quadratic programming (SQP) as well as the proposed analog simulation method along with base case values of these variables are given in Table 3.2. To confirm the existence of the saddle node bifurcation obtained by the two methods, minimum eigenvalues were determined at base case and the predicted saddle node bifurcation points. The minimum eigenvalue at base case was 9.2012 and was of the order of 10^{-6} at saddle node points determined by either the sequential quadratic programming or the proposed method. Thus at the predicted saddle node bifurcation points, the minimum eigenvalues are quite close to zero. The stability margin were also computed as the Euclidean distance between the base case loading parameters and the values (λ) at the saddle node bifurcation (λ^*) point defined as $M = \|\lambda - \lambda^*\|$.

The margin values, computed by the two methods are comparable which are given in Table 3.2.

Table 3.3: Parameters of 9-bus system (in p.u.)

Parameter	Initial	At saddle node Bifurcation	
		with S.Q.P.	Analog simulation
P_{L_5}	1.2500	1.9844	1.9851
Q_{L_5}	0.5000	2.7023	2.7028
P_{L_6}	0.9000	1.0896	1.0891
Q_{L_6}	0.3000	1.1705	1.1708
P_{L_8}	1.0000	1.1307	1.1312
Q_{L_8}	0.3500	1.4580	1.4581
Margin (M)	- -	2.71571	2.72614

Appendix -B presents the 9-bus system. The parameters considered as variables were the loadings at bus-5 (P_{L_5} + j Q_{L_5}), bus-6 (P_{L_6} + jQ_{L_6}) and bus-8 (P_{L_8} + jQ_{L_8}). The value of these parameters obtained at saddle node bifurcation using sequential quadratic programming and the proposed method along with the base case values of the variables are given in Table 3.3. To justify the saddle node bifurcation obtained with the two methods, minimum eigenvalue was computed at base case as well as the saddle node bifurcation points determined by sequential quadratic programming and the proposed analog simulation methods. The value was 6.8267 at the base case and of the order of 10^{-5} at saddle node bifurcation points computed by the both methods. The stability margins (M) computed using bifurcation points computed by the proposed method and SQP are also presented in Table 3.3. At the saddle node bifurcation point the eigenvalues are close to zero and the margins are nearly equal obtained with both the methods.

Table 3.4 compares the CPU time required by the SQP and the proposed method to determine the saddle node bifurcation point. CPU time required by the analog simulation method is much less as compared to the Sequential Quadratic Programming method for both the test systems.

3.6 Conclusion

This chapter has presented a new approach utilizing an analog simulation based ANN method for determining the closest saddle node bifurcation point. The results obtained

Table 3.4: The comparison of CPU time

System	CPU time required in sec.	
	S.Q.P.	Analog simulation
3-bus	2.24	0.28
9-bus	15.01	0.37

on two sample systems were compared with sequential quadratic programming (SQP) method. The studies conducted in this chapter reveal the following.

(i) The parameter values obtained by the proposed method and the SQP method are comparable. Stability margin defined as the Euclidean distance from base case operating point to the predicted saddle node bifurcation point by the two methods are almost equal.

(ii) The proposed method can be effectively used for real time prediction of the closest saddle node bifurcation point, as the CPU time required is much less compared to the SQP method.

(iii) The minimum eigenvalue of the load flow Jacobian at the predicted saddle node bifurcation point is close to zero obtained either by the proposed method or the SQP method.

The results obtained in this chapter were limited to smaller systems mainly due to the limitation of the available SPICE (version-3) package. However, the proposed approach is quite modular in nature and can be easily extended to large size systems.

Chapter 4

Estimation of Closest Hopf Bifurcation

4.1 Introduction

Today's stressed power system networks provided with various types of controllers interacting with each other, exhibit highly non-linear dynamical behavior. This has necessitated a close examination of different types of bifurcations that may take place and lead to new types of instabilities in the system. In the phenomenon of voltage instability leading to collapse [233], both static and dynamic factors are involved. Saddle-node and Hopf bifurcations have been recognized as the reasons behind instability of the system [43,90,99]. Saddle-node bifurcation is a static bifurcation as described in chapter 3 while Hopf bifurcation is a generic case of dynamic bifurcation which leads to oscillatory instability. It has been shown that even some simplified power system models become oscillatory unstable in Hopf bifurcation before the saddle-node bifurcation occurs [160, 164], i.e., before the system reaches its maximum loadability limit. However, very little attention has been focused on predicting stability margin with respect to Hopf bifurcation. Dobson et al. [145] derived the first order factors showing sensitivity of system parameters with respect to the Hopf bifurcation. However, no proper method has been suggested to predict numeric values of stability margin with respect to the Hopf bifurcation. For secure operation of the system, it is essential to know how much margin is available with respect to the Hopf bifurcation which may probably occur before the saddle node bifurcation.

In this chapter a new method based on an optimization technique has been propose

for estimating the minimum distance to Hopf bifurcation and tested on a simple single machine infinite bus system as well as multi machine 3-bus and 9-bus systems.

4.2 Hopf Bifurcation

In 1942, E. Hopf observed the bifurcation from an equilibrium point to a family of periodic solutions in non-linear systems of dimension greater than or equal to two. The Hopf bifurcation, attributed to his name, is characterized by emergence of periodic orbit (limit cycle) around an equilibrium point. The Hopf bifurcation point can be determined with the help of linearized analysis. At Hopf bifurcation, the number of equilibrium points are preserved but the Jacobian admits a pair of purely imaginary eigenvalues.

Consider a dynamical system modeled by a vector differential equation

$$\dot{x} = f(x,p) \quad x \in R^n, \quad p \in R^p \tag{4.1}$$

where x is the n-dimensional state vector and p is the parameter vector. When the parameter p is varied, the state vector x and eigenvalues of the corresponding Jacobian $\left[\frac{\partial f}{\partial x}\right]$ evaluated on this path changes. At the equilibrium point the left hand side derivative term $\dot{x}$ of equation (4.1) becomes zero and the static model of the system is given by

$$f(x,p) = 0 \tag{4.2}$$

Equation (4.2) specifies the position of the equilibrium point x as a function of p. The hypersurface defined by equation (4.2) is asymptotically stable if the eigenvalues of the Jacobian have negative real parts at that point. When a complex conjugate pair of eigenvalues reaches at the imaginary axis, by varying the parameter p, there exists a Hopf bifurcation (say at $p = p_0$ and $x = x_0$) as shown in Figure 4.1. At Hopf bifurcation, the following conditions should be satisfied.

- $f(x_0, p_0) = 0$
- The Jacobian matrix $\left[\frac{\partial f}{\partial x}\right]_{(x_0,p_0)}$ should have a simple pair of purely imaginary eigenvalues $\mu(p_0) = \pm j\omega_0$
- The rate of change of real part of the eigenvalues should be non zero $\frac{d(Re(\mu(p_0)))}{dp} \neq 0$

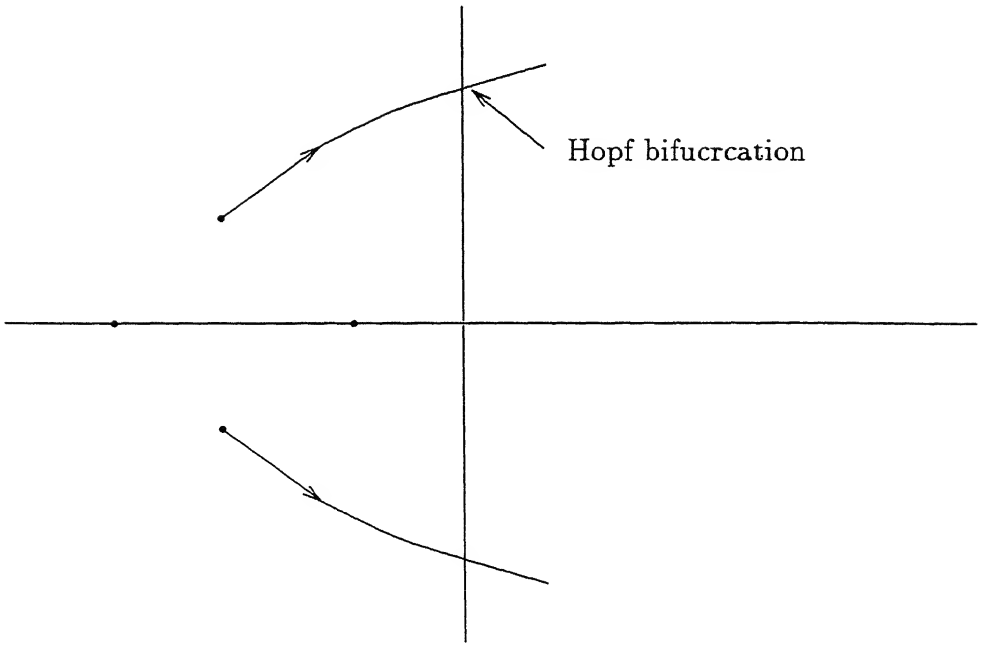

Figure 4.1: Locus of eigen values for Hopf Bifurcation

If the $\frac{d(Re(\mu(p_0)))}{dp} = 0$, it signifies the presence of a degenerate Hopf bifurcation. The above conditions imply that for $p \neq p_0$ the system has an equilibrium and a closed trajectory. A limit cycle exists near this equilibrium point on one side of the parameter values ($p > p_0$ or $p < p_0$). Limit cycle can be unstable or stable. Depending upon the nature of the limit cycle the Hopf bifurcation can be classified into two categories namely *subcritical* and *supercritical.*

The Hopf bifurcation is said to be subcritical when an unstable periodic orbit (u.p.o.) emerges around fixed or equilibrium point and shrinks into a stable equilibrium point (s.e.p.) as shown in Figure 4.2.

The Hopf bifurcation is said to be supercritical when a stable periodic orbit (s.p.o.) emerges around unstable equilibrium points (u.e.p.) as shown in Figure 4.3. The stable equilibrium becomes unstable and a stable periodic orbit is born at the supercritical Hopf bifurcation.

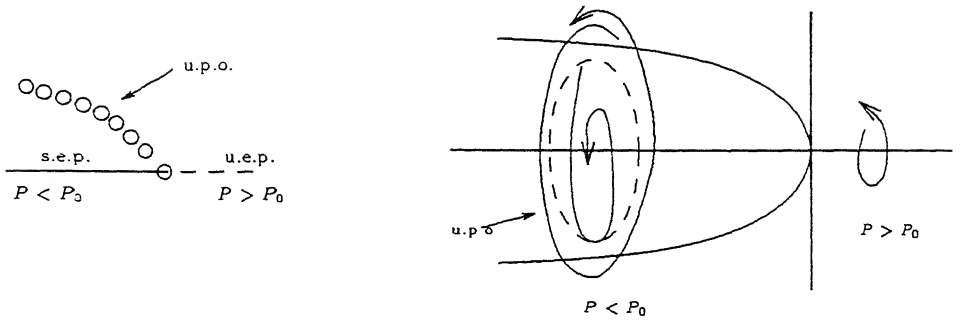

Figure 4.2: Subcritical Hopf bifurcation

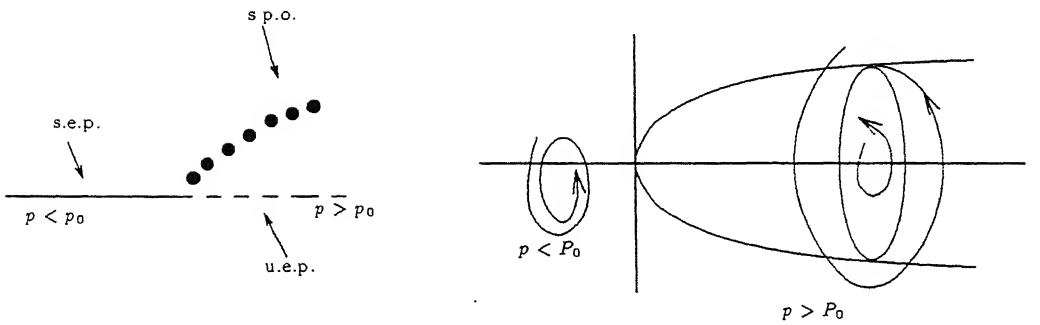

Figure 4.3: Supercritical Hopf bifurcation

4.3 Prediction of Closest Hopf Bifurcation

The power system model can be described by a set of differential and algebraic equations

$$\dot{x} = F(x, y, \lambda) \quad F : R^{n+m+p} \rightarrow R^n \tag{4.3}$$

$$0 = G(x, y, \lambda) \quad G : R^{n+m+p} \rightarrow R^m \tag{4.4}$$

where x is a vector of states governing dynamics of generators, loads and controls, y represents state variables of load flow equations and λ is composed of system parameters such as transmission line parameters λ_s and operating parameters λ_p (e.g. loads). In this study λ_s were assumed to be known and constant while operating parameters λ_p were considered as variables. Consider an operating point λ_p^0 in R^p dimensional load parameter space which includes active and reactive power demand of the system. A set of critical loadings at which Hopf bifurcation forms a hypersurface (say Σ) in a parameter space having dimension $p-1$ is a curved surface. Security margin to Hopf bifurcation is the minimum distance between operating point λ_p^* on hypersurface Σ of critical loading and λ_p^0. This security margin must be greater than or equal to some specified tolerance ϵ to operate the power system securely. If security margin is less than ϵ, some corrective action must be taken to increase this margin. The point λ_p^* on Σ, closest to λ_p^0 in euclidean sense, is called the closest Hopf bifurcation point. For this the line joining λ_p^0 and λ_p^* will be normal to the hypersurface Σ.

Hopf bifurcation occurs when the system has a nonhyperbolic equilibrium with a pair of purely imaginary eigenvalues and all other eigenvalues having non-zero real part and in addition the following transversality conditions are satisfied [213]

- reduced matrix $\tilde{A}$ defined in equation (4.5) linearized around the steady state equilibrium (x^*, y^*) has unique simple pair of only imaginary eigenvalues μ at λ_p^*.

$$\dot{x} = \tilde{A}x = (A - BD^{-1}C)x \tag{4.5}$$

- $\left.\frac{\partial Re(\mu)}{\partial \lambda}\right|_{\lambda_p = \lambda_p^*} \neq 0$

where

$$A = \left.\frac{\partial F}{\partial x}\right|_{(x^*,y^*)} \quad B = \left.\frac{\partial F}{\partial y}\right|_{(x^*,y^*)}$$

$$C = \left.\frac{\partial G}{\partial x}\right|_{(x^*,y^*)} \quad D = \left.\frac{\partial G}{\partial y}\right|_{(x^*,y^*)}$$

The basic equation for finding an eigenvalue of matrix $\tilde{A}$ is given by

$$\tilde{A}v = \mu v \tag{4.6}$$

where μ is the eigenvalue and v is the associated eigenvector.

At Hopf bifurcation, one pair of eigenvalues μ is a purely imaginary number say $j\mu_i$. The associated eigenvector v becomes a complex vector say $(v^r)^T + j(v^i)^T$. Substituting these in equation (4.5) and separating real and imaginary parts, we get

$$\tilde{A}v^r = -\mu_i(v^i) \tag{4.7}$$

$$\tilde{A}v^i = \mu_i(v^r) \tag{4.8}$$

Using equations (4.7) and (4.8), along with differential and algebraic equations of the system, point on Σ can be computed by solving following sets of nonlinear equations.

$$F(x, y, \lambda) = 0 \tag{4.9}$$

$$G(x, y, \lambda) = 0 \tag{4.10}$$

$$\tilde{A}v^r = -\mu_i(v^i) \tag{4.11}$$

$$\tilde{A}v^i = \mu_i(v^r) \tag{4.12}$$

$$\|v^r\| \neq 0 \tag{4.13}$$

$$\|v^i\| \neq 0 \tag{4.14}$$

The closest Hopf bifurcation point λ_p^* from an operating point λ_p^0 can be estimated by minimizing Euclidean norm of distance between λ_p^0 and λ_p^* (on hypersurface Σ). it can be formulated as an optimization problem to minimize an objective function

$$f = \|\lambda_p^0 - \lambda_p^*\|^2 \tag{4.15}$$

Subject to equality constraints represented by equations (4.9) to (4.12) and inequality constraints given by equations (4.13) and (4.14). To solve this optimization problem, sequential quadratic programming has been used in the present work.

4.4 Power System Model

The mathematical model of an m machine n bus system can be described by a set of differential equations representing the dynamics of the machines, exciters and other controls and algebraic equations representing the network relation. The models considered in the present study are briefly described below:

4.4.1 Generator Model

Fourth order model of generators [10, 42, 220] has been used in the present study as described below:

The dynamics of the synchronous generator can be represented by the following equations:

$$\frac{d\delta}{dt} = \omega \tag{4.16}$$

$$M_g \frac{d\omega}{dt} = P_M - P_{ge} - D\omega \tag{4.17}$$

where δ is generator's internal bus voltage angle, ω the speed deviation, M_g the moment of inertia of generator, P_{ge} the electrical power output of the generator, D the damping constant and P_M is the mechanical power input to the generator.

If the effect of saliency is considered, the changes in flux linkage of the field winding have to be accounted for along the d and q axes. Therefore, two more additional state equations (4.18) and (4.19) along with the swing equations (4.16) and (4.17) have to be considered.

$$T'_{do}\frac{dE'_q}{dt} = E_{fd} + (X_d - X'_d)I_d - E'_q \tag{4.18}$$

$$T'_{qo}\frac{dE'_d}{dt} = -(X_q - X'_q)I_q - E'_d \tag{4.19}$$

along with the voltage equation,

$$\begin{bmatrix} E'_q - V_q \\ E'_d - V_d \end{bmatrix} = \begin{bmatrix} R_a & -X'_d \\ X'_q & R_a \end{bmatrix} \begin{bmatrix} I_q \\ I_d \end{bmatrix} \tag{4.20}$$

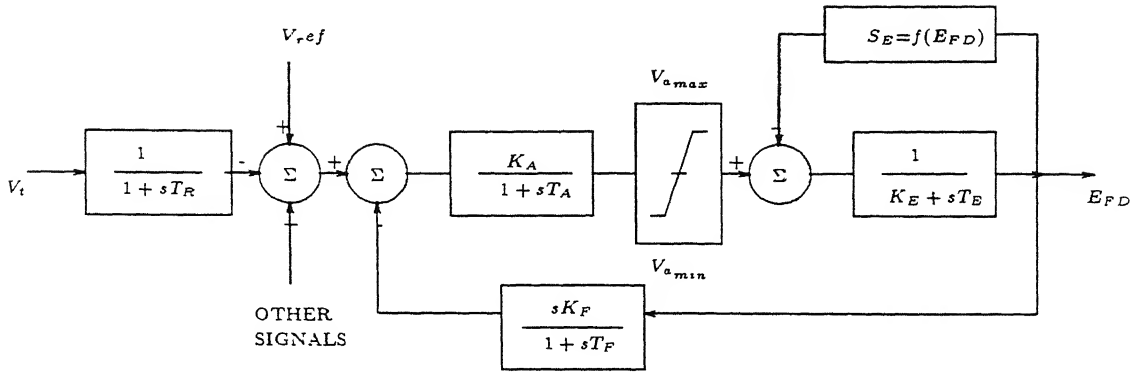

Figure 4.4: IEEE type–1 exciter

where, T'_{qo} is the q-axis open circuit transient time constant, R_a the armature resistance, X_q the steady state q-axis reactance, X'_q the q-axis transient reactance, E'_d the voltage behind X'_q, I_d & I_q the d and q axes armature current and V_d and V_q are the generator terminal voltage along d and q axes.

Further equations (4.18) to (4.20) can be converted into two equations (4.21) and (4.22) by neglecting saliency effect during transients (i.e. $X'_q = X'_q$) and the rotor resistance.

$$T'_{d_0}\dot{E}'_{q_i} = \frac{X_{d_i} - X'_{d_i}}{X'_{d_i}} V_i \cos(\theta_i - \delta_i) + E_{fd_i} - \frac{X_{d_i}}{X'_{d_i}} E'_{q_i} \tag{4.21}$$

$$T'_{q_0}\dot{E}'_{d_i} = -\frac{X_{q_i} - X'_{d_i}}{X'_{d_i}} V_i \sin(\theta_i - \delta_i) - \frac{X_{q_i}}{X'_{d_i}} E'_{d_i} \tag{4.22}$$

where $V_i\angle\theta_i$ is the terminal voltage of the synchronous generator. Equations (4.16), (4.17), (4.21) and (4.22) form the fourth order model of the synchronous generator.

4.4.2 Exciter Model

IEEE type-1 exciter [10, 42] as shown in Figure 4.4 has been considered in this study and equations governing the dynamics are given as follows:

$$T_E \frac{dE_{FD}}{dt} = V_a - (K_E + S_E)E_{FD} \tag{4.23}$$

$$T_F \frac{dV_f}{dt} = K_F E_{FD} - V_f \tag{4.24}$$

$$T_A \frac{dV_a}{dt} = K_A(V_{ref} - V_t - V_f) - V_a \tag{4.25}$$

and $V_a^{min} < V_a < V_a^{max}$

where $S_E = A_{ex} \exp(B_{ex} E_{FD})$ is a saturation function

V_a = Regulator amplifier output voltage

K_A = Regulator amplifier gain

T_A = Regulator amplifier time constant

V_f = Stabilizing circuit output voltage

K_F = Stabilizing circuit gain

T_F = Stabilizing circuit time constant

K_E = Exciter gain

T_E = Exciter time constant

V_{ref} = Reference voltage setting

V_t = Terminal voltage

4.4.3 Network Equations

The power flow equations governing the interaction between the terminals of generators and the system network can be given as:

$$0 = \frac{V_i}{X'_{d_i}}(E'_{q_i} \sin(\delta_i - \theta_i) - E'_{d_i} \cos(\delta_i - \theta_i)) - V_i \sum_{j=1}^{n} V_j(g_{ij} \cos\theta_{ij} + b_{ij} \sin\theta_{ij}) \tag{4.26}$$

$$0 = \frac{V_i}{X'_{d_i}}(E'_{q_i} \cos(\delta_i - \theta_i) + E'_{d_i} \sin(\delta_i - \theta_i) - V_i) - V_i \sum_{j=1}^{n} V_j(g_{ij} \sin\theta_{ij} - b_{ij} \cos\theta_{ij}) \tag{4.27}$$

for i = 1,..., m, where m is number of generators in the system. In addition following load flow equations should also be satisfied.

$$0 = P_{L_k} - V_k \sum_{j=1}^{n} V_j(g_{kj} \cos\theta_{kj} + b_{kj} \sin\theta_{kj}) \tag{4.28}$$

$$0 = Q_{L_k} - V_k \sum_{j=1}^{n} V_j(g_{kj} \sin\theta_{kj} - b_{kj} \cos\theta_{kj}) \tag{4.29}$$

for k = 1, ..., nl, where nl is the total number of load buses in the system (load buses numbered as 1, ..., nl), $(P_{L_k} + jQ_{L_k})$ is the complex load at a bus-k. Constant P, Q load model was considered in the present study. However, it can be easily extended to consider the voltage dependent and/or dynamic models of the loads.

4.5 Computational Procedure

To determine the closest Hopf bifurcation using sequential quadratic programming as described in section 4.3, it is necessary to provide initial estimate of variables. These initial conditions were obtained by following procedural steps.

(1) A load flow was run to solve equation (4.4) for a base case operating point λ_p^0 to obtain the values of load flow variables y.

(2) The solution of dynamic state variables x was obtained by solving set of nonlinear equations described by equation (4.3) with $\dot{x} = 0$ by using Gauss-Seidal iterative technique.

(3) Reduced Jacobian $\tilde{A}$ as defined in equation (4.6) was obtained for the values of x and y computed in steps 1 and 2.

(4) After computing the eigenvalues of matrix $\tilde{A}$, the eigenvalue λ having smallest real part and its imaginary part $\mu = imag(\lambda)$ was obtained.

(5) Vectors v^r and v^i representing the real and imaginary part of eigenvector corresponding to the eigenvalue λ, respectively, were calculated.

(6) To ensure conditions imposed by equations (4.13) and (4.14), i.e., $\|v^r\| \neq 0$ and $\|v^i\| \neq 0$, the vector v^r and v^i were normalized by dividing each of them by their first element. The first element of each vector was thus forced to 1, which ensures their non zero norm.

With the initial conditions obtained as above, the sequential quadratic programming was used to minimize the objective function described by equation (4.15) while satisfying the equality constraints represented by equations (4.9) to (4.12).

4.6 Results

The proposed method to calculate closest distance to Hopf bifurcation point has been tested on sample 2-bus, 3-bus and 9-bus systems. Generators were represented by their fourth order model along with type-1 exciter. Static model of loads (constant P-Q type

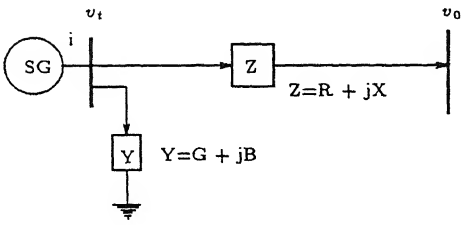

Figure 4.5: A one-machine infinite-bus system

Table 4.1: Machine and excitation system data for single machine ∞ bus system

Generator	$M_g = .04913$	$T'_{d_0} = 7.76$	$D = 0.002$
	$X_d = .973$	$X'_d = 0.19$	$X_q = 0.55$
Excitation	$K_A = 50$	$T_A = 0.05$	
Transmission line	$R = 0.034$	$X = 0.997$	

except in 2-bus system where it was represented by the corresponding admittance) was used.

Figure 4.5 shows the two bus system [42] consisting of a synchronous generator at bus-i connected to infinite bus-o through a transmission line having series impedance $Z = R + jX$ and shunt load having admittance Y connected at $node_i$. The system details are given in Table 4.1. For this system, the parameters λ_p include, load parameter (G, B) and mechanical power input P_m. These variables have been used to minimize $\|\lambda_p^0 - \lambda_p^*\|^2$ to find the closest distance to Hopf bifurcation. The minimum distance to the Hopf bifurcation (stability margin) using the proposed method was found to be 0.59953 p.u. The values of the parameters are given in Table 4.2

Appendix-A describes the 3-bus system considered for the study. The parameters considered as variables were the loading at bus-2 $(P_l + jQ_l)$ and mechanical power input to generator (P_m) at bus-1. Ignoring the generator losses, the output of generator (P_g) will be same as mechanical power input (P_m). To compute minimum distance to Hopf bifurcation, three different base case loadings were considered. The minimum distance predicted in loading case-1, case-2 and case-3 were 3.2770 p.u., 0.1865 p.u. and 0.0 p.u.

Table 4.2: Parameter values for single machine ∞ bus system

Loading	Initial Value	Final Value
G	0.249	0.00000
B	0.262	0.26271
P_m	0.420	1.04538

Table 4.3: Parameter values for 3-Bus system

Initial Values			Final Values at Hopf Bifurcation		
P_m	P_L	Q_L	P_m	P_L	Q_L
0.5	3.41	0.6	0.46	4.9500	3.4940
1.5	7.413	1.6	1.510	7.530	1.744
1.0	8.413	1.0	1.0	8.413	1.0

respectively. The initial and final values of variables in p.u. are given in Table 4.3. Loading case-3 was purposely selected to test the effectiveness of the proposed model. Starting from the base case it was found that the Hopf bifurcation point corresponds to P_l = 8.413 p.u., Q_l = 1.0 p.u. and P_m = 1.0. p.u. These were considered as initial conditions of the variables in case 3 and as expected zero stability margin was found with the proposed method. Minimum distance from the base case to saddle node bifurcation for the 3-bus system was found to be 5.5363 p.u.

The 9-bus system has been described in Appendix-B. The parameters considered as

Table 4.4: Parameter values for 9-Bus system

Loading	Initial Value	Final Value
$P_L(5)$	1.25	1.9120
$Q_L(5)$	0.50	1.1620
$P_L(6)$	0.90	1.5620
$Q_L(6)$	0.30	0.962039
$P_L(8)$	1.00	1.66204
$Q_L(8)$	0.35	1.0120

variables were loading at bus-5 (P_5+jQ_5), bus-6 (P_6+jQ_6) and bus-8 (P_8+jQ_8). As loading on system was increased, the output of each generator was increased in proportional to their inertia. The minimum distance to Hopf bifurcation predicted at base loading condition was 0.9967 p.u. while distance to saddle node bifurcation was found as 2.8357 p.u. Table 4.4 shows the initial and final values of the load parameters in p.u.

4.7 Conclusion

In this chapter a new method based on optimization technique has been developed and demonstrated to estimate the closest Hopf bifurcation point in parameter space. This method does not require any assumption of pattern or the direction in which the load is to be increased.

The distance to saddle node bifurcation point was found to be more than the closest Hopf bifurcation point in all the test systems. Hence the power margin to the closest Hopf bifurcation can be used as a useful index of proximity to voltage instability. The security boundary Σ to Hopf bifurcation defines limitation on power system performance and must be avoided to prevent instability of the system.

Chapter 5

Determination of Voltage Control Area using Entropy Concept

5.1 Introduction

Voltage collapse has been shown [131] to occur due to the weakness of the boundaries of groups of load (PQ) and generator (PV) buses and insufficient voltage control within these groups of buses. The voltage changes within such a group of buses are coherent for any disturbance that occurs out side the group. This coherency is due to the weakness of the boundary branches that connect the group of buses to the rest of the power system network. Such a group of buses is called a *voltage control area* (VCA). The control of voltage by voltage control devices within a particular voltage control area would be virtually independent of the voltage controls in other voltage control areas due to the weakness of the transmission boundaries that separate voltage control areas. However, the voltage control devices within a voltage control area must be coordinated.

The concept of the voltage control area is relatively new. Utility planners have used it to assess voltage security and reliability. Paul et al. [79] used this concept for estimating the secondary voltage control. Zaborszky [53] utilized the concept of nested clusters to describe voltage VAR planning. To determine the voltage control areas Schlueter et al. [131] developed an algorithm using the load flow Jacobian sensitivities to identify group of buses that experiences voltage collapse in interconnected system. The above algorithm identifies the branches at the boundaries between different voltage control areas by observing the elements of normalized Jacobian. However, control areas determined by

this method do not remain valid for change in system operating conditions.

Hence, a new method to find voltage control area valid for wide range of operating points has been explored in this chapter. An approach based on system entropy [19,95,151] has been employed to identify features i.e., buses where bus voltages are affected most by change in reactive power loading at given buses. These features and network connectivity information have been used to determine the voltage control areas. The new approach has been tested on IEEE 14-bus, IEEE 30-bus and a practical 75-bus Indian systems and the results have been compared with the method developed in [131].

5.2 Entropy Concept

The term *entropy* has been used to describe the degree of uncertainty, surprise or information about an event. Let the events be defined as discrete random variables S_i (i = 1, 2, ..., q) with q possible values and let their respective probability distribution function be $prob(S = S_i) = P_i$. Then the entropy function to the event S is defined [95] as

$$H(S) = \sum_{i=1}^{q} P_i \ln(1 \ P_i) \tag{5.1}$$

A large value of entropy indicates high degree of uncertainty and minimum information about an event. In a physical system, entropy is associated with a measure of disorder in the system. The most disorderly system is one where all the values of S_i occur with equal probability.

For example, the entropy for a fair die with equal probability of occurrence for each number is given by

$$H_1 = 6 * 1/6 * \ln 6 = 1.792$$

If we do not have any information about the die except that it is fair (since we are uncertain about outcome of any number from trial).i.e., all events have equal probability to appear in the trial, the entropy will be high. Suppose we conduct some experiment on die and find that the die is unfair and probability of occurrence based on experiment for these numbers are 0.5, 0.1, 0.1, 0.1, 0.1 and 0.1. The entropy now becomes

$$H_2 = 0.5 \cdot \ln 2 + 5 \cdot 0.1 \cdot \ln 10 = 1.4898$$

It is observed that this additional information results in reduction of 0.294 in the entropy value. The change in the entropy for given informationS_1 (fair die) and S_2 (information about die from trials) is defined as the information Gain (G)

$$\begin{aligned} G &= H_1 - H_2 \\ &= \sum_{i=1}^{q} P_{1i} \ln(1/P_{1i}) - \sum_{i=1}^{q} P_{2i} \ln(1/P_{2i}) \end{aligned} \tag{5.2}$$

The above equation can be rewritten as,

$$G = \sum_{i=1}^{q} P_{1i} \ln(1/P_{1i}) + \sum_{i=1}^{q} P_{1i} \ln(1/P_{2i}) - \sum_{i=1}^{q} P_{1i} \ln(1/P_{2i}) - \sum_{i=1}^{q} P_{2i} \ln(1/P_{2i}) \tag{5.3}$$

Since, sum of the probabilities of all the events is unity i.e.,

$$\sum_{i=1}^{q} P_{1i} = \sum_{i=1}^{q} P_{2i} = 1$$

Equation 5.3 for the information gain becomes,

$$G = \sum_{i=1}^{q} P_{1i} \ln(P_{2i}/P_{1i}) \tag{5.4}$$

This information gain provides a basis for feature selection. The features are selected on the basis of maximum information gain provided by various trials. Hence for selecting the features, the information gain provided by various trials are arranged in descending order of their values.

5.3 Voltage Control Area Using Jacobian Sensitivity

The algorithm suggested by Schlueter et al. [131] to identify voltage control area was based on identification of weakest transmission elements connected to each bus. These elements were first identified by exploiting the sensitivity information provided by the power flow Jacobian and corresponding elements were eliminated from the Jacobian. The groups of buses after elimination of the weak transmission elements, found isolated from each other, were called as *voltage control areas.* The algorithm had been applied to the decoupled submatrix J of complete Jacobian or a reduced Jacobian J^* both describing the sensitivity of reactive power with respect to voltage as defined below.

The Newton Raphson load flow Jacobian considering all the buses (PV and PQ buses) can be defined as follows

$$\begin{bmatrix} \Delta P_G \\ \Delta P_L \\ \Delta Q_G \\ \Delta Q_L \end{bmatrix} = \begin{bmatrix} A_1 & B_1 & C_1 & D_1 \\ A_2 & B_2 & C_2 & D_2 \\ A_3 & B_3 & C_3 & D_3 \\ A_4 & B_4 & C_4 & D_4 \end{bmatrix} \begin{bmatrix} \Delta\delta \\ \Delta\theta \\ \Delta E/E \\ \Delta V/V \end{bmatrix} = \left[\hat{J}\right] \begin{bmatrix} \Delta\delta \\ \Delta\theta \\ \Delta E/E \\ \Delta V/V \end{bmatrix} \tag{5.5}$$

where,

$P_G =$ Real power injections at synchronous machine buses excluding the swing bus.
$P_L =$ Real power injections at generator (PV) and load (PQ) buses excluding the synchronous machines and swing bus.
$Q_L =$ Reactive power injections at load (PQ) buses.
$Q_V =$ Reactive power injections at generator buses.

$\left[\hat{J}\right]$ becomes $\left[\hat{J}_N\right]$, the normal load flow Jacobian by forcing $\Delta E = 0$.

$$\left[\hat{J}_N\right] = \begin{bmatrix} A_1 & B_1 & D_1 \\ A_2 & B_2 & D_2 \\ A_4 & B_4 & D_4 \end{bmatrix} \tag{5.6}$$

Decoupled submatrix J corresponding to reactive power - voltage sensitivity is defined as

$$J = \begin{bmatrix} C_3 & D_3 \\ C_4 & D_4 \end{bmatrix} \tag{5.7}$$

Reduced Jacobian J^* can be obtained from equation 5.5 by first setting $\begin{bmatrix} \Delta P_G \\ \Delta P_L \end{bmatrix} = 0$ and solving for $\begin{bmatrix} \Delta\delta \\ \Delta\theta \end{bmatrix}$

$$\begin{bmatrix} \Delta\delta \\ \Delta\theta \end{bmatrix} = -\begin{bmatrix} A_1 & B_1 \\ A_2 & B_2 \end{bmatrix}^{-1} \begin{bmatrix} C_1 & D_1 \\ C_2 & D_2 \end{bmatrix} \begin{bmatrix} \Delta E/E \\ \Delta V/V \end{bmatrix} \tag{5.8}$$

Substituting values of $\begin{bmatrix} \Delta\delta \\ \Delta\theta \end{bmatrix}$ in equation 5.5 we get

$$\begin{bmatrix} \Delta Q_G \\ \Delta Q_L \end{bmatrix} = [J^*] \begin{bmatrix} \Delta E/E \\ \Delta V/V \end{bmatrix} \tag{5.9}$$

where,

$$[J^*] = \begin{bmatrix} C_3 & D_3 \\ C_4 & D_4 \end{bmatrix} - \begin{bmatrix} A_3 & B_3 \\ A_4 & B_4 \end{bmatrix} \begin{bmatrix} A_1 & B_1 \\ A_2 & B_2 \end{bmatrix}^{-1} \begin{bmatrix} C_1 & D_1 \\ C_2 & D_2 \end{bmatrix} \tag{5.10}$$

Once J or J^* is obtained, the following steps for determining the control area has been applied.

(i) Search for the largest diagonal element of Jacobian $d = max(J)_{ii}$ or $max(J^*)_{ii}$.

(ii) Normalize J (or J^*) by dividing every element by d.

(iii) In each row i of the normalized Jacobian, the absolute values of the off-diagonal Jacobian elements are ranked from the smallest to the largest. The smallest absolute values are eliminated, from each row i until the sum of the eliminated elements of the normalized Jacobian is close to but still less than α, where α is a prespecified threshold value.

(iv) The group of buses, that are still inter-connected after the weakest branches are eliminated, form the *voltage control areas.*

Since the elements of Jacobian matrix J or J^* are computed at a given operating point, the *voltage control areas* obtained with the above method may not remain valid for change in the system loading or operating conditions.

5.4 Voltage Control Area Using Entropy Concept

The voltage control area can be obtained by identifying a group of buses where voltages are affected significantly for reactive power disturbance at buses within the group and quite insignificant for the disturbance at buses outside the group. If the information regarding certain bus voltage change to the disturbance results in significant information gain (change in entropy) the bus voltage has significant impact of reactive power disturbance and the bus is selected as a feature for determining voltage control area. On the other hand, the bus voltage which results in minor information gain is regarded as having no significant effect of the reactive power disturbance and will not be selected as a feature. This implies that the bus does not belong to particular control area.

To determine control areas, different loading conditions were simulated by perturbing the loading on all the buses randomly in wide range of system operating conditions. Once the loading pattern (1000 in the present study) were created, AC load flow was performed to obtain voltage profile for each case. These loading conditions were used

to find the effect of the reactive power disturbance for obtaining information gain and feature selection which have been utilized to identify the voltage control areas.

5.4.1 Feature Selection Procedure

After obtaining the load flow results the information gain was computed by observing the voltages at each bus for load disturbance at various buses in the system using following steps.

(i) Pick up a bus p at which voltage variation is being observed when load is changed at bus q.

(ii) Equally divide the range of loading variation at bus q into various groups (only reactive power loadings were considered). Five groups gQ_1 to gQ_5 were considered in the present study, which were experimentally found to be adequate. Thus each group contains 200 cases.

(iii) Scan all 1000 values of voltages at selected bus p and equally divide them in to several categories. Five categories say gV_1 to gV_5 were considered in the study.

(iv) Count the number of cases n_{ij} common to voltage group i and load group j. Calculate the corresponding probability as

$$P_{ij} = \frac{n_{ij}}{\sum_{j=1}^{5} n_{ij}} \qquad (i = 1, \ldots, 5) \tag{5.11}$$

(v) For each voltage group i, calculate entropy

$$H_i = \sum_{j=1}^{5} P_{ij} \ln \frac{1}{P_{ij}} \tag{5.12}$$

(vi) Calculate average entropy H_{avg} and entropy gain G using equation (5.13) and equation (5.14)

$$H_{\text{avg}} = \frac{1}{5} \sum_{i=1}^{5} H_i \tag{5.13}$$

$$G = H^0 - H_{\text{avg}} \tag{5.14}$$

Where H^0 is the maximum entropy value when probability of occurrence for all five groups is equal to 0.2 i.e. $H^0 = 5 * .2 \ln 1/.2 = 1.609$.

(vii) Once the information gain for all the combination of buses were found, the information gain was ranked according to their magnitude for particular bus-p (p = 1, ..., n) and first X ranked buses were selected as features i.e. buses where voltages were maximum affected by change in loading at bus-q.

5.4.2 Criterion for Selection of Voltage Control Area

Once the features were selected, the following procedural steps have been applied to find voltage control areas. Assume that elem $(j, k) = P$ implies that the k^{th} element of j^{th} control area is bus P and feature set $F(P) = \{\mu_i/\mu_i \in$ buses selected as feature for load disturbance at bus $P\}$.

Step1: Set control area $j = 1$, bus count $k = 1$, and select bus 1 as first element of control area j i.e. $P =$ elem $(j, k) = 1$. Set a counter $kk = 1$.

Step2: Take feature set $F(P)$ and for all $\mu_i \in F(P)$ check whether $P \in F(\mu_i)$. If $P \notin F(\mu_i)$, then μ_i is not selected in control area j. If $P \in F(\mu_i)$, then go to next step.

Step3: Check the connectivity of μ_i with buses in control area j. If μ_i is connected to any of the buses in the control area then μ_i belongs to the control area j. Set $k = k + 1$ and elem $(j, k) = \mu_i$.

Step4: Increment $kk = kk + 1$. Repeat the procedural steps 2 and 3 for all the buses in control area j till $k = kk$.

Step5: Increment control area $j = j + 1$. Select a bus P which is not belonging to any of the control area already selected and set $k = 1, kk = 1$, elem $(j, k) =$ P.

Step6: Repeat the procedural steps 2 to 5 till all the buses are selected in the respective control area.

Figure 5.1 shows a detailed flow chart for selecting the voltage control area.

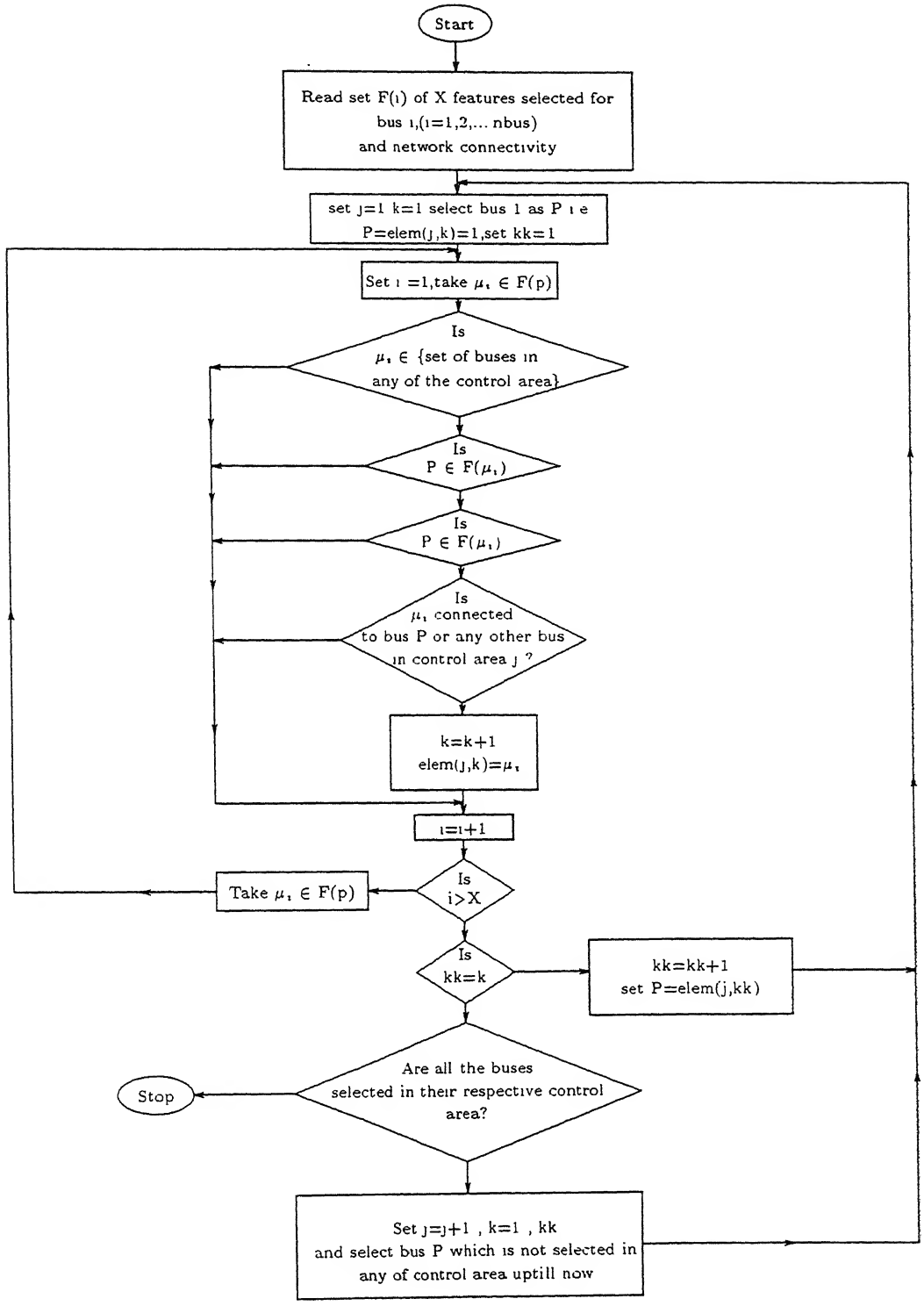

Figure 5.1: Flowchart for selecting the control areas

5.5 Results and Discussion

To establish the effectiveness of the proposed method for determining voltage control areas, studies were conducted on the following three sample systems on HP-9000/735 computer.

(i) IEEE 14-bus system as described in Appendix-C.

(ii) IEEE 30-bus system as described in Appendix-D.

(iii) A practical 75-bus UP state electricity board (UPSEB) system representing 220 KV and 400 KV network as described in Appendix-E.

To determine the control areas, different loading conditions were generated by perturbing the loadings randomly in the range of 80% to 130% of their base values and voltages of P-V buses between 0.95 p.u. to 1.05 p.u. of their base values. A set of 1000 loading patterns were simulated in this way for all the three test systems and load flow was run for each of the cases to generate sensitivity patterns required for entropy calculation.

The entropy and the information gain were computed for each bus corresponding to the load change at different buses of the system as described in section 5.4.1. The effect of number of features on the occurrence of voltage control areas were studied for all the three systems.

Initially a maximum number of features (X) were selected which were taken as two third of the total number of buses in each system. A table was formed showing these maximum selected features (in descending order of their entropy gain) corresponding to each bus. A total of 10 features for the 14-bus system, 20 features for the 30-bus system and 50 features for the 75-bus system were selected. The results of the three systems are described below.

5.5.1 IEEE 14-bus system

Table 5.1 shows the ten features selected against each bus for the IEEE 14-bus system where the voltages are maximum affected when there is reactive power disturbance. Table 5.2 shows the buses belonging to different control areas of the IEEE 14-bus system when features were varied from 2 to 9 for the selection of control areas using the proposed method.

Table 5.1: Features selected for IEEE 14-Bus system

Bus NO.	FEATURES SELECTED
1	1, 5, 2,14, 4, 9, 8,13, 7,11
2	5, 1, 2, 3, 8, 4, 9,14,12,13
3	5, 1,14, 2, 7,12,10, 3,13, 9
4	5, 4, 1, 2, 9,14,12, 3,10, 8
5	5, 1, 7,14, 2, 9,10,12,11, 4
$\star$ 7	5, 7, 1,14, 2,10,11, 9,12, 3
8	5, 1, 2.14, 4, 9, 8, 3,12,13
9	5, 1, 2, 4, 9,14,12, 8,13, 3
10	5, 7, 1,10, 2,14,11, 3,12, 4
11	5, 1, 7, 2,14.10, 3.11, 9,13
12	5, 1,14, 7, 2.13, 3.12,10.11
13	5, 1,14, 7, 2,13,11,12,10, 3
14	5, 1,14, 7, 2, 8,10, 9, 3, 4

$\star$Bus *no.*6 is internal bus of a three winding transformer

Voltage control areas were also determined using the Jacobian sensitivity method [131]. To separate weakly coupled buses from strongly coupled buses different values of threshold α was used. Table 5.3 shows control areas of IEEE 14-bus system obtained by different values of threshold α varying from 0.05 to 0.921. At $\alpha = 0.921$ each bus of the system forms individual control area.

The control areas obtained by the proposed method for different values of features selected and the Jacobian based method [131] for different threshold 'α' values were validated by comparing the Q-V[1] curves of buses belonging to the same control area. It was found that the buses within each of the control areas, when the features selected are five in number and $\alpha = 0.24$, exhibit identical Q-V curves. Figure 5.2 shows typical Q-V curves for control area no. 2. Control areas obtained with the proposed method are 8 in number (fea. = 5) and with the sensitivity method these are 7 in number($\alpha = 0.24$).

From the Table 5.2 and Table 5.3 it can be seen that the buses belonging to different control areas obtained by the two methods are almost same but not identical.

In the sensitivity based method the Jacobian was estimated at the base loading condition. In order to explore the validity of the control areas obtained by the sensitivity

[1]Q-V curves were obtained by varying the value of voltage magnitude at a bus selected one at a time and computing injected reactive power (Q) at the same bus from load flow.

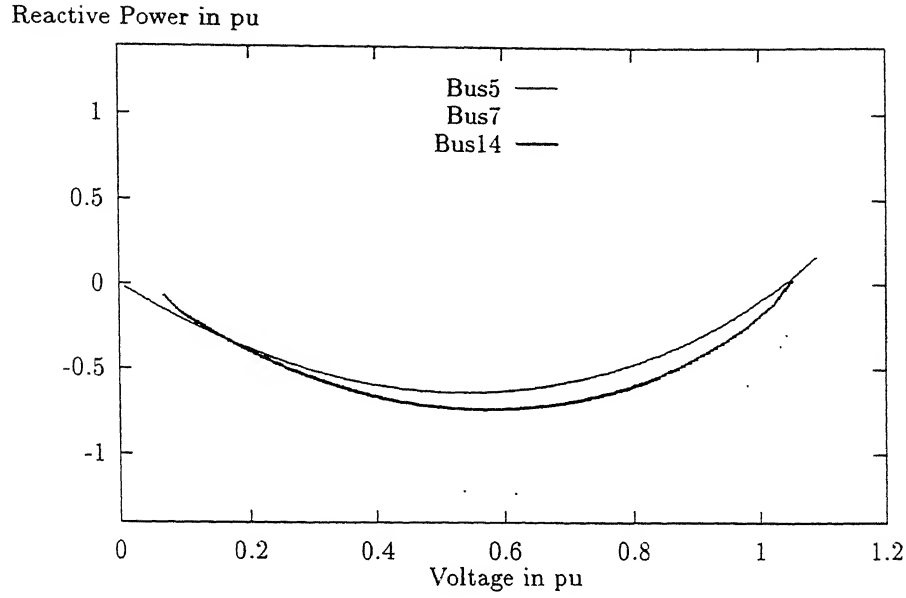

Figure 5.2: $Q - V$ Curves of control area 2 of 14 bus system

Table 5.2: Voltage control areas of IEEE 14-Bus by entropy method

Sr. No.	Bus No.	Control areas with different features							
		$fe. = 2$	$fe. = 3$	$fe. = 4$	$fe. = 5$	$fe. = 6$	$fe. = 7$	$fe. = 8$	$fe. = 9$
1	1	1	1	1	1	1	1	1	1
2	2	1	1	1	1	1	1	1	1
3	4	3	2	2	1	1	1	1	1
4	9	4	3	3	1	1	1	1	1
5	5	5	4	4	2	1	1	1	1
6	7	6	4	4	2	1	1	1	1
7	14	7	5	4	2	1	1	1	1
8	8	8	6	5	3	1	1	1	1
9	10	9	7	6	4	1	1	1	1
10	3	10	8	7	5	2	1	1	1
11	11	11	9	8	6	3	1	1	1
12	12	12	10	9	7	4	2	1	1
13	13	13	11	10	8	5	3	2	1

Table 5.4: Features selected for IEEE 30-Bus system

Bus NO.	FEATURES SELECTED
1	1, 27, 11, 3, 9, 14, 13, 15, 23, 6, 28, 18, 16, 17, 20, 25, 19, 21, 22, 24
2	1, 14, 27, 11, 3, 12, 13, 28, 9, 14, 15, 20, 6, 5, 19, 16, 18, 17, 22, 21
3	3, 28, 15, 16, 13, 9, 8, 14, 6, 23, 11, 18, 20, 22, 21, 19, 17, 24, 26, 25
4	4, 27, 11, 2, 13, 3, 28, 12, 1, 8, 9, 21, 15, 23, 14, 24, 22, 17, 6, 16
5	11, 5, 1, 27, 2, 11, 23, 15, 18, 20, 9, 17, 14, 6, 16, 19, 24, 8, 28, 13
6	13, 28, 3, 26, 24, 23, 25, 14, 15, 11, 21, 8, 22, 18, 10, 16, 17, 20, 27, 9
⋆ 8	15, 4, 2, 1, 11, 27, 13, 5, 29, 9, 15, 6, 3, 28, 25, 30, 12, 14, 24, 26
9	27, 9, 14, 16, 28, 15, 13, 11, 9, 12, 23, 10, 24, 17, 18, 25, 26, 30, 19, 4
10	5, 12, 3, 14, 21, 22, 18, 8, 13, 28, 17, 9, 26, 24, 15, 20, 10, 11, 19, 25
11	17, 12, 21, 22, 8, 14, 1, 30, 4, 20, 16, 23, 19, 5, 25, 29, 27, 18, 24, 6
12	22, 8, 21, 20, 17, 9, 24, 10, 19, 15, 11, 14, 4, 18, 25, 23, 16, 6, 30, 26
13	1, 27, 15, 12, 11, 28, 4, 25, 3, 26, 10, 13, 5, 6, 17, 23, 8, 16, 9, 21
14	19, 17, 21, 5, 22, 20, 16, 8, 24, 18, 9, 4, 15, 6, 13, 23, 14, 28, 29, 30
15	15, 2, 30, 9, 25, 14, 15, 29, 26, 27, 1, 19, 6, 20, 18, 23, 10, 24, 13, 12
16	2, 28, 15, 12, 20, 10, 18, 25, 17, 19, 27, 29, 30, 26, 9, 23, 21, 16, 22, 8
17	5, 6, 17, 10, 20, 19, 22, 8, 18, 21, 11, 18, 16, 25, 15, 2, 23, 14, 13, 26
18	29, 2, 4, 3, 26, 25, 16, 30, 6, 10, 5, 16, 15, 17, 1, 23, 24, 21, 19, 22
19	9, 28, 27, 5, 14, 26, 10, 25, 10, 2, 13, 15, 16, 23, 6, 1, 3, 24, 17, 30
20	13, 12, 26, 5, 2, 24, 27, 21, 6, 10, 4, 25, 22, 30, 8, 29, 18, 9, 20, 28
21	13, 12, 21, 28, 22, 5, 3, 24, 8, 16, 1, 29, 14, 15, 17, 4, 23, 18, 9, 20
22	3, 24, 23, 11, 18, 27, 14, 29, 8, 14, 13, 12, 15, 20, 19, 22, 9, 28, 16, 21
23	14, 8, 22, 29, 17, 20, 21, 25, 3, 6, 26, 24, 18, 30, 23, 10, 19, 13, 16, 1
24	22, 8, 6, 21, 24, 26, 18, 19, 25, 5, 20, 23, 15, 16, 20, 17, 4, 14, 10, 9
25	21, 22, 8, 17, 3, 5, 24, 19, 12, 20, 19, 13, 11, 9, 18, 14, 23, 16, 28, 6
26	5, 27, 1, 2, 13, 14, 13, 23, 18, 11, 16, 26, 24, 12, 15, 4, 25, 9, 6, 19
27	21, 22, 24, 23, 8, 17, 16, 4, 30, 19, 10, 18, 20, 26, 15, 25, 13, 28, 27, 1
28	28, 5, 13, 10, 11, 16, 18, 14, 27, 9, 3, 8, 24, 30, 23, 15, 2, 20, 17, 22
29	29, 30, 10, 25, 26, 24, 22, 21, 23, 20, 19, 8, 18, 17, 15, 16, 9, 6, 14, 27
30	20, 27, 19, 8, 20, 23, 21, 24, 22, 17, 2, 29, 4, 18, 13, 30, 16, 15, 5, 1

⋆Bus *no.*7 is internal bus of a three winding transformer

Table 5.5: Voltage control areas of IEEE 30-Bus by entropy method

Sr. No.	Bus No.	Control areas with different features					
		$fea. = 10$	$fea. = 11$	$fea. = 12$	$fea. = 13$	$fea. = 14$	$fea. = 16$
1	29	1	1	1	1	1	1
2	30	1	1	1	1	1	1
3	13	2	2	2	2	1	1
4	28	2	2	2	2	1	1
5	2	3	2	2	2	1	1
6	9	4	3	3	3	1	1
7	15	4	3	3	3	1	1
8	14	4	3	3	3	1	1
9	16	4	3	3	3	1	1
10	11	4	3	3	3	1	1
11	27	5	4	3	3	1	1
12	23	6	5	3	3	1	1
13	21	7	6	4	4	1	1
14	22	8	7	5	4	1	1
15	24	9	8	6	4	1	1
16	25	10	9	7	4	1	1
17	26	11	10	8	4	1	1
18	10	12	11	9	5	1	1
19	12	13	12	10	6	1	1
20	17	14	13	11	7	1	1
21	18	15	14	12	8	1	1
22	19	16	15	13	9	1	1
23	3	17	16	14	10	1	1
24	4	18	17	15	11	1	1
25	5	19	18	16	12	1	1
26	6	20	19	17	13	1	1
27	20	21	20	18	14	1	1
28	8	22	21	19	15	1	1
29	1	23	22	20	16	2	1

Table 5.6: Voltage control areas of IEEE 30-Bus using Jacobian sensitivity

Sr. No.	Bus No.	Control areas for different threshold (α) value										
		0.01	0.03	0.05	0.07	0.09	0.11	0.13	0.15	0.25	0.35	0.63
1	21	1	1	1	1	1	1	1	1	1	1	1
2	22	1	1	1	1	1	1	1	1	1	1	2
3	7	1	1	1	1	1	1	1	2	2	2	3
4	8	1	1	1	1	1	1	1	2	3	3	4
5	17	1	1	1	1	1	1	1	2	4	4	5
6	13	1	1	1	2	2	2	2	3	5	5	6
7	11	1	1	1	2	2	2	2	3	5	5	7
8	27	1	1	1	2	2	2	2	3	5	5	8
9	3	1	1	1	2	2	2	2	3	5	6	9
10	28	1	1	1	2	2	2	2	3	5	7	10
11	12	1	1	1	2	2	2	2	3	6	8	11
12	1	1	1	1	2	2	2	3	4	7	9	12
13	2	1	1	1	2	2	2	3	4	7	10	13
14	5	1	1	1	2	2	3	4	5	8	11	14
15	9	1	1	1	3	3	4	5	6	9	12	15
16	15	1	1	1	3	3	4	5	6	10	13	16
17	6	1	1	1	3	3	5	6	7	11	14	17
18	23	1	1	1	3	4	6	7	8	12	15	18
19	4	1	1	1	4	5	7	8	9	13	16	19
20	16	1	1	1	5	6	8	9	10	14	17	20
21	29	1	1	2	6	7	9	10	11	15	18	21
22	19	1	1	2	6	7	9	10	11	16	19	22
23	16	1	1	2	6	8	10	11	12	17	20	23
24	10	1	1	3	7	9	11	12	13	18	21	24
25	25	1	1	3	7	9	12	13	14	19	22	25
26	14	1	1	4	8	10	13	14	15	20	23	26
27	24	1	1	5	9	11	14	15	16	21	24	27
28	29	1	1	6	10	12	15	16	17	22	25	28
29	26	1	2	7	11	13	16	17	18	23	26	29
30	30	1	3	8	12	14	17	18	19	24	27	30

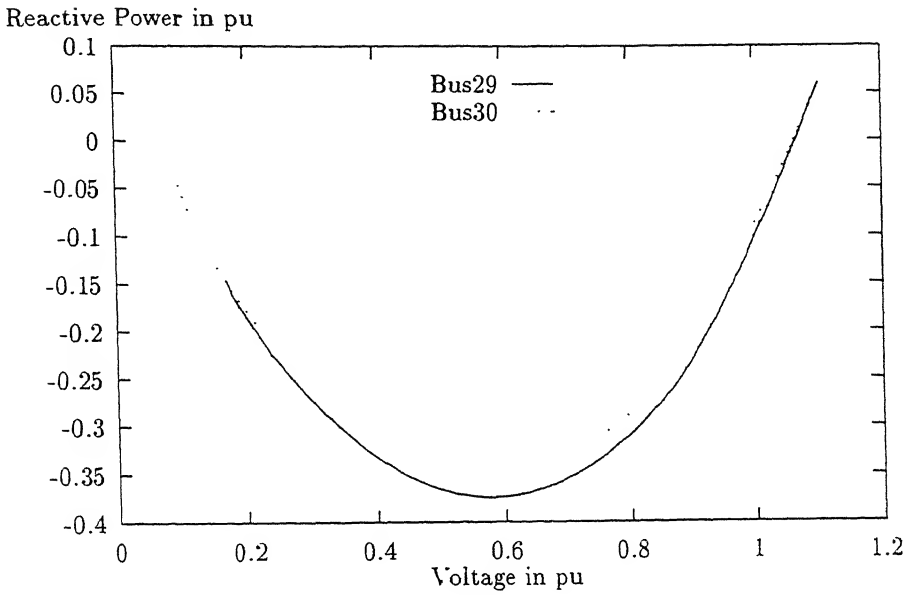

Figure 5.3: $Q - V$ Curves of control area 1 of 30 bus system

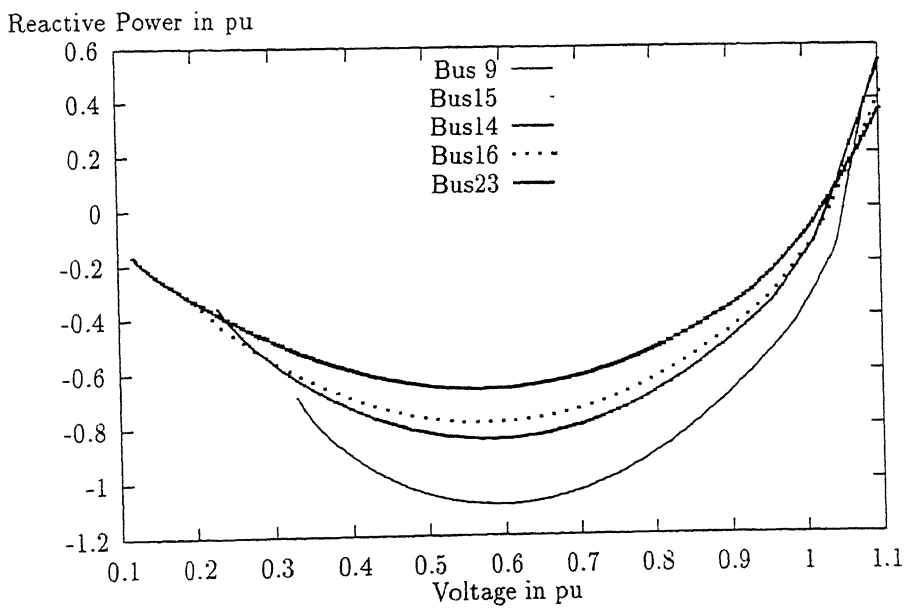

Figure 5.4: $Q - V$ Curves of control area 3 of 30 bus system

selected and the Jacobian based method [131] for different threshold (α) values were validated by comparing Q-V curves belonging to the same control area. It was found that the buses within each control area, when the features selected are 13 in number and α = 0.09, exhibit identical Q-V curves. Typical Q-V curves for buses in control area 1 and 3 are given in Figures 5.3 and 5.4 respectively.

The control areas obtained with the proposed method are 16 in number (feature = 13) and with the sensitivity based method, these are 14 in number ($\alpha = 0.09$).

From Table 5.5 and Table 5.6 it can be seen that the buses belonging to different control areas with the two methods are almost same but not identical. In the sensitivity based method, the Jacobian was estimated at base loading condition. In order to explore the validity of the control areas obtained by the sensitivity method at loading different from the base case, the number of control areas were obtained at 80% and 120% of the base loading values. The same threshold value $\alpha = 0.09$ was used to determine the number of control areas by the Jacobian sensitivity method. At 80% and 120% loading the number of control areas were obtained as 15 and 19 respectively which was 14 at the base loading condition. Thus, the control areas obtained using the sensitivity method at a loading condition do not remain valid for change in the operating condition in the IEEE 30-bus system.

5.5.3 75-Bus UPSEB System

For the 75-bus Indian system the features were varied between 20 to 50. The control areas and associated buses for this system determined with the help of these features and network bus connectivity information are given in Table 5.7. The control areas were also determined by using the Jacobian sensitivity method [131] for different values of threshold (α) varied from 0.01 to 0.982. At $\alpha = 0.982$ all the buses form individual control areas. Table 5.8 shows control areas corresponding to different values of threshold (α).

The validation of control areas obtained by the proposed method for different values of features selected and the Jacobian based method [131] for different threshold values (α) has been done by comparing Q-V curves of buses belonging to the same control area. It was found that when the feature selected is 30 in number and α=0.03 the buses within each of the control areas exhibit identical Q-V curves. Typical Q-V curves for buses in control area 1 are shown in Figures 5.5 and 5.6 and for control area-3 in Figure 5.7.

Table 5.7: Voltage control areas of 75-bus system by entropy method

Sr. No.	Bus No.	Control areas with diff. features						Sr. No.	Bus No.	Control areas with diff. features					
		20	30	35	40	45	50			20	30	35	40	45	50
1	3	1	1	1	1	1	1	29	72	18	2	1	1	1	1
2	71	1	1	1	1	1	1	30	60	18	2	1	1	1	1
3	15	2	1	1	1	1	1	31	70	19	2	1	1	1	1
4	73	2	1	1	1	1	1	32	53	20	3	1	1	1	1
5	55	2	1	1	1	1	1	33	61	21	3	1	1	1	1
6	16	3	1	1	1	1	1	34	62	22	3	1	1	1	1
7	46	3	1	1	1	1	1	35	4	23	4	1	1	1	1
8	50	3	1	1	1	1	1	36	5	24	5	1	1	1	1
9	37	3	1	1	1	1	1	37	6	25	6	1	1	1	1
10	69	3	1	1	1	1	1	38	30	26	7	1	1	1	1
11	24	4	1	1	1	1	1	39	32	27	8	1	1	1	1
12	27	4	1	1	1	1	1	40	39	28	9	1	1	1	1
13	74	4	1	1	1	1	1	41	56	29	10	1	1	1	1
14	8	5	1	1	1	1	1	42	57	30	11	1	1	1	1
15	54	6	1	1	1	1	1	43	58	31	12	1	1	1	1
16	63	6	1	1	1	1	1	44	59	32	13	1	1	1	1
17	10	7	1	1	1	1	1	45	65	33	14	1	1	1	1
18	12	8	1	1	1	1	1	46	75	34	15	1	1	1	1
19	13	9	1	1	1	1	1	47	2	35	16	2	2	2	1
20	14	10	1	1	1	1	1	48	11	36	17	3	3	3	2
21	28	11	1	1	1	1	1	49	49	36	17	3	3	3	2
22	34	12	1	1	1	1	1	50	20	37	17	3	3	3	2
23	47	13	1	1	1	1	1	51	64	38	18	4	3	3	2
24	51	14	1	1	1	1	1	52	66	39	19	5	3	3	2
25	52	15	1	1	1	1	1	53	48	40	20	6	4	3	2
26	67	16	1	1	1	1	1	54	1	41	21	7	5	4	3
27	68	17	1	1	1	1	1	55	7	42	22	8	6	5	4
28	25	18	2	1	1	1	1	56	9	43	23	9	7	6	5

Table 5.8: Voltage control areas of 75-bus system using Jacobian sensitivity

Sr. No.	Bus No.	Control areas for different threshold (α) value						
		0.01	0.03	0.1	0.4	0.62	0.63	0.982
1	21	1	1	1	1	1	1	1
2	22	1	1	1	2	2	2	2
3	25	1	1	1	3	3	3	3
4	28	1	1	1	4	4	4	4
5	29	1	1	1	5	5	5	5
6	30	1	1	1	6	6	6	6
7	56	1	1	1	7	7	7	7
8	65	1	1	1	8	8	8	8
9	75	1	1	1	9	9	9	9
10	14	1	1	2	10	10	10	10
11	38	1	1	3	11	11	11	11
12	43	1	1	4	12	12	12	12
13	53	1	1	5	13	13	13	13
14	54	1	1	6	14	14	14	14
15	57	1	1	7	15	15	15	15
16	58	1	1	7	16	16	16	16
17	59	1	1	9	17	17	17	17
18	61	1	1	10	18	18	18	18
19	12	1	2	11	19	19	19	19
20	13	1	2	11	20	20	20	20
21	41	1	2	11	21	21	21	21
22	42	1	2	11	21	21	22	22
23	23	1	2	12	22	22	23	23
24	74	1	2	12	22	22	23	24
25	18	1	2	13	23	23	24	25
26	47	1	2	14	24	24	25	26
27	24	1	2	15	25	25	26	27
28	27	1	2	16	26	26	27	28
29	67	1	2	17	27	27	28	29
30	19	1	2	18	28	28	29	30
31	20	1	2	19	29	29	30	31
32	36	1	2	20	30	30	31	32
33	3	1	2	21	31	31	32	33
34	11	1	2	22	32	32	33	34
35	26	1	2	23	33	33	34	35
36	40	1	2	24	34	34	35	36
37	37	1	2	25	35	35	36	37

Contd. ...

Table 5.8 ... Contd.

Sr. No.	Bus No.	Control areas for different threshold (α) value						
		0.01	0.03	0.1	0.4	0.62	0.63	0.982
38	48	1	2	26	35	36	37	38
39	68	1	2	27	37	37	38	39
40	71	1	2	28	38	38	39	40
41	31	1	3	29	39	39	40	41
42	32	1	3	29	40	40	41	42
43	5	1	3	30	41	41	42	43
44	33	1	3	31	42	42	43	44
45	39	1	3	32	43	43	44	45
46	62	1	3	33	44	44	45	46
47	1	1	4	34	45	45	46	47
48	16	1	4	34	46	46	47	48
49	17	1	4	34	47	47	48	49
50	35	1	4	34	47	48	49	50
51	2	1	4	35	48	49	50	51
52	9	1	4	36	49	50	51	52
53	46	1	4	37	50	51	52	53
54	45	1	5	38	51	52	53	54
55	73	1	5	38	52	53	54	55
56	15	1	5	39	53	54	55	56
57	44	1	5	39	54	55	56	57
58	8	1	6	40	55	56	57	58
59	34	1	6	41	56	57	58	59
60	55	1	7	42	57	58	59	60
61	63	1	7	43	58	59	60	61
62	70	1	8	44	59	60	61	62
63	72	1	8	45	60	61	62	63
64	4	1	9	46	61	62	63	64
65	6	1	10	47	62	63	64	65
66	7	1	11	48	63	64	65	66
67	10	1	12	49	64	65	66	67
68	49	1	13	50	65	66	67	68
69	50	1	14	51	66	67	68	69
70	51	1	15	52	67	68	69	70
71	52	1	16	53	68	69	70	71
72	60	1	17	54	69	70	71	72
73	64	1	18	55	70	71	72	73
74	66	1	19	56	71	72	73	74
75	69	1	20	50	72	73	74	75

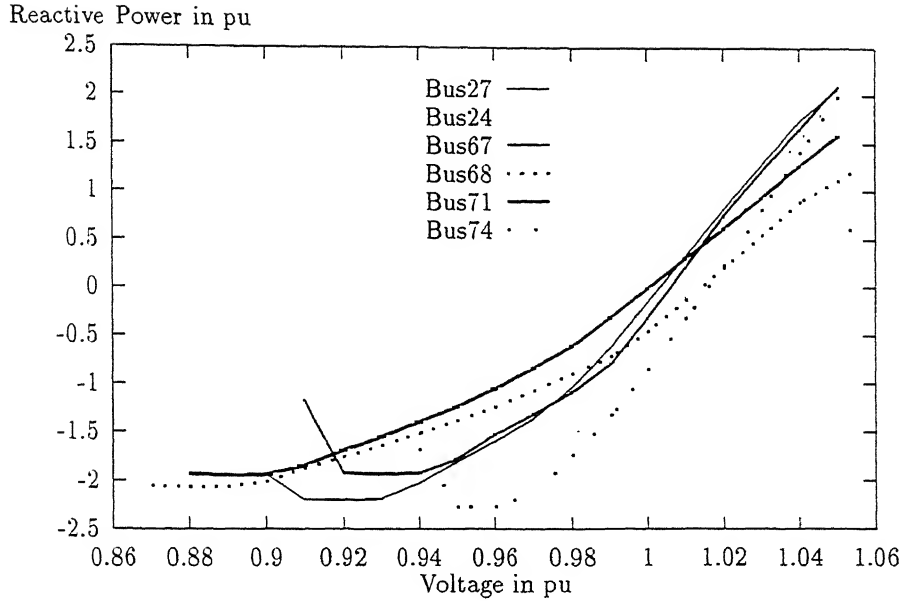

Figure 5.5: $Q - V$ Curves of control area 1 of 75 bus system
(see Figure 5.6 also)

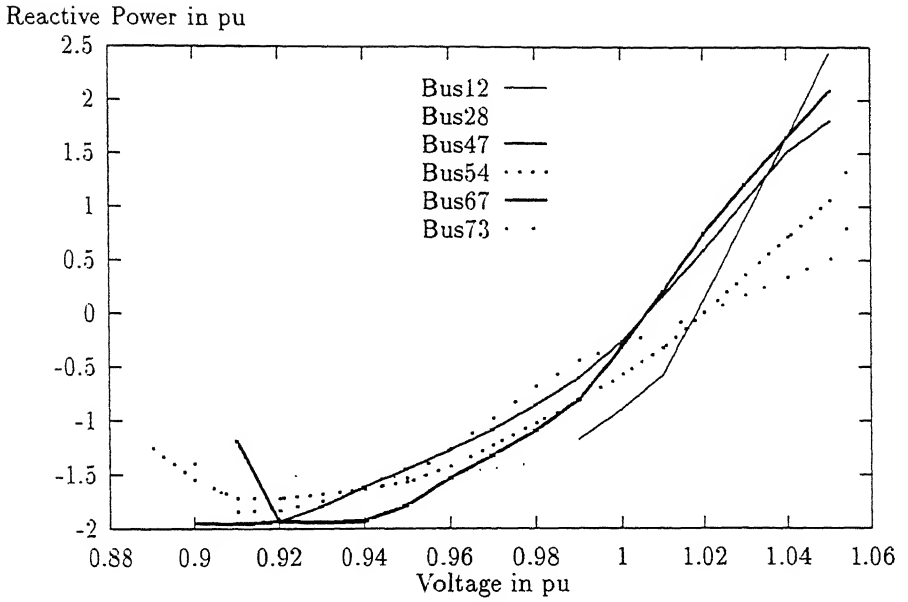

Figure 5.6: $Q - V$ Curves of control area 1 of 75 bus system (see Figure 5.5 also)

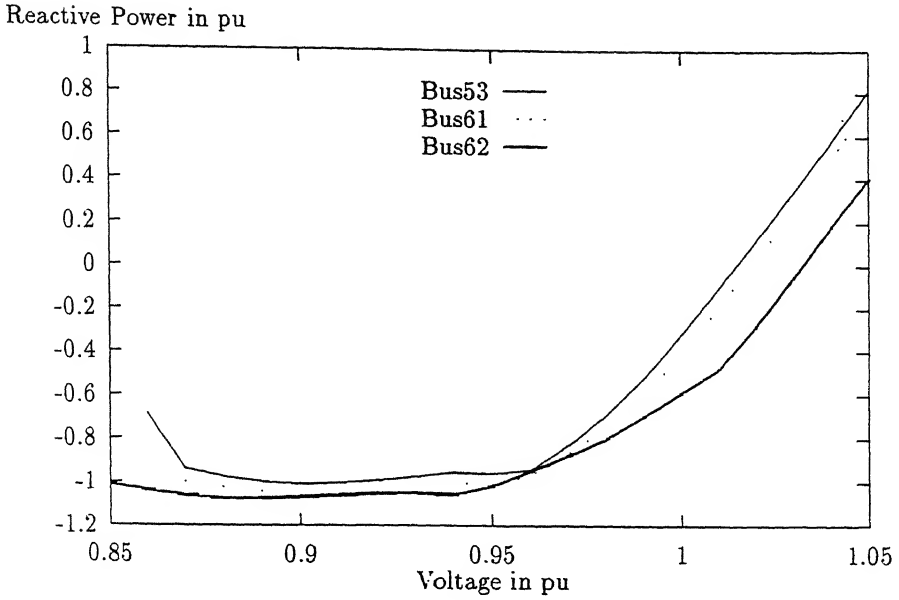

Figure 5.7: $Q - V$ Curves of control area 3 of 75 bus system

Number of control areas obtained with the proposed method is 23 and with the sensitivity method it is 20. From Tables 5.7 and 5.8 it can be seen that the buses belonging to different control areas, obtained with the two methods, are almost same but not identical.

In the sensitivity based method the Jacobian was estimated at the base loading condition. In order to explore the validity of the control areas obtained by the sensitivity method at loading different from the base case, the number of control areas were obtained at 80% and 120% of the base loading values. The same threshold value $\alpha = 0.03$ was used to determine the number of control areas by the Jacobian sensitivity method. At 80% and 120% loading, the number of control areas obtained were 19 and 23 respectively which was 20 at the base loading condition. Thus the control areas obtained using the sensitivity method at a loading condition do not remain valid for change in operating condition in the 75-bus UPSEB system also.

5.6 Conclusion

A new method of determining the voltage control areas, using entropy concept, has been suggested and demonstrated on three sample systems viz. IEEE 14-bus, IEEE 30-bus and a practical 75-bus Indian system. The results have been compared with a sensitivity

based method [131]. The studies conducted in this chapter reveal the following

(i) The control areas determined with the proposed method remain valid for wide range of loading conditions where as in case of the Jacobian sensitivity method voltage control areas have to be recomputed for small change in loading conditions.

(ii) As the number of features selected to determine the control areas increases in the proposed method or the threshold value (α) decreases in the sensitivity based method. the number of control areas decreases.

(iii) The buses within each control area, obtained with the proper choice of features or values of threshold, exhibit identical $Q - V$ curves.

The present work has considered a fixed topology of the network for determining the control areas. However, the proposed method is quite general and can be easily extended to cover different network topologies and much wider range of loading conditions.

Chapter 6

Impact of Generator and FACTS Devices' Rescheduling on Voltage Stability Margin

6.1 Introduction

For secure operation of stressed power systems, it is essential to provide operators the information regarding voltage stability margin. The system should be operated with an adequate voltage margin which can be achieved through appropriate control actions. In chapters 3 and 4, methods were developed to predict the static as well as dynamic stability margins. To increase static stability margin, Tiranuchit et al. proposed [83] an optimal generation scheduling scheme which maximizes the minimum singular value of the power flow Jacobian using a linear programming technique. Begovic et al. [118] demonstrated that by using an optimal power flow strategy, which minimizes the weighted sum of the absolute values of the control actions, voltage stability margin can be enhanced. Dynamic bifurcations, which reduce the stability margin, can be avoided by using FACTS devices with proper feed-back signal and gain of controllers [231].

Traditionally, generation rescheduling is performed in view of minimization of total fuel cost of thermal plants or system transmission loss. These schemes form a part of modern energy management system. Reference [122] presents a review of various optimal power flow strategies being used in practice. However, effect of these conventional optimal power flow schemes considering the FACTS devices on the stability margin, probably, has not

been reported in the literature. Some of the FACTS devices include controllable series capacitors (CSC), static phase angle regulators (PAR) and static VAR compensators (SVC).

In this chapter, following optimal power flow schemes have been considered for determining the setting of generators and FACTS devices and their relative impact on voltage stability margin has been studied.

(i) Minimization of total real power transmission loss.

(ii) Minimization of total reactive power transmission loss.

A simple scheme based on identification of weakest bus / control area through continuation power flow method has been suggested for optimal location of FACTS devices.

The voltage stability margin has been obtained and compared for the above two formulations in terms of total system reactive power margin for IEEE-14 bus, IEEE-30 bus and 75 bus UPSEB systems. The reactive power margin has been computed by estimating the closest distance of operating point to the saddle node bifurcation point in reactive power load parameter space [174].

6.2 Identification of Weakest Bus and Control Area

For identification of weakest bus, continuation power flow [139] method has been used. This method overcomes the non- convergence of conventional load flow algorithms near the voltage stability limit. The continuation power flow analysis described below, overcomes this problem by reformulating the power flow equations so that they remain well conditioned at all possible loading conditions.

6.2.1 Continuation Power Flow

The continuation power flow analysis uses an iterative process involving predictor and corrector steps as shown in Figure 6.1. From a known initial solution (A), a tangent predictor is used to estimate the solution (B) for a specified pattern of load increase. The corrector step then determines the exact solution (C) using conventional power flow analysis with the system load assumed to be constant.

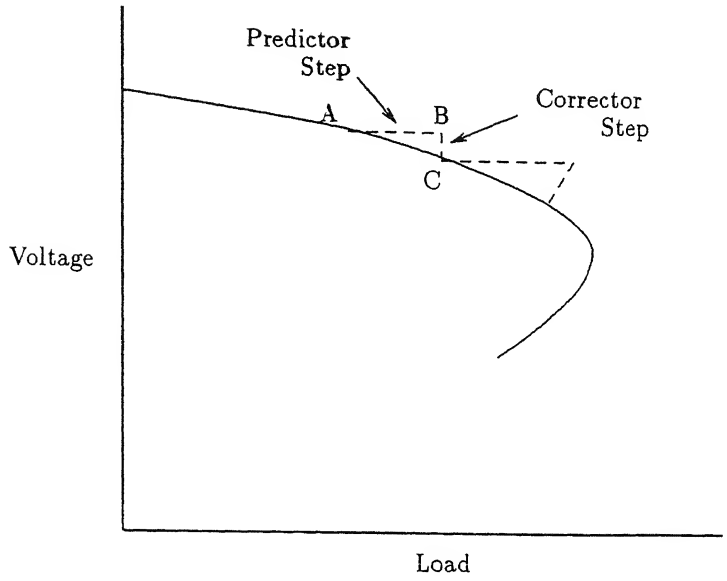

Figure 6.1: Contineuation power flow analysis

The basic equations are similar to those of standard power flow analysis except that the increase in load is added as parameter. The inclusion of this load parameter results in the steady state power flow equations expressed as

$$F(\theta, V, \lambda) = 0 \tag{6.1}$$

where
λ is the load parameter
θ is the vector of bus voltage angles
V is the vector of bus voltage magnitudes
The above set of non-linear equations is solved by specifying a value of λ such that

$$0 \leq \lambda \leq \lambda_{critical}$$

$\lambda = 0$ represents the base load condition and $\lambda = \lambda_{critical}$ represents critical load parameter value.

Predictor step:

In the predictor step, a linear approximation is used to estimate the next solution for a change in one of the state variables (i.e. θ, V, or λ). Differentiation of equation (6.1) with respect to the state variables at the initial solution point results in the following set of linear equations

$$dF = \frac{\partial F}{\partial \theta} d\theta + \frac{\partial F}{\partial V} dV + \frac{\partial F}{\partial \lambda} d\lambda = 0$$

or

$$\begin{bmatrix} F_\theta & F_V & F_\lambda \end{bmatrix} \begin{bmatrix} d\theta \\ dV \\ d\lambda \end{bmatrix} = 0 \tag{6.2}$$

The insertion of λ in power flow equations adds one more unknown variable. Hence to solve the equation (6.2), one of the components of the tangent vector is set to +1 or -1. This also helps in removing the ill-conditioning of the matrix. This component is referred as the *Continuation Parameter*. Equation (6.2) now becomes

$$\begin{bmatrix} F_\theta & F_V & F_\lambda \\ & e_k & \end{bmatrix} \begin{bmatrix} d\theta \\ dV \\ d\lambda \end{bmatrix} = \begin{bmatrix} 0 \\ \pm 1 \end{bmatrix} \tag{6.3}$$

where e_k is a row vector with all elements equal to zero except for the kth element corresponding to the continuation parameter being equal to 1.

Initially, the load parameter λ is chosen as the continuation parameter and the corresponding component of the tangent vector is set to +1. During the subsequent predictor steps. the continuation parameter is chosen to be the state variable that has the greatest rate of change near the given solution, and sign of its slope determines the sign of the corresponding component of tangent vector.

Once the tangent vector is found, the prediction for the next solution is given by equation (6.4)

$$\begin{bmatrix} \theta \\ V \\ \lambda \end{bmatrix} = \begin{bmatrix} \theta_0 \\ V_0 \\ \lambda_0 \end{bmatrix} + \sigma \begin{bmatrix} d\theta \\ dV \\ d\lambda \end{bmatrix} \tag{6.4}$$

Where θ_0, V_0, λ_0 are the values of state variables at the beginning of the predictor step.

The step size σ is chosen so that a power flow solution exists with the specified continuation parameter. If for a given step size a solution is not found in corrector step, the step size is reduced and the corrector step is repeated until a successful solution is obtained.

Corrector Step:

In the corrector step. the original set of equations $F(\theta, V, \lambda) = 0$ is augmented by one equation that specifies the state variable . which is selected as the continuation parameter. Thus the new set of equations is

$$\begin{bmatrix} F(\theta, V, \lambda) \\ X_k - \eta \end{bmatrix} = 0 \tag{6.5}$$

In the above, X_k is the state variable selected as the continuation parameter and η is equal to predicted value of X_k. This set of equation can be solved using a slightly modified Newton-Raphson power flow method. The introduction of additional equation specifying X_k makes the Jacobian non-singular at the critical operating point and thus solutions corresponding to the lower portion of V-P curve can also be obtained.

6.2.2 Determination of Weak Buses

In continuation power flow analysis. the elements of the tangent vector represent differential change in the state variables in response to a differential change in system load. Therefore. the dV elements in a given tangent vector are useful in identifying *weak buses*. i.e., buses which experience large voltage change in response to a change in load. Sensitivity of bus voltage magnitude can be expressed with respect to total change in active power or total change in reactive power. i.e.,

$$\frac{dV_i}{dP_{total}} \quad or \quad \frac{dV_i}{dQ_{total}}$$

If,

K_{L_i} = a multiplier to designate the rate of load change at bus-i as λ changes.
ψ_i = power factor angle of load change at bus i. and
$S_{\Delta BASE}$ = apparent power which is chosen to provide appropriate scale of λ

then,

$$\begin{aligned} dP_{total} &= \sum_n P_{L_i} = (S_{\Delta BASE} \sum_n K_{L_i} cos(\psi_i)) d\lambda \\ &= C d\lambda \end{aligned}$$

The weakest bus-j is one which has maximum sensitivity

$$\left| \frac{dV_j}{C d\lambda} \right| = max \left[\left| \frac{dV_1}{C d\lambda} \right|, \left| \frac{dV_2}{C d\lambda} \right|, \cdots, \left| \frac{dV_n}{C d\lambda} \right| \right] \tag{6.6}$$

6.3 Placement of FACTS Devices

For determining the location of FACTS devices in a power system, following two heuristic rules have been proposed.

Rule:1 The SVC should be placed at the weakest bus of the system. Since the weakest bus undergoes maximum voltage deviation and has maximum deficit of reactive power, it has been considered to be an ideal choice for the placement of SVC.

Rule:2 The placement of CSC/PAR has been considered in a line connecting weakest control area containing the weakest bus to the strongest area of the system. CSC/PAR effectively helps in reducing the electrical distance of two buses and thus in transmitting more power. In order to facilitate transfer of power to the weakest bus/area facing deficit of reactive power, the line in which these devices are placed should be connected at the other end to a bus/area having maximum surplus power (strongest area).

To implement these rules, set of weakest buses was determined with the help of continuation power flow. Rule:1 is simple to execute. SVC is placed at the weakest bus. However, to apply Rule:2, information of weak buses/areas and strong buses / areas and their connectivity is needed. A procedure for the selection of line for placement of these devices are described below through a simple example.

Consider a network shown in Figure 6.2 which represens a part of the complete system. Suppose the weakest bus is bus-C belonging to control area - I and the areas - II (containing bus - A) and IV (containing bus - D) are weak as compared to area - III (containing buses B and E). Assume that the descending order of the weakest areas are area - I, area - IV. area - II and area - III.

Since, amongst the areas directly connected to area - I, area - III is in a stronger position to supply reactive power to area - I, CSC or PAR can be placed in the line joining area - I and area - III.

If both the devices (CSC and PAR) are required to be placed for supporting area - I, it has been suggested to place CSC in a line joining weakest and the strongest area (i.e., area - I and area - III) and PAR in a line joining the weakest area and the next strongest area (area- I and area - II in the present case).

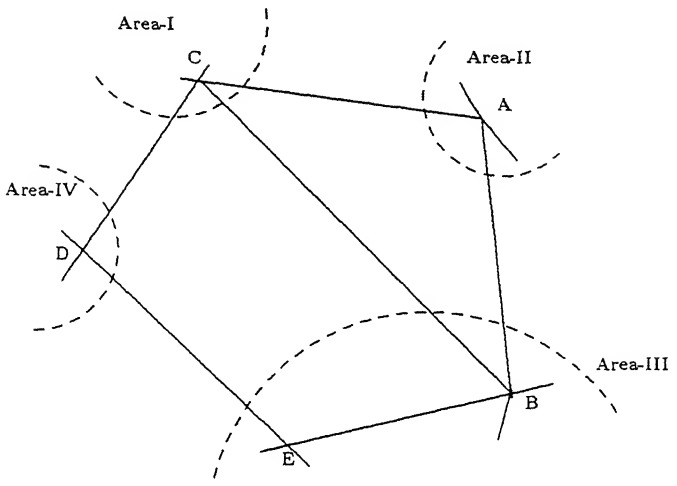

Figure 6.2: Connectivity of a partial system

6.4 Modeling of FACTS Devices

Flexible ac transmission system (FACTS) consisting of controllable series compensator (CSC), phase angle regulator (PAR) and static VAR compensator (SVC) can be used in the system for greater control of power, secure loading of transmission lines to levels near to their thermal limits, and to increase ability to transfer power between control areas. The static models of these devices used for optimal load flow analysis are described below.

6.4.1 Controllable Series Compensator (CSC)

Controllable series compensators (CSC) are connected in series with the line conductors to compensate for the inductive reactance of the line. This reduces the transfer reactance between the buses to which the line is connected, increases maximum power that can be transmitted and reduces the effective reactive power losses. Though the series capacitors are not usually installed for voltage control, they do contribute for improved voltage control and reactive power balance.

Figure 6.3 shows a series compensated transmission line-l represented by its lumped Π equivalent parameters connected between bus-i and bus-j. The complex power flowing from bus-i to bus-j ($\bar{S}_{ij} = P_{ij} + jQ_{ij}$) can be expressed as

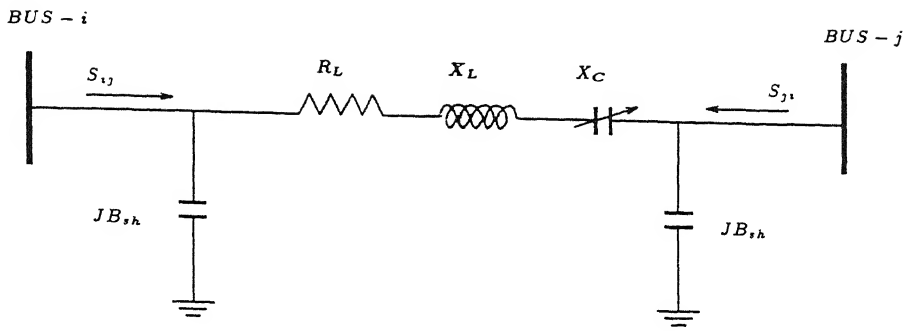

Figure 6.3: Π-Equivalent model of series compensated tranmsssion line

$$\begin{aligned}\bar{S}_{ij}^{*} &= P_{ij} - jQ_{ij} = \bar{V}_i^{*}\bar{I}_{ij} \\ &= \bar{V}_i^{*}[(\bar{V}_i - \bar{V}_j)\bar{Y}_{ij} + \bar{V}_i(jB_{sh})] \\ &= V_i^2[G_{ij} + j(B_{ij} + B_{sh})] - \bar{V}_i^{*}\bar{V}_j(G_{ij} + jB_{ij}) \qquad (6.7)\end{aligned}$$

where

$G_{ij} + jB_{ij}$=Y_{ser}=$1/Z_{ser}$

Z_{ser}=$R_L + jX_L - jX_C$

Equating the real and imaginary parts of the above equation. the expression for real and reactive power flows can be written as.

$$P_{ij} = V_i^2 G_{ij} - V_i V_j G_{ij}\cos(\delta_i - \delta_j) - V_i V_j B_{ij}\sin(\delta_i - \delta_j) \qquad (6.8)$$

$$Q_{ij} = -V_i^2(B_{ij} + B_{sh}) - V_i V_j G_{ij}\sin(\delta_i - \delta_j) + V_i V_j B_{ij}\cos(\delta_i - \delta_j) \qquad (6.9)$$

Similarly. the real and reactive power flows from bus-j to bus-i can be expressed as.

$$P_{ji} = V_j^2 G_{ij} - V_i V_j G_{ij}\cos(\delta_i - \delta_j) + V_i V_j B_{ij}\sin(\delta_i - \delta_j) \qquad (6.10)$$

$$Q_{ji} = -V_j^2(B_{ij} + B_{sh}) + V_i V_j G_{ij}\sin(\delta_i - \delta_j) + V_i V_j B_{ij}\cos(\delta_i - \delta_j) \qquad (6.11)$$

Equations (6.8) to (6.11) form the model of CSC for optimal power flow formulation.

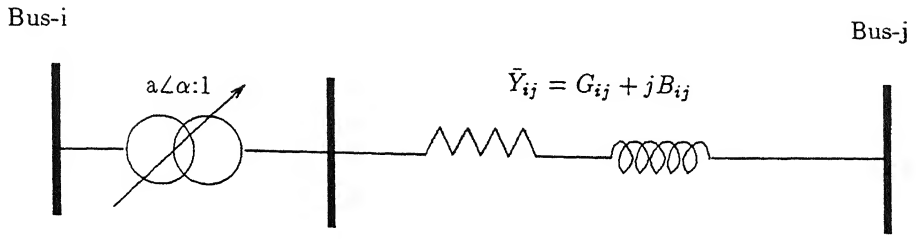

Figure 6.4: Phase angle regulator - single-line diagram

6.4.2 Phase Angle Regulator

In a phase angle regulator, the phase shift is accomplished by adding or subtracting a variable voltage component in perpendicular to the phase voltage of the line. Figure 6.4 shows static model of phase angle regulator connected between bus-i and bus-j and having complex taping $a\angle\alpha : 1$ $[(a_r + ja_i) : 1]$. $\bar{Y}_{ij}$ is the series admittance of the transformer. The real and reactive power flows from bus-i to bus-j can be derived similar to the controllable series compensator and can be expressed as

$$\begin{aligned} P_{ij} &= Re\left\{V_i^*\left[V_i\frac{Y_{ij}}{a^2} - V_j\frac{Y_{ij}}{a^*}\right]\right\} \\ &= \frac{V_i^2 G_{ii}}{a^2} - \frac{V_i V_j}{a}G_{ij}cos(\delta_i - \delta_j + \alpha) - \frac{V_i V_j}{a}B_{ij}sin(\delta_i - \delta_j + \alpha) \end{aligned} \tag{6.12}$$

and

$$\begin{aligned} Q_{ij} &= -Im\left\{V_i^*\left[V_i\frac{Y_{ij}}{a^2} - V_j\frac{Y_{ij}}{a^*}\right]\right\} \\ &= -\frac{V_i^2 B_{ii}}{a^2} + \frac{V_i V_j}{a}B_{ij}cos(\delta_i - \delta_j + \alpha) - \frac{V_i V_j}{a}G_{ij}sin(\delta_i - \delta_j + \alpha) \end{aligned} \tag{6.13}$$

Similarly real and reactive power flows from bus-j to bus-i can be written as

$$\begin{aligned} P_{ji} &= Re\left\{V_j^*\left[V_j\frac{Y_{ij}}{a^2} - V_i\frac{Y_{ij}}{a}\right]\right\} \\ &= \frac{V_j^2 G_{ii}}{a^2} - \frac{V_i V_j}{a}G_{ij}cos(\delta_i - \delta_j + \alpha) + \frac{V_i V_j}{a}B_{ij}sin(\delta_i - \delta_j + \alpha) \end{aligned} \tag{6.14}$$

and

$$\begin{aligned} Q_{ji} &= -Im\left\{V_j^*\left[V_j\frac{Y_{ij}}{a^2} - V_i\frac{Y_{ij}}{a}\right]\right\} \\ &= -\frac{V_j^2 B_{ii}}{a^2} + \frac{V_i V_j}{a}B_{ij}cos(\delta_i - \delta_j + \alpha) - \frac{V_i V_j}{a}G_{ij}sin(\delta_i - \delta_j + \alpha) \end{aligned} \tag{6.15}$$

Equations (6.12) to (6.15) form the model of PAR for optimal power flow formulation.

6.4.3 Static VAR Compensator

The static VAR compensator (SVC) is an important component for voltage control in power systems, which can help to maintain a bus voltage magnitude at a desired value during load variations. The SVC can both generate and absorb reactive power by means of thyristor controlled elements. It is usually continuously controllable over the full operating range determined by rating of the component.

The inclusion of SVC models in the power flow program is fairly straight forward. The reactive power output of an SVC can be computed as

$$Q_{SVC} = V_t(V_t - V_{ref})/X_{SL} \tag{6.16}$$

Where X_{SL} is the equivalent slope reactance in p.u., equal to slope of the voltage control characteristics, and V_t and V_{ref} are the node and reference voltage magnitudes. respectively. The equation (6.16) is valid as long as the reactive power Q_{SVC} is between limits. set by available inductive (B_{ind}) and capacitive (B_{cap}) susceptances, defined below:

$$Q_{max} = B_{ind} * V_{ref}^2 \tag{6.17}$$

$$Q_{min} = B_{cap} * V_{ref}^2 \tag{6.18}$$

If slope X_{SL} is small $V_{t_{min}}$ and $V_{t_{max}}$ will be close to V_{ref}. If the SVC is operating at limit. the corresponding susceptance value i.e. B_{cap} or B_{ind} is added to the bus admittance matrix Y_{BUS}.

6.5 Optimal Power Flow Model

The proposed model of optimal power flow has been formulated to obtain both real and reactive power setting of sources and also the the settings of FACTS devices in view of minimizing either the total system real power loss or the total system reactive power loss subject to the system operating constraints. It can be expressed as

$$Minimize\ P_{Loss}\ or\ Minimize\ Q_{Loss} \tag{6.19}$$

Subject to real and reactive power balance equations.

$$\sum_{i=1}^{N_g} P_{Gi} - P_{Loss} - P_D = 0 \tag{6.20}$$

$$\sum_{i=1}^{N_q} Q_{Gi} - Q_{Loss} - Q_D = 0 \tag{6.21}$$

and set of inequality constraints

$$P_{Gi}^{\min} \leq P_{Gi} \leq P_{Gi}^{\max} \qquad i = 1,.....N_g \tag{6.22}$$

$$Q_{Gi}^{\min} \leq Q_{Gi} \leq Q_{Gi}^{\max} \qquad i = 1,.....N_q \tag{6.23}$$

$$V_i^{\min} \leq V_i \leq V_i^{\max} \qquad i = 1,.....N \tag{6.24}$$

where

P_{Loss}	=	Total system real power loss
Q_{Loss}	=	Total system reactive power loss
P_{G_i}	=	Real power output of generator-i
Q_{G_i}	=	Reactive power output of source-i
P_D	=	Total real power demand of the system
Q_D	=	Total reactive power demand of the system
V_i	=	Voltage magnitude at bus-i
N_g	=	Total number of generators
N_q	=	Total number of reactive power sources including generators.

Additional constraints for FACTS devices are:

$$X_c^{\min} \leq X_c \leq X_c^{\max} \tag{6.25}$$

$$\phi^{\min} \leq \phi \leq \phi^{\max} \tag{6.26}$$

$$Q_{SVC}^{\min} \leq Q_{SVC} \leq Q_{SVC}^{\max} \tag{6.27}$$

The objective functions P_{Loss} and Q_{Loss} have been expressed as

OBJ-I : Real power loss minimization

$$P_{loss} = \sum_{i=1}^{Nl} P_{LM} + P_{ML} \tag{6.28}$$

OBJ-II : Reactive power loss minimization

$$Q_{loss} = \sum_{i=1}^{Nl} Q_{LM} + Q_{ML} \tag{6.29}$$

Where line i is connected between buses M & L (Total Nl lines in the system) and
P_{LM} = Real power flow from bus-L to bus-M in line-i
P_{ML} = Real power flow from bus-M to bus-L in line-i
Q_{LM} = Reactive power flow from bus-L to bus-M in line-i
Q_{ML} = Reactive power flow from bus-M to bus-L in line-i

With the above two objectives, five test cases were simulated for each system as given below:

Case-I: Rescheduling of generators with FACTS devices were made inoperative i.e. their outputs set to zero.

Case-II: Optimal rescheduling of CSC with other FACTS devices made inoperative and generators' output fixed to their base values.

Case-III: Same as case-II but considering the rescheduling of only PAR.

Case-IV: Same as case-II but considering the rescheduling of only SVC.

Case-V: Rescheduling of generators and all the FACTS devices, simultaneously.

6.6 Reactive Power Margin

For a given stable operating state and reactive loading vector ($Q_L = Q_L^0$), when Q_L is varied, the operating state may change. Let at $Q_L = Q_L^*$ the load flow Jacobian is singular. In reactive parameter space set of all Q_L, such that the load flow Jacobian is singular. define a boundary of the feasible region (say Σ) for stable operation. Σ typically forms a hypersurface. When the reactive loads encounter Σ, the saddle node bifurcation can result in catastrophic voltage collapse and may lead to system blackout [90,105]. One of the ways to monitor the proximity of an operating point to voltage collapse is to measure the closest distance between operating point Q_L^0 and the hypersurface Σ. Although the geometry of Σ is not known, Σ has been assumed to be convex in the present study. It is useful to calculate a critical reactive load power Q_L^* in Σ for which $\|Q_L^* - Q_L^0\|_2$ is a local minimum [148,174,175,208]. The line segment Q_L^0 to Q_L^* represents a worst case reactive load variation and $\|Q_L^* - Q_L^0\|_2$ measures the proximity of Q_L^0 to Σ.

This problem has been formulated as an optimization problem and it was solved by

using Newton-Raphson method in reference [174, 208]. A sequential quadratic programming algorithm has been used in the present work, to find Q_L^* such that $\|Q_L^* - Q_L^0\|_2$ is a minimum while satisfying various constraints.

6.7 Results

The studies were conducted on the following three sample systems using HP 9000/735 computer:

System–A: IEEE-14 bus system given in Appendix–C
System–B: IEEE-30 bus system given in Appendix–D
System–C: 75-bus Indian system given in Appendix–E.

For location of FACTS devices the eight most weak buses/areas were selected using continuation power flow. SVC was located at the weakest bus. PAR and CSC were located with the knowledge of the eight weakest buses and areas along with the network connectivity information as described in section 6.3. The range of SVC was considered to be -1.0 p.u. to 1.0 p.u. CSC was assumed to provide compensation of 0 to 80%. PAR was assumed to operate in the range of ±30 degrees. Sequential quadratic programming was used for rescheduling of generators' output and optimal setting of FACTS devices to minimize either the real power transmission loss (P_{Loss}) or the reactive power transmission loss (Q_{Loss}). The results of studies conducted on the three systems are described below.

6.7.1 System–A

The eight most weakest buses computed by continuation power flow method, in their rank order, for the IEEE-14 bus system were bus-14, bus-10, bus-7, bus-11, bus-6, bus-13, bus-9 and bus-12. These buses belong to the control areas - 2,4,2,6(transformer internal bus),8,1 and 7 respectively as found in chapter 5 (Table 5.2,fea = 5). Hence, SVC was placed at the weakest bus-14(area -2). Area -2 is directly connected to areas - 1,4 and 8. Although area - 1 is less weaker compared to area - 8, CSC has been placed in the line joining area -2(bus-14) and area - 8(bus-13). This was done due to the fact that element between areas - 2 and 1 is a transformer where CSC cannot be placed. PAR was located in the line joining area - 2 and area - 4.

Table 6.1: Reactive power (voltage stability) margin for system-A

Objective function	Measure	Base Case	Case-1	Case-2	Case-3	Case-4	Case5
OBJ-I	$Q_m(L_1)$	1.056600	1.106956	1.127756	1.060989	1.151047	1.152053
	$Q_m(L_2)$	0.362286	0.367045	0.387748	0.362901	0.395007	0.395338
OBJ-II	$Q_m(L_1)$	1.056600	1.107990	1.128756	1.066404	1.179748	1.186609
	$Q_m(L_2)$	0.362286	0.369935	0.388848	0.365454	0.404995	0.407582

The optimization program was run using sequential quadratic programming for minimizing both the OBJ-I and OBJ-II separately for all the five cases defined in section 6.5. The L_1 and L_2 norm of reactive power margin (Q_m) were calculated using method described in section 6.6 for all the test cases at the final optimal values of the system states and also at the base case. These margin values have been presented in Table 6.1.

The optimal settings of the generators and FACTS devices for only case-5, obtained with the OBJ-I and OBJ-II along with their base values, are given in Table 6.2.

From Table 6.1 it can be observed that the reactive power margin increases more with optimal setting of generators and FACTS devices using OBJ-II as compared to the OBJ-I. Amongst all the three FACTS devices placed individually, the SVC has been found to be the most effective in maximizing the margin followed by PAR and CSC in sequence. When only generator rescheduling (case-1) was considered, it has also effectively increased the reactive power margin. With all the devices considered simultaneously (case-5), the increase in reactive power margin is maximum.

6.7.2 System–B

The eight most weakest buses as determined by Continuation Power Flow Method, in their rank order for the IEEE 30-bus system, were bus-30, bus-26, bus-29, bus-24, bus-19, bus-20 and bus-23. These buses belong to control areas 1,17,1,15,10,11 and 9 respectively as given in chapter 5 (Table - 5.5, fea = 13). Hence, SVC has been placed at the weakest bus (bus-30). Area - 1(bus - 30) is directly connected to area - 9 only. Hence CSC was

Table 6.2: Optimal settings of Generators and FACTS devices of System-A

Variable	Base case	OBJ-I	OBJ-II
P_{G_1}	2.1061	0.6573	0.6696
P_{G_2}	0.4000	1.0000	1.0000
P_{G_3}	0.2000	1.0000	0.9892
Q_{G_1}	-0.1624	-0.2305	-0.3955
Q_{G_2}	0.3362	0.0161	0.3352
Q_{G_3}	0.2033	0.2400	0.2400
Q_{G_4}	0.2173	0.2429	0.3195
Q_{G_5}	0.1708	0.1486	0.1011
SVC	0.0000	0.0805	0.0401
CSC	0.0000	0.0073	0.0000
PAR	0.0000	-0.6896	-0.3772

placed in the line joining area - 1(bus-30) and area - 9(bus-10). Location of PAR was considered in the line connecting bus-28 and bus-3 to facilitate more power flow from stronger control area (area - 14)to the weakest area via transformer between buses 28 and 10.

The optimization program was run using sequential quadratic programming for minimizing both OBJ-I and OBJ-II separately for all the five cases and reactive power margin (Q_m) was determined for all the test cases at the final optimal values of the system states and also at the base case. These margins have been presented in Table 6.3.

The optimal setting of the generators and FACTS devices for only case-5 obtained with the two objectives along with their base values are given in Table 6.4.

From Table 6.3 it can be observed that the reactive power margin increases more with optimal setting of generators and FACTS devices using OBJ-II compared to OBJ-I. Amongst all the three FACTS devices placed individually, the SVC in this system also has been found to be the most effective in maximizing the margin followed by PAR and CSC in sequence. Only generator rescheduling (Case-1) has also effectively increased the reactive power margin. With all the devices considered simultaneously (Case-5), the increase in reactive power margin is maximum.

Table 6.3: Reactive power (voltage stability) margin for system-B

Objective function	Measure	Base Case	Case-1	Case-2	Case-3	Case-4	Case5
OBJ-I	$Q_m(L_1)$	0.590885	0.726689	0.732648	0.768940	0.796919	0.809230
	$Q_m(L_2)$	0.130104	0.206266	0.204177	0.198372	0.224532	0.225717
OBJ-II	$Q_m(L_1)$	0.590885	0.741618	0.740053	0.785958	0.819913	0.821598
	$Q_m(L_2)$	0.130104	0.206949	0.206527	0.200721	0.227055	0.228845

Table 6.4: Optimal settings of Generators and FACTS devices of System-B

Variable	Base case	OBJ-I	OBJ-II
P_{G_1}	2.3517	0.5000	0.4782
P_{G_2}	0.4000	1.1800	1.0765
P_{G_3}	0.2000	1.2197	1.3545
Q_{G_1}	-0.1590	-0.0925	-0.1428
Q_{G_2}	0.5000	0.1654	0.2096
Q_{G_3}	0.1988	0.3612	0.4099
Q_{G_4}	0.2280	0.1841	0.0412
Q_{G_5}	0.3625	0.2953	0.34351
Q_{G_6}	0.1944	0.1453	0.10243
SVC	0.0000	-0.0084	-0.0115
CSC	0.0000	0.0024	0.0105
PAR	0.0000	0.1627	0.0720

Table 6.5: Reactive power (voltage stability) margin for system-C

Objective function	Measure	Base Case	Case-1	Case-2	Case-3	Case-4	Case5
OBJ-I	$Q_m(L_1)$	1.8322	1.9527	1.8473	1.8227	1.9556	2.1045
	$Q_m(L_2)$	0.0867	0.0934	0.0871	0.0871	0.1025	0.1587
OBJ-II	$Q_m(L_1)$	1.8322	2.0814	1.8612	1.8583	1.9824	2.4904
	$Q_m(L_2)$	0.0867	0.0938	0.0878	0.0876	0.1092	0.1605

6.7.3 System–C

The eight most weakest buses in their rank order, for UPSEB 75-bus system as computed by continuation power flow method, were bus-52, bus-70, bus-72, bus-51, bus-60, bus-25, bus-22 and bus-29. Hence, the SVC was placed at the weakest bus (bus-52). Out of these eight buses bus-70, bus-72, bus-60 and bus-25 belong to one control area - 2(refer Table 5.7,fea = 30) and bus-52 and bus-51 form another control area - 1 as determined in chapter 5. In order to provide reactive power support to weakest bus - 52(area - 1), CSC was placed in the only link between bus - 51(area - 1) and stronger bus - 27(not included in the list of 8 weakest buses). Next weakest control area - 2 is directly connected to only area - 3(bus-22). However, element between weakest area - 2 and area - 3 is a transformer where PAR can not be placed. Hence, it was placed between bus - 22 and stronger bus-26.

The optimization program was run using sequential quadratic programming for minimizing both objectives OBJ-I and OBJ-II separately for all the test cases and reactive power margin (Qm) has been computed for all the test cases at final optimal values of the system states and also at the base case. These margins have been presented in Table 6.6.

The optimal settings of the generators and FACTS devices for only case-5 obtained with the OBJ-I and OBJ-II along with their base values are given in Table 6.5.

From Table 6.5 it can be observed that the reactive power margin increases more with optimal setting of generators and FACTS devices using OBJ-II compared to the OBJ-I. Amongst all the three FACTS devices placed individually the SVC has been found to be the most effective in maximizing the margin followed by CSC and PAR in sequence. When only generator rescheduling (case-1) was considered, it has also effectively increased the

Table 6.6: Optimal settings of Generators and FACTS devices of System-C

Variable	Base case	OBJ-I	OBJ-II
P_{G_1}	7.7515	5.2587	5.3752
P_{G_2}	2.6000	1.4922	3.0000
P_{G_3}	1.8000	2.0000	2.0000
P_{G_4}	1.0000	1.7000	1.7000
P_{G_5}	1.8000	2.4000	2.4000
P_{G_6}	1.2000	1.2000	1.2000
P_{G_7}	0.6000	1.0000	1.0000
P_{G_8}	0.8000	1.0000	1.0000
P_{G_9}	5.5000	5.3458	3.7495
$P_{G_{10}}$	0.8000	1.2000	1.2000
$P_{G_{11}}$	1.0900	2.0000	2.0000
$P_{G_{12}}$	18.0000	18.0000	18.0000
$P_{G_{13}}$	9.0000	9.0000	9.0000
$P_{G_{14}}$	1.5000	1.5000	1.5000
$P_{G_{15}}$	4.5400	4.5400	4.5400
Q_{G_1}	0.2016	0.2653	0.1007
Q_{G_2}	0.9600	0.4279	0.4046
Q_{G_3}	0.6876	0.5519	0.4790
Q_{G_4}	0.4962	0.0543	0.0000
Q_{G_5}	0.1948	0.2200	0.20850
Q_{G_6}	0.1161	0.1176	0.1120
Q_{G_7}	0.0485	0.0592	0.0546
Q_{G_8}	0.6800	0.3656	0.0490
Q_{G_9}	0.9691	0.3638	0.1579
$Q_{G_{10}}$	0.3165	0.2333	0.0000
$Q_{G_{11}}$	0.6242	0.48154	0.4046
$Q_{G_{12}}$	2.4890	1.44807	1.3082
$Q_{G_{13}}$	1.2186	0.7906	0.7253
$Q_{G_{14}}$	0.3074	0.0738	0.2464
$Q_{G_{15}}$	-0.3000	-0.3000	-0.3000
SVC	0.0000	-0.0386	-0.2385
CSC	0.0000	0.0203	0.0490
PAR	0.0000	2.80	3.34

reactive power margin in this system also. With all the devices considered simultaneously (case-5), the increase in reactive power margin is maximum.

6.8 Conclusion

In this chapter, a simple method based on the identification of weakest buses obtained by continuation power flow method and the control areas has been used to decide the placement of FACTS devices. The optimal setting of FACTS devices and generators have been computed and their effect on maximization of stability margin were studied.

The studies presented in this chapter on three sample systems reveal the following,

(i) Considering either the real power loss minimization (OBJ-I) or the reactive power loss minimization (OBJ-II) in all the five cases have resulted into increase in voltage stability margin.

(ii) Reactive power loss minimization (OBJ-II) has been found to be more effective as compared to the real power loss minimization (OBJ-I) in enhancing the reactive power margin.

(iii) When the optimal adjustment of the FACTS devices were considered one at a time, the optimal adjustment of SVC (Case-IV) was found to be the most effective amongst the three devices with either of the two objectives.

(iv) The optimal adjustment of all the FACTS devices and source outputs, simultaneously, provide maximum increase in the stability margin.

Chapter 7

Conclusions

7.1 General

The developments in fast protective devices, controllers and their use in the power system networks has increased the transient stability limit of the system allowing more real power transfer through transmission lines. However, the stressed operation of power system, due to increased loading on generation and transmission network has made the possible threat of voltage instability more pronounced and the systems have become voltage stability limited. Since, the voltage itself is a poor indicator of voltage stability, specially in the presence of reactive power compensating devices, it is essential to determine voltage stability margin also for secure operation of the system. This thesis has addressed to certain aspects of voltage contingency selection forming a part of the security analysis, static and dynamic voltage stability margin prediction and the static voltage stability margin enhancement. The main contribution of the thesis include the development of,

- a new method for contingency selection consisting of a fast model based on Artificial Neural Network (ANN) for post outage voltage prediction and a fuzzy logic based contingency ranking method considering the bus voltage deviations as well as system voltage stability margin as described in chapter 2,

- a fast method for prediction of nearest saddle node bifurcation point in the system using an analog simulation based Neural Network given in chapter 3,

- a new method for determining the dynamic voltage stability margin with respect to the distance to closest Hopf bifurcation using an optimization technique covered in

chapter 4,

- a new method to determine voltage control area based on entropy concept valid for wide range of operating conditions reported in chapter 5, and
- a simple approach for siting of flexible A C Transmission system (FACTS) devices and studying the impact of optimal adjustment of generators and FACTS devices' output on static voltage stability margin enhancement given in chapter 6.

The objective of this chapter is to highlight the main findings of the work carried out in this thesis and provide suggestions for further research work in this area. Some of the main findings are given below.

7.2 Summary of Important Findings

In chapter 2, a new method based on ANN using Functional Link Network (FLN) model was developed for post-outage bus voltage prediction. Fuzzy logic has been used to compute the performance indices of the contingencies required for ranking them in order of their relative severities. Voltage stability margin has been included, probably for the first time, for contingency selection. Results of three systems reveal the following:

(1) Voltages predicted by the proposed FLN based ANN models are quite accurate and can be used for contingency selection. The average error in all the test cases were within 1%.

(2) The ANN based voltage prediction method is extremely fast. The maximum CPU time in all the three systems was found to be 0.24 seconds.

(3) Fuzzy logic can be effectively used for obtaining the performance indices (PIs) for various contingencies. It is free from misranking effect as it does not depend on the choice of weighting factors.

(4) The contingency ranking changes when the PI is calculated based on the voltage stability margin as compared to those obtained by using only the bus voltage deviations.

Chapter 3 has presented a new approach utilizing an analog simulation based ANN method for determining the closest saddle node bifurcation point. The results obtained on two sample systems were compared with sequential quadratic programming (SQP) method. The studies conducted in this chapter reveal the following.

(i) The parameter values at saddle node bifurcation point, obtained by the proposed method and the SQP method are comparable. Voltage stability margin defined as the Euclidean distance from base case operating point to the predicted saddle node bifurcation point by the two methods are almost equal.

(ii) The proposed analog simulation based method can be effectively used for real time prediction of the closest saddle node bifurcation point, as the CPU time required is much less compared to the SQP method.

(iii) The minimum eigenvalue of the load flow Jacobian at the predicted saddle node bifurcation point is close to zero obtained either by the proposed method or the SQP method.

(iv) The proposed analog simulation based approach is quite modular in nature and can be easily extended to large size systems.

In chapter 4, a new method based on optimization technique has been developed and demonstrated to estimate the closest Hopf bifurcation point in parameter space. The studies conducted in this chapter reveal the following:

(1) The proposed method effectively predicts the closest Hopf bifurcation point and does not require any assumption of pattern or the direction in which the load is to be increased.

(2) The distance to saddle node bifurcation point was found to be more than the closest Hopf bifurcation point in all the test systems.

(3) The minimum power margin to the Hopf bifurcation can be utilized as an useful index of proximity to voltage instability. The security boundary Σ to Hopf bifurcation defines limitation on power system performance and must be avoided to prevent instability of the system.

A new method for determining the voltage control areas, using entropy concept, has been suggested and demonstrated on three sample systems in chapter 5. The results have been compared with a sensitivity based method [131]. The studies conducted in this chapter reveal the following:

(1) The control areas determined with the proposed method remain valid for wide range of loading conditions whereas in case of the Jacobian sensitivity method [131] voltage control areas have to be recomputed for small change in loading conditions.

(2) As the number of features selected to determine the control areas increases in the proposed method or the threshold value (α) decreases in the sensitivity based method, the number of control areas decreases.

(3) The buses within each control area obtained with the proper choice of features or values of threshold exhibit identical $Q-V$ curves.

In chapter 6, a simple method based on the knowledge of identification of weakest buses obtained by continuation power flow and the control area has been used to decide the placement of FACTS devices. The optimal setting of FACTS devices and generators have been computed and their effect on maximization of stability margin was studied.

The studies presented in this chapter on three sample systems reveal the following.

(1) Considering either the real power loss minimization (OBJ-I) or the reactive power loss minimization (OBJ-II) as objective in all the five cases, increase in voltage stability margin is observed.

(2) Reactive power loss minimization (OBJ-II), as an objective to determine outputs of generators and/or FACTS devices, was found to be more effective as compared to the real power loss minimization (OBJ-I) in enhancing the voltage stability (reactive power) margin.

(3) When the optimal adjustment of the FACTS devices (CSC,PAR,SVC) were considered one at a time, the optimal adjustment of SVC alone (Case-IV) is found to be the most effective amongst the three devices with either of the two objectives (OBJ-I or OBJ-II) utilized.

(4) The optimal adjustment of all the FACTS devices and generator outputs simultaneously, results into maximum increase in the voltage stability margin.

7.3 Scope for Further Research

As consequence of investigations carried out in this thesis, the following aspects are being suggested as future research work to be carried out.

(i) The results obtained in chapter 3 and 4 were restricted to the smaller systems (3-bus and 9-bus systems) due to limitation of the available softwares (SPICE in chapter-3 and SQP in chapter-4). The approach can be demonstrated on larger practical sized systems with the new versions of these softwares having capabilities of handling large size problems. Further, the studies in chapter 4 can be extended to consider the dynamic models of loads.

(ii) In chapter 5 the work presented has considered a fixed topology of the network for determining the control area. However, the proposed method is quite general and can be easily extended to cover different network topologies and much wider range of loading conditions. Moreover the approach is required to be extended to define control areas from dynamic consideration, so that they can be utilized for dynamic voltage stability studies.

(iii) In chapter 6, a very simple approach was used to site the FACTS devices and the impact of rescheduling of these devices and generator outputs were studied on static voltage stability margin. A more rigorous studies considering the detailed models of FACTS devices can be used to find their optimum locations not only from point of enchancing static voltage stability / maximum power transfer, but also to increase the system dynamic voltage stability. Impact of optimum setting of these devices and generators can be studied in enhancing the dynamic voltage stability margin.

Bibliography

[1] T.E. DyLiacco, *The Adaptive Reliability Control System*, IEEE Trans. on Power Apparatus and Systems, Vol-PAS-86, 1967, pp. 517-531.

[2] J.F. Dopazo, O.A. Klitin, G.W. Stagg and M. Watson, *An Optimization Technique for Real and Reactive Power Allocation,* IEEE Proc., Vol-55, 1967, pp. 1877-1885.

[3] B. M. Weedy and B. R. Cox, *Voltage Stability of Radial Power Links,* Proc. IEE vol. 115 April 1968, pp. 528-536.

[4] B. Stott, *Decoupled Newton Load Flow,* IEEE Trans. on Power Apparatus and System, Vol-PAS-91, No.5, September/October 1972, pp. 1955-1959.

[5] N.M. Peterson, W.F. Tinney and D.W. Bree, *Iterative Linear AC Power Flow Solution for Fast Approximate Outage Studies,* IEEE Trans. on Power Apparatus and Systems, Vol-PAS-91, No.5, September/October 1972, pp. 2048-2058.

[6] T.E. DyLiacco, *Real-time Computer Control of Power Systems*, IEEE Proc., Vol. 62, No.7, July 1974, pp. 884-891.

[7] B. Stott and O. Alsac, *Fast Decoupled Load Flow,* IEEE Trans. on Power Apparatus and Systems, Vol-PAS-93, No.5, May 1974, pp. 859-869.

[8] Y. Yoshida, *Development of a Calculation Model of AC Voltage Stability in HVDC Transmission System*, Electrical Engg. in Japan, Vol. 94, No. 2, 1974, pp. 77-85.

[9] V.A. Venikov, V.A. Stroev, V.I. Idelchick and V.A. Torasov, *Estimation of System Steady State Stability in Load Flow Calculations*, IEEE Transactions on Power Apparatus and Systems, Vol. 94, May/June 1975, pp. 1034-1040.

[10] P.M. Anderson and A.A. Fouad, *Power System and Stability,* The Iowa University Press, 1977.

[11] H.H. Happ, *Optimal Power Dispatch - A Comprehensive Survey,* IEEE Trans. on Power Apparatus and Systems, Vol-PAS-96, No.3, May/June 1977 , pp. 841-854.

[12] P. J. King and E. H. Mamdami, *The application of Fuzzy Control System to Industrial Process,* Fuzzy Automata and Decision Process, 1977, pp. 321-330.

[13] V.A. Venikov, *Transient Processes in Electrical Power Systems*, Mir Publishers. Moscow, 1977.

[14] S. Abe, N. Hamada, A.Isono and K. Okudo, *Load Flow Convergence in Vicinity of Voltage Instability Limit,* IEEE Trans. on Power Apparatus and Systems Vol-PAS-97. Nov/Dec 1978, pp. 1983-1993.

[15] A. Capasso and E. Mariani, *Influnce of Generator Capability Curves Representation on System Voltage and Reactive Power Control Studies*, IEEE Trans. on Power Apparatus and Systems Vol-PAS-97, July/Aug 1978. pp. 1036-1041.

[16] L.H. Fink and K. Carlsen, *Operating Under Stress and Strain.* IEEE Spectrum. March 1978, pp. 48-53.

[17] W.R. Lachs, *System Reactive Power Limitations.* Paper # A 79 015-9, presented at the IEEE PES Winter Meeting, New York, Feb 4-9, 1979.

[18] G.C. Ejebe and B.F. Wollenberg, *Automatic Contingency Selection*, IEEE Trans. on Power Apparatus and Systems, Vol-PAS-98. No.1. January/February 1979. pp. 97-109.

[19] R.W.Hamming, *Coding and information theory.* Prentice-Hall. Englewood cliffs. NJ. 1980.

[20] Y. Tamura. K. Iba and S. Iwamoto, *A Method of Finding Multiple Load Flow Solutions for General Power Systems*, Paper # A80043-OD. IEEE PES Winter Meeting. February 1980.

[21] J. Zaborsky, K.W. Whang and K. Prasad, *Fast Contingency Evaluation Using Concentric Relaxation*, IEEE Trans. on Power Apparatus and Systems, Vol-PAS-99. No.1, January/Febraury 1980, pp 28-36.

[22] B.D. Hassard. N.D. Kazarinoff and Y.H. Wan. *Theory and Applications of Hopf Bifurcation*, Cambridge University Press, Cambridge, UK, 1981.

[23] T. Hayashi, *Analysis of Voltage Instability of AC-DC Interconnected Systems.* Electrical Engg. in Japan, Vol. 101, No. 4, 1981, pp. 46-53.

[24] IEEE Working Group, *Discription and Bibiliography of Major Economic-Security Functions Part-II- Bibiliography (1959-1972),* IEEE Trans. on Power Apparatus and Systems, Vol-PAS-100, No.1, January 1981, pp. 215-223.

[25] IEEE Working Group, *Discription and Bibiliography of Major Economic-Security Functions Part-III- Bibiliography (1973-1979),* IEEE Trans. on Power Apparatus and Systems, Vol-PAS-100, No.1, January 1981, pp. 224-235.

[26] J. Jaris, F.D. Galiana, *Quantitative Analysis of Steady State Stability in Power Networks*, IEEE Trans. on Power Apparatus and Systems, Vol. PAS-100, Jan. 1981, pp. 318-326.

[27] T.A. Mikolinnas and B.F. Wollenberg, *An Advance Contingency Selection Algorithms*, IEEE Trans. on Power Apparatus and System. Vol-PAS-100, No.2, February 1981, pp. 608-617. M.A. Pai, *Power System Stability Analysis by the Direct Method*. North Holland, New York, 1981.

[28] S.N. Talukdar and F.F. Wu, *Computer Aided Dispatch for Electric Power System*. IEEE Proc., Vol-69, No.10. October 1981, pp. 1212-1231.

[29] S. Abe, Y. Fukunaga, A. Isono and B. Kondo. *Power System Voltage Stability*, IEEE Trans. on Power Apparatus and System, Vol. PAS-101. No. 10. October 1982, pp. 3830-3840.

[30] F. Albuyeh, A. Bose and B. Heath, *Reactive Power Consideration in Automatic Contingency Selection*, IEEE Trans. on Power Apparatus and Systems, Vol-PAS-101, No.1, January 1982, pp. 107-112.

[31] L. O. Chua, G. N. Lin and J. J. Lum. *The (P + Q)-Port Transformer*. Int. Journal of Circuit Theory and Applications, Vol-10, 1982. pp. 335-359.

[32] T. Medicherla and S. Rastogi. *A Voltage Criterion Based Contingency Selection Technique*, IEEE Trans. on Power Apparatus and Systems. Vol-PAS-101. September 1982. pp. 3523-3531.

[33] K.T. Khu. M.G. Lauby and D.W. Bowen, *A Fast Linearization Method to Evaluate the Effects of Circuit Contingency Upon System Load Bus Voltages*. IEEE Trans. on Power Apparatus and Systems. Vol-PAS-101, October 1982. pp. 3926-3932.

[34] J. Arrillaga, C.P. Arnold and B.J. Harker, *Computer Modelling of Electrical Power Systems*, Wiley, Chichester, UK. 1983.

[35] R.C. Burchett and H.H. Happ., *Large Scale Security Dispatching : An Exact Model*. IEEE Trans. on Power Apparatus and Systems, Vol-PAS-102, No.9. September 1983. pp. 2995-2999.

[36] L. O. Chua, G. N. Lin, *Nonlinear Optimization with Constraint: a Cookbook Approach*, Int. Journal of Circuit Theory and Applications, Vol-11. 1983. pp. 141-159.

[37] C. S. Indulkar and B. Viswanathan. *Voltage Stability of EHV Lines with Series Compensation; Evaluation taking into Consideration Uncertainty of Load Parameters* IEEE Trans. on Power Apparatus and Systems, Vol-PAS-102, No., pp. 2317-2322. 1983

[38] M.G. Lauby, T.A. Mikolinnas and N.D. Reppen, *Contingency Selection of Branch Outage Causing Voltage Problems*. IEEE Trans. on Power Apparatus and Systems. Vol-PAS-102, No.12, December 1983, pp. 3899-3904.

[39] R.E. Palmer, R.C. Burchett, H.H. Happ. and D.R. Vierath, *Reactive Power Dispatching for Power System Voltage Security*, IEEE Trans. on Power Apparatus and Systems, Vol-PAS-102, No.12, December 1983, pp. 3905-3909.

[40] Y. Tamura, K. Iba and S. Iwamoto, *Relationship between Instability and Multiple Load Flow Solutions in Electric Power Systems*, IEEE Trans. on Power Systems, Vol. 102, No. 2, May 1983, pp. 1115-1125.

[41] R.G. Wasley and M. Daneshdoost, *Identification and Ranking of Critical Contingencies in dependent Variable Space,* IEEE Trans. on Power Apparatus and Systems, Vol-PAS-102, No.4, April 1983, pp. 888-892.

[42] Y.N. Yu, *Electric Power System Dynamics*, Academic Press, New York, 1983.

[43] E.H. Abed and P. Varaiya, *Nonlinear Oscillations in Power Systems*, Int. Jr. of Electric Power and Energy Systems. Vol. 6, No. 1, Jan. 1984, pp. 37-43.

[44] P. Borremans, A. Calvaer, J.P. de Reuck, J. Gooserens, E. Van Geert, J. Van Hecke and A. Van Ranst, *Voltage Stability: Fundamental Concepts and Comparison of Practical Criteria*, CIGRE report 38-11, August 1984.

[45] J. Carpentier, R. Girard and E. Scano, *Voltage Collapse Proximity Indicators Computed from an Optimal Power Flow*, Proc. 8th Power System Computation Conference, Helsinki, Finland, 1984, Butterworth London, pp. 671-678.

[46] T.F. Halpin, R. Fischl and R. Fink, *Analysis of Automatic Contingency Selection Algorithms*, IEEE Trans. on Power Apparatus and Systems, Vol-PAS-103, No. 5, May 1984, pp. 938-945.

[47] L. O. Chua and G. Lin, *Nonlinear Programming without computation*. IEEE Tarns. on Circuits and Systems, Vol-CAS-31, No. 2, February 1984, pp. 182-188.

[48] A.J. Wood and B.F. Wollenberg, *Power Generation, Operation and Control*. John Wiley & Sons. Inc., 1984.

[49] M. Brucoli, F. Torelli, M. Trovato, G. Carpinelli and F. Rossi *Voltage Stability Analysis of Electric Power Systems by Nonlinear Programming,* Electric Machines and Power Systems, Vol. 10, No. 5, 1985, pp. 403-416.

[50] W.R. Lachs, *Dynamic Study of Extreme System Reactive Power Deficit*, IEEE Trans. on Power Apparatus and System, Vol. 104, No. 9, September 1985, pp. 2420-2426.

[51] C.C. Liu and F.F. Wu, *Steady State Voltage Stability Regions of Power Systems*, Systems & Control Letter, Vol. 6, June 1985, pp. 23-31.

[52] K. Nara, H. Kodama, K. Tanaka, R.R. Shoultz, M.S.Chen and P.V. Olinda, *On Line Contingency Selection Algorithms for Voltage Security Analysis*. IEEE Trans. on Power Apparatus and Systems, Vol-PAS-104, No.4, April 1985, pp. 847-856.

[53] J. Zaborszky, G. Huang and K. W. Lu, *A Textured Model for Computationally Efficient Reactive Power Control and Management,* IEEE Trans. on Power Apparatus and Systems, Vol-PAS-104, No.7, July 1985, pp. 1718-1727.

[54] J.C. Alexander, *Oscillatory Solutions of a Model System of Nonlinear Swing Equations*, Int. Jr. of Electric Power and Energy Systems, Vol. 8 , No. 3, July 1986, pp. 130-136.

[55] M. Brucoli, M. L. Scala and F. Torelli, *Probablistic Approch to the Voltage Stability Analysis Interconnected Power System,* Electric Power System Research, Vol. 10, March 1986, pp 157-166.

[56] I. Dabbaghchi and G. Irisarri, *AEP automatic Contingency Selector : Branch Outage Impacts on Load Bus Volatge Profile,* IEEE Trans. on Power Systems, Vol-PWRS-1, No.1, Febraury 1986, pp. 37-45.

[57] H.G. Kwatny, A.K. Pasrija and L.Y. Bahar, *Static Bifurcation in Electric Power Networks: Loss of Steady-State Stability and Voltage Collapse*, IEEE Trans. on Circuits and Systems, Vol. 33, No. 10, October 1986, pp 981-991.

[58] C.C. Liu and K.L. Tomsovic, *An Expert System Assisting Decision - Making of Reactive Power/Voltage Control*, IEEE Trans. on Power Systems, Vol-PWRS-1, No.3, August 1986, pp. 195-201.

[59] D. W. Tank and J. J. Hopfield, *Simple Neural Optimization Networks: An A/D converter. Signal decision network. and Linear programming circuit,* IEEE Tarns. on Circuits and Systems, Vol-CAS-33, No. 5, May 1986, pp. 533-541.

[60] Y. Wallach, *Calculations and Programs for Power System Networks*, Prentice–Hall, Inc, Englewood Cliffs, New Jersey, 1986.

[61] K. Walve, *Modelling of Power System Components at Severe Disturbances*, CIGRE report 38-18, 1986.

[62] F.F. Wu and C.C. Liu, *Characterization of Power System Small Disturbance Stability with Models Incorporating Voltage Variation*, IEEE Trans. on Circuits and Systems, Vol. CAS-33, No. 4, April 1986, pp. 406-417.

[63] *Planning Against Voltage Collapse*, CIGRE Task Force report 38-01.03, Electra, No. 111, March 1987.

[64] C.L. DeMarco and A.R. Bergen, *A Security Measure for Random Load Disturbances in Nonlinear Power System Models*, IEEE Trans. on Circuits and Systems, Vol. 34, No. 12, Dec. 1987, pp. 1546-1557.

[65] Richard P. Lippmann, *An Introduction to Computing with Neural Nets*, IEEE ASSP Magazine, Vol. 4 No. 2, April 1987, pp. 4-21.

[66] J. Medanic, M. Ilic-Spong and J. Christensen, *Discrete Models of Slow Voltage Dynamics for Under Load Tap-Changing Transformer Coordination*, IEEE Trans. on Power Systems, Vol. 2, No. 4, Nov. 1987, pp. 873-882.

[67] B. Stott, O. Alsac and A.J. Monticelli, *Security Analysis and Optimization,* IEEE Proc. Vol.75, No.12, pp. 1622-1644, December 1987.

[68] W.F. Tinney and J.M. Bright, *Adaptive Reduction for Power Flow Equivalent,* IEEE Trans. on Power Systems, Vol-PWRS-2, No.2, pp. 351-360, May 1987.

[69] V. Brandwajn, *Efficient Bounding Method for Linear Contingency Analysis,* IEEE Trans. on Power Systems, Vol-PWRS-3, No.1, Febraury 1988, pp. 34-43.

[70] H.D. Chiang and F.F. Wu, *Stability of Nonlinear Systems Described by a Second Order Vector Differential Equations*, IEEE Trans. on Circuits and Systems, Vol. 35, No. 6, June 1988, pp. 703-711.

[71] H.D. Chiang, M.W. Hirsch and F.F. Wu, *Stability Regions of Nonlinear Autonomous Dynamical Systems*. IEEE Trans. on Automatic Control, Vol. 33, No. 1, Jan. 1988, pp. 16-27.

[72] R.L. Chen and P.P. Varaiya, *Degenerate Hopf Bifurcations in Power Systems*, IEEE Trans. on Circuits and Systems, Vol. 35, No. 7, June 1988, pp. 818-824.

[73] R.D. Christie and S.N. Talukdar, *Expert System for On-line Security Assesement-I Preliminary Design*, IEEE Trans. on Power Systems, Vol-PWRS-3, No.2, May 1988, pp. 654-659.

[74] M.P. Kennedy and L.O. Chua, *Neural Networks for Nonlinear Programming,* IEEE Trans. on Circuits and Systems, Vol.35, No.5, May 1988, pp. 554-562.

[75] M.G. Lauby, *Evaluation of Local DC Load Flow Screening Method For Branch Contingency Selection of Overloads*, IEEE Trans. on Power Systems, Vol-PWRS-3, No.3, pp. 923-928, May 1988.

[76] K.L. Lo, M.A. Bismil, R.D. MacColl and A.M. Moffatt, *A Comparision of MW Ranking Methods*, Electric Power Systems Research, Vol-15, 1988, pp. 157-171.

[77] F. Mercede, J.C. Chow, H. Yan and R. Fischl, *A Framework to Predict Voltage Collapse in Power Systems*, IEEE Trans. on Power Systems, Vol. 3, No. 4, Nov. 1988, pp. 1807-1813.

[78] O.O. Obadina and G.J. Berg, *Determination of Voltage Stability Limit in Multimachine Power Systems*, IEEE Trans. on Power Systems, Vol. 3, No. 4, Nov. 1988, pp. 1545-1554.

[79] J. P. Paul, J. Y. Leost and J. M. Tesseron, *Survey of Secondary Voltage Control in France. Present Realization and Investigation,* IEEE Trans. on Power Systems, Vol-PWRS-3, No.2, May 1988, pp. 505-511.

[80] R. Seydel, *From Equilibrium to Chaos: Practical Bifurcation and Stability Analysis*, Elsevier Science Publishers, North-Holland, 1988.

[81] D.J. Sobajic and Y.H. Pao, *An Artificial Intelligence System for Power System Contingency Screening,* IEEE Trans. on Power Systems, Vol-PWRS-3, No.2, May 1988, pp. 647-653.

[82] S.C. Tripathi, M.A. Rasheed and P.S. Satsangi, *Fast Contingency Analysis using System Theory Approach,* The Journal of The Institution of Engineers(India), Vol. 69, August 1988, pp. 26-32.

[83] A. Tiranuchit and R.J. Thomas, *A Posturing Strategy against Voltage Instabilities in Electric Power Systems*, IEEE Trans. on Power Systems, Vol. 3, No. 1, Feb. 1988, pp. 87-93.

[84] A. Tiranuchit, L.M. Ewerbring, R.A. Duryea, R.J. Thomas and F.T. Luk, *Towards a Computationally Feasible On-Line Voltage Instability Index*, IEEE Trans. on Power System, Vol. 3, No. 2, May 1988, pp. 669-675.

[85] F.F. Wu, *Real Time Network Security Monitoring, Assessment and Optimization*, Int. Journal of Electric Power and Energy Systems, Vol-10, No.2, April 1988, pp. 83-100.

[86] F.L. Alvarado and T.H. Jung, *Direct Detection of Voltage Collapse Conditions*, Proceedings: Bulk Power System Voltage Phenomena—Voltage Stability and Security, EPRI EL-6183, pp. 5.23-5.38, Jan. 1989.

[87] V. Brandwajn and M.G. Lauby, *Complete Bounding Method for AC Contingency Screening*, IEEE Trans. on Power Systems, Vol-PWRS-4, No.2, May 1989, pp. 724-729.

[88] Y. Chen and A. Bose, *Adaptive Pre-filter for the Voltage Contingency Selection Function*, paper presented at IEEE/PES Winter Meeting, New York, Feb. 1989.

[89] Y. Chen and A. Bose, *Direct Ranking for Voltage Contingency Ranking,* IEEE Trans. on Power Systems, Vol-PWRS-4, No.4 , November 1989, pp. 1335-1344.

[90] I. Dobson and H.D. Chiang, *Towards a Theory of Voltage Collapse in Electric Power Systems*, Systems & Control Letters, Vol. 13, 1989, pp. 253-262.

[91] I.A. Hiskens and D.J. Hill, *Energy Functions, Transient Stability and Voltage Behaviour in Power Systems with Nonlinear Loads*, IEEE Trans. on Power Systems, Vol. 4, No. 4, Oct 1989, pp. 1525-1533.

[92] C.C. Liu and K.T. Vu, *Analysis of Tap-Changer Dynamics and Construction of Voltage Stability Regions*, IEEE Trans. on Circuit and Systems, Vol. 36, No. 4, April 1989, pp. 575-590.

[93] K.L. Lo and M.A. Bismil, *A Comparison of Voltage Ranking Methods*, Electric Power Systems Research, Vol.16, 1989, pp. 127-140.

[94] M.A. Pai and M.G.O' Grady, *Voltage Collapse Analysis with Reactive Generation and Voltage Dependent Constraints*, Journal of Electric Machines and Power Systems, Vol. 17, No. 6, 1989, pp. 379-390.

[95] Yoh-Han Pao, *Adaptive pattern recognition and Neural networks*, Addition - Wesley publishing company Inc., 1989.

[96] C. Rajagopalan, P.W. Sauer and M.A. Pai, *Analysis of Voltage Control Systems exhibiting Hopf Bifurcation*, Proceedings of 28th IEEE Conference on Decision and Control, Tampa, FL, 1989, pp. 332-335.

[97] C. Rajagopalan, P.W. Sauer and M.A. Pai, *An Integrated Approach to Dynamic and Static Voltage Stability*, Proc. of 1989 American Control Conference, Pittsburg PA, Vol. 3, June 1989, pp. 1231-1235.

[98] Philip D. Wasserman, *Neural Computing Theory and Practice*, Van Nostarand Reinhold, New York, 1989.

[99] M.M. Begovic and A.G. Phadke, *Dynamic Simulation of Voltage Collapse*, IEEE Trans. on Power Systems, Vol. 5, No. 4, Nov. 1990, pp. 1529-1534.

[100] M.M. Begovic and D.R. Ostojic, *Determination of Critical Zones for Voltage Instability in Power Systems*, Proc. of 29th IEEE Conference on Decision and Control, Honolulu, Hawaii, December 1990, pp. 3011-3013.

[101] M.M. Begovic and A.G. Phadke, *Voltage Stability Assesment through Measurement of a Reduced State Vector* IEEE Trans. on Power Systems, Vol. 5, No. 1, Feb. 1990, pp. 198-203.

[102] T.J. Bertram, K.D. Demaree and L.C. Dangelmaier, *An Integrated Package for Real-time Security Enhancement*, IEEE Trans. on Power Systems, Vol-PWRS-5, No.2, May 1990, pp. 592-600.

[103] C.S. Chang, T.S. Chung and K.L. Lo, *Application of Pattern Recognition Techniques to Power System Security Analysis and Optimization*, IEEE Trans. on Power Systems, Vol PWRS 5, No.3, August 1990, pp. 835-841.

[104] Y. Chen and A. Bose, *Security Analysis for Voltage Problems Using a Reduced Model*, IEEE Trans. on Power Systems, Vol-PWRS-5, No.3, August 1990, pp. 933-940.

[105] H.D. Chiang, Ian Dobson, R.J. Thomas, J.S. Thorp and L.F. Ahmed, *On Voltage Collapse in Electric Power Systems*, IEEE Trans. on Power Systems, Vol. 5, No. 2, May 1990, pp. 601-611.

[106] J.C. Chow, R. Fischl and H. Yan, *On the Evaluation of Voltage Collapse Criteria*, IEEE Trans. on Power Systems, Vol. 5, No. 2, May 1990, pp. 612-620.

[107] C.L. DeMarco and T.J. Overbye, *An Energy Based Security Measure for Assessing Vulnerability to Voltage Collapse*, IEEE Trans. on Power Systems, Vol. 5, No. 2, May 1990, pp. 419-427.

[108] N. Flatabo, R. Ognedal and T. Carlsen, *Voltage Stability Conditions in a Power System Calculated by Sensitivity methods*, IEEE Trans. on Power Systems, Vol. 5 No. 4, Nov. 1990, pp. 1286-1293.

[109] R.K. Gupta, Z.A. Alaywan, R.B. Stuart and T.A. Reece, *Steady State Voltage Instability Operations Perspective*, IEEE Trans. on Power Systems, Vol. 5, No. 4, Nov. 1990, pp. 1345-1352.

[110] J.F. Hauer, *Eigenvalue Analysis and Frequency Domain Methods for System Dynamic Performance*, IEEE publication # 90 TH 0293-3 PWR.

[111] IEEE system dynamic performance subcommittee, *Voltage Stability of Power Systems: Concepts, Analytical Tools and Industry Experience*, IEEE document 90TH0358-2-PWR-1990.

[112] H.G. Kwatny and G.E. Piper, *Frequency Domain Analysis of Hopf Bifurcations in Electric Power Networks*, IEEE Trans. on Circuits and Systems CAS-37, No. 10, Dec. 1990, pp. 1317-1321.

[113] C. Lemaitre, J.P. Paul, J.M. Tesseron, Y. Harmand and Y.S. Zhao, *An Indicator of the Risk of Voltage profile Instability for Real-Time Control Applications*, IEEE Trans. on Power Systems, Vol. 5, No. 1, Feb. 1990, pp. 154-161.

[114] P.W. Sauer and M.A. Pai, *Power System Steady-State Stability and the Load Flow Jacobian*, IEEE Trans. on Power Systems, Vol. 5, No. 4, Nov. 1990, pp. 1374-1383.

[115] K.F. Schafer and J.F. Verstege, *Adaptive Procedure for Masking Effect Compensation in Contingency Selection Algorithms*, IEEE Trans. on Power Systems, Vol-PWRS-5, No.2, May 1990, pp. 539-546.

[116] Y. Sekine and H. Ohtsuki, *Cascaded Voltage Collapse*, IEEE Trans. on Power Systems, Vol. 5, No. 1, Feb. 1990, pp. 250-256.

[117] Patrick K. Simpson, *Artificial Neural Systems,* Pergamon Press, New York, 1990.

[118] M. Begovic, A. Meliopoulos and X. Chao, *Control of Voltage Stability via Optimal Power Flow*, Proc. of International NSF Workshop 'Bulk Power System Voltage Phenomena: Voltage Stability and Security', Deep Creek Lake, MD, August 1991, pp. 321-332.

[119] C. Concordia, *Voltage Instability*, Int. Jr. of Electrical Power & Energy System, Vol. 13, No. 1, Feb. 1991, pp. 14-20.

[120] N. Fernandopulle and R.S. Ramshaw, *Analysis of Synchronous Motor Stability using Hopf Bifurcation*, Electric Machines and Power Systems, Vol. 19, 1991, pp. 239-250.

[121] I.A. Hiskens and D.J. Hill, *Failure Modes of a Collapsing Power System*, Proceedings of the Workshop on Bulk Power System Voltage Phenomena, Deep Creek, MD, Aug. 1991.

[122] M. Huneault F.D. Galiana, *A Survey of the Optimal Power Flow Literature*, IEEE Trans. on Power Systems, Vol. 6, No. 2, May 1991, pp. 762-770.

[123] K. Iba, H. Suzuki, M. Egawa and T. Watanabe, *Calculation of Critical Loading Condition with Nose Curve using Homotopy Continuation Method*, IEEE Trans. on Power Systems. Vol. 6, No. 2, May 1991, pp. 584-593.

[124] B.H. Lee and K.Y. Lee, *A Study on Voltage Mechanism in Electric Power Systems*, IEEE Trans. on Power Systems, Vol. 6, No. 3, Aug. 1991, pp. 966-973.

[125] G. Leonidopoloulos, *Linear Power System Equations and Security Assessment*, Int. Journal of Electric Power and Energy Systems, Vol.13, No.2, 1991, pp. 100-102.

[126] M.A. Nayfeh, A.M.A. Hamdan and A.H. Nayfeh, *Chaos and Instability in a Power System: Sub-Harmonic Resonant Case*, Nonlinear dynamics 2, 1991, pp. 53-72.

[127] H. Ohtsuki, A. Yokoyama and Y. Sekine, *Reverse Action of On-Load Tap Changer in Association with Voltage Collapse*, IEEE Trans. on Power Systems, Vol. 6, No. 1, Feb. 1991, pp. 300-306.

[128] T.J. Overbye and C.L. DeMarco, *Improved Techniques for Power System Voltage Stability Assessment using Energy Methods*, IEEE Trans. on Power Systems, Vol. 6, No. 4, Nov. 1991, pp. 1446-1452.

[129] T.J. Overbye and C.L. DeMarco, *Voltage Security Enhancement using Energy Based Sensitivities*, IEEE Trans. on Power Systems, Vol. 6, No. 3, Aug. 1991, pp. 1196-1202.

[130] *Survey of the Voltage Collapse Phenomenon*, North American Electric Reliability Council report, 1991.

[131] R.A. Schlueter, I. Hu, M.W. Chang, J.C. Lo and A. Costi, *Methods for Determining Proximity to Voltage Collapse*, IEEE Trans. on Power Systems, Vol. 6, No. 1, Feb. 1991, pp. 285-292.

[132] A. Semlyen, B. Gao and W. Janischewskyj, *Calculation of Extreme Loading Condition of a Power System for the Assessment of Voltage Stability*, IEEE Trans. on Power Systems, Vol. 6, No. 1, Feb. 1991, pp. 307-315.

[133] T. Smed, G. Andersson, G.B. Sheble and L.L. Grigsby, *A New Approach to AC/DC Power Flow*, IEEE Trans. on Power Systems, Vol. 6, 1991, pp. 1238-1244.

[134] S.C. Srivastava, P.K. Kalra, Ranjan Bose and Manu Agarwal, *Voltage Collapse in Electric Power System*, Proc. of 1st IEE Int. Conf. on Advances in Power System Control, Operation and Management, HongKong, 1991.

[135] D.G. Taylor and L.J. Maahs, *A Reactive Contingency Analysis Algorithm Using MW and MVAR Distribution Factors*, IEEE Trans. on Power Systems,

[136] L.D.B. Terra and M.J. Short, *Security Constrained Reactive Power Dispatch*, IEEE Trans. on Power Systems, Vol-PWRS-6, No.1, February 1991, pp. 109-117.

[137] T. Van Cutsem, *A Method to Compute Reactive Power Margins with respect to Voltage Collapse*, IEEE Trans. on Power Systems, Vol. 6, No. 1, Feb. 1991, pp. 145-156.

[138] T. Van Cutsem, *Voltage Collapse Mechanisms: A Case Study*, Proc. of the 1991 Workshop on Bulk Power System Voltage Phenomena: Voltage Stability and Security, Mc Henry, USA, August 1991.

[139] V. Ajjarapu and C. Christy, *The Continuation Power Flow: A Tool for Steady State Voltage Stability Analysis*, IEEE Trans. on Power Systems, Vol. 7, No. 1, Feb. 1992, pp. 416-423.

[140] V. Ajjarapu and B. Lee, *Bifurcation Theory and its Application to Nonlinear Dynamical Phenomena in an Electric Power System*, IEEE Trans. on Power Systems, Vol. 7, No. 1, Feb. 1992, pp. 424-431.

[141] F.L. Alvarado, M. Gu and Y.Hu, *Direct Ditection of Instability Points Using an Augmented Formulation*,North American Power Symposium, Reno, NV, Oct. 5-6, 1992, pp.2-7.

[142] N. Balu et al , *On line Power System Security and Analysis*, IEEE Proc., Vol-80, No.2, February 1992, pp. 260-280.

[143] M.M. Begovic and A.G. Phadke, *Control of Voltage Stability using Sensitivity Analysis*, IEEE Trans. on Power Systems, Vol. 7, No. 1, Feb. 1992, pp. 114-123.

[144] C.A. Canizares, F.L. Alvarado, C.L. DeMarco, I. Dobson and W.F. Long, *Point of Collapse Methods Applied to AC/DC Power Systems*, IEEE Trans. on Power Systems, Vol. 7, No. 2, May 1992, pp.673-683.

[145] I. Dobson, F. Alvarado and C.L. DeMarco, *Sensitivity of Hopf Bifurcations to Power System Parameters*, Proc. 31st IEEE Conference on Decision and Control, Tucson, AZ, December 1992, pp. 2928-2933.

[146] I. Dobson and L. Lu, *Voltage Collapse Precipitated by the Immediate Change in Stability when Generator Reactive Power Limits are Encountered*, IEEE Trans. on Circuits and Systems–I, Vol. 39, No. 9, Sept. 1992, pp. 762-766.

[147] I. Dobson, *Observations on the Geometry of Saddle Node Bifurcations and Voltage Collapse in Electrical Power System*, IEEE Trans. Circuits and Systems–I, Vol. 39, No. 3, March 1992, pp. 241-243.

[148] I. Dobson and L. Lu, *Computing an Optimum Direction in Control Space to Avoid Saddle Node Bifurcation and Voltage Collapse in Electric Systems*, IEEE Trans. on Automatic Control, Vol. 37, No. 10, October 1992, pp. 1616-1620.

[149] J. Douglas, *FACTS: the Delivery System of the Future*, EPRI Journal, 17(7), October 1992, pp. 4-11.

[150] A.A. Fouad and V. Vittal. *Power System Transient Stability Analysis*, The Prentice Hall, New Jersey, 1992.

[151] James A. Freeman and David M. Skapura, *Neural Networks Algorithms, Applications, and Programming Techniques,* Addison-Wesley Publishing Company, New York, 1992.

[152] B. Gao, G.K. Morison and P. Kundur, *Voltage Stability Evaluation using Modal Analysis.* IEEE Trans. on Power Systems, Vol. 7, No. 4, Nov. 1992, pp. 1529-1542.

[153] I.A. Hiskens and C.B. McLean, *SVC Behaviour under Voltage Collapse Conditions.* IEEE Trans. on Power Systems, Vol. 7, No. 3, Aug. 1992, pp. 1078-1087.

[154] Yoan-Yih Hsu and Han-Ching Kuo,*Fuzzy set based contingency ranking,* IEEE Trans. on Power Systems, Vol.7,No.3,pp. 1189-1196, Aug 1992.

[155] W.R. Lachs and D. Sutanto, *Voltage Instability in Interconnected Power Systems: A Simulation Approach,* IEEE Trans. on Power Systems, Vol. 7, No. 2, May 1992, pp. 753-761.

[156] C. Lee and N. Chen, *Distribution Factors of Reactive Power Flow in Transmission Line and Transformer Outage Studies,* IEEE Trans. on Power Systems, Vol-PWRS-7, No.1, February 1992, pp. 194-200.

[157] P.A. Lof, T. Smed, G. Anderson and D.J. Hill, *Fast Calculation of a Voltage Stability Index,* IEEE Trans. on Power Systems, Vol. 7, No. 1, Feb. 1992, pp 54-64.

[158] V. Miranda and J.T. Saraiva, *Fuzzy Modelling of Power System Optimal Load Flow.* IEEE Trans. on Power Systems, Vol-PWRS-7, No. 2, May 1992, pp. 843-849.

[159] M.K. Pal, *Voltage Stability Conditions considering Load Characteristics*, IEEE Trans. on Power Systems, Vol. 7, No. 1, Feb. 1992, pp. 243-249.

[160] C. Rajagopalan, B. Lesieutre, P.W. Sauer and M.A. Pai, *Dynamic Aspects of Voltage/Power Characteristics*, IEEE Trans. on Power Systems, Vol. 7, No. 3, Aug. 1992, pp. 990-1000.

[161] M.V. Rao, *Fast Algorithm for Voltage Contingency Selection,* M.Tech Thesis in Electrical Engg. Department, I.I.T. Kanpur, June 1992.

[162] R.A. Schlueter and A. Costi, *Multiple Contingency Selection for Transmission Reliability and Transfer Capability Studies,* Electric Machines and Power Systems, Vol-20, 1992, pp. 223-237.

[163] M. Suzuki, S. Wada, M. Sato, T. Asano and Y. Kudo, *Newly Developed Voltage Security Monitoring System*, IEEE Trans. on Power Systems, Vol. 7, No. 3, Aug. 1992, pp. 965-973.

[164] P. Varaiya, F. Wu and H.D. Chiang, *Bifurcation and Chaos in Power System: A Survey*, EPRI TR-100834, August 1992, Final Report.

[165] V. Venkatasubramanian, H. Schattler and J. Zaborszky, *Voltage Dynamics; Study of a Generator with Voltage Control, Transmission and Matched MW Load*, IEEE Trans. Automatic Control, Vol. 37, No. 11, Nov. 1992, pp. 1717-1733.

[166] K.T. Vu and C.C. Liu, *Shrinking Stability Regions and Voltage Collapse in Power System*, IEEE Trans. on Circuits and Systems—I: Fundamental Theory and Applications, Vol. 39, No. 4, April 1992, pp. 271-289.

[167] H.O. Wang, E.H. Abed and A.M.A. Hamdan, *Bifurcations, Chaos and Crises in Power System Voltage Collapse*, Technical Research Report # TR 92-72, University of Maryland, USA.

[168] N. Yorino, H. Sasaki, Y. Masuda, Y. Tamura, M. Kitagawa and A. Oshimo, *An Investigation of Voltage Instability Problems*, IEEE Trans. on Power Systems, Vol. 7, No. 2, May 1992.

[169] C.A. Canizares and F.L. Alvarado, *Point of Collapse and Continuation Methods for Large AC/DC Systems*, IEEE Trans. on Power Systems, Vol. 8, No. 1, Feb. 1993, pp 1-8.

[170] *Modeling of Voltage Collapse Including Dynamic Phenomena*, CIGRE Task Force # 38.02.10.

[171] C. Concordia (ed.), *Special Issue on Voltage Stability and Collapse*, Int. Jr. of Electrical Power & Energy Systems, Vol. 15, No. 4, August 1993.

[172] C. Counan, M. Trotignon, E. Corradi, G. Bortoni, M. Stubbe and J. Deuse, *Major Incidents on the French Electric System: Potentiality and Curative Measures Studies*, IEEE Trans. on Power Systems, Vol. 8, No. 3, Aug. 1993, pp 879-886.

[173] J. Deuse and M. Stubbe, *Dynamic Simulation of Voltage Collapse*, IEEE Trans. on Power Systems, Vol. 8, No. 3, Aug. 1993, pp 894-904.

[174] I. Dobson and L. Lu, *New Methods for Computing a Closest Saddle Node Bifurcation and Worst Case Load Power Margin for Voltage Collapse*, IEEE Trans. on Power Systems, Vol. 8, No. 3, Aug. 1993, pp 905-913.

[175] I. Dobson, *Computing a Closest Bifurcation Instability in Multidimentional Parameter Space*, Jr. of Nonlinear Science, Vol. 3, 1993, pp. 307-327.

[176] N. Flatabo, O.B. Fosso, R. Ognedal, T. Carlsen and K.R. Heggland, *A Method for Calculating of Margins to Voltage Instability Applied on the Norwegian System for Maintaining Required Security Level*, IEEE Trans. on Power Systems, Vol. 8, No. 3, Aug. 1993, pp 920-928.

[177] A.M.A. Hamdan, *Modes, State Variables and Local Bifurcations in Power System Dynamics*, Electrical Machines and Power Systems, Vol. 21, 1993, pp. 241-255.

[178] D.J. Hill, *Nonlinear Load Models with Recovery for Voltage Stability Studies*, IEEE Trans. on Power Systems, Vol. 8, No. 1, Feb. 1993, pp. 166-176.

[179] N.G. Hingorani. *Flexible AC Transmission*, IEEE Spectrum, Vol. 30, No. 4, April 1993. pp. 40-45.

[180] N.G. Hingorani and K.E. Stahlkopf, *High Power Electronics*, Scientific American, Vol. 269, No. 5, November 1993, pp. 78-85.

[181] Yuan-Yih Hsu and Chien-Chun Yang. Fast voltage estimation using and artificial neural network.*Electrical power system Research.* Vol.27. pp.1-9, 1993.

[182] S. Iwamoto. M. Kinoshita and C. C. Liu, *Aritficial Neural Network Application to Voltage Stability Considering Power System Configuration,* Procedings of Expert System application to power System IV (ESAP'93), Melbourne, Australia, Jan, 4-8 1993. pp. 16-21.

[183] A.K. Jana. P.B. Duttagupta and G.D. Prasad, *An Improved Linearized Method for Evaluation of Bus Voltage for Line Outage Contingency,* Int. Journal of Electric Power and Energy Systems, Vol-15, No.5, 1993 ,pp. 301-305.

[184] B. Lee and V. Ajjarapu, *Period-doubling Route to Chaos in an Electric Power System*, Proc. IEE Pt-C, Vol-140. No. 6, November 1993. pp. 490-496.

[185] B.H. Lee and K.Y. Lee, *Dynamic and Static Voltage Stability Enhancement of Power Systems*. IEEE Trans. on Power Systems, Vol. 8, No. 1. Feb. 1993, pp 231-238.

[186] P.A. Lof. G. Andersson and D.J. Hill, *Voltage Stability Indices for Stressed Power Systems*. IEEE Trans. on Power Systems, Vol. 8, No. 1. Feb. 1993, pp 326-335.

[187] P.A. Lof. G. Andersson and D.J. Hill, *Generator Modelling for Static Voltage Stability Studies*. Proc. of the 11th Power System Computation Conference, Avignon, France. Aug/Sept 1993, pp 923-929.

[188] P.A. Lof. D.J. Hill, S. Arnborg and G. Andersson, *On the Analysis of Long-Term Voltage Stability*. Int. Jr. of Electrical Power and Energy Systems, Vol. 15. No. 4, 1993. pp. 229-237.

[189] F.K. Mak and M.D. Ilic, *Classification of Voltage Problems in Electric Power Systems*. Int. Jr. of Electrical Power and Energy Systems. Vol. 15, No. 6, 1993, pp. 377-385.

[190] J.D. McCalley, J.F. Dorsey, J.F. Luini, R.P. Mackin and G.H. Molina, *Subtransmission Reduction for Voltage Instability Analysis*, IEEE Trans. on Power Systems. Vol. 8, No. 1, Feb. 1993, pp. 349-356.

[191] N.W. Miller. R.D. Aquila, K.M. Jimma. M.T. Sheehan and G.L. Comegys. *Voltage Stability of Puget Sound System under Abnormally Cold Weather Conditions*. IEEE Trans. on Power Systems, Vol. 8. No. 3, Aug. 1993, pp 1133-1142.

[192] A Roman-Messina and B.J. Cory. *Enhancement of Dynamic Stability by Coordinated Control of Static VAR Compensators*, Int. Journal of Electrical Power and Energy Systems, Vol. 15, No. 2, 1993, pp. 85-93.

[193] G.K. Morison, B. Gao and P. Kundur, *Voltage Stability Analysis using Static and Dynamic Approaches*, IEEE Trans. on Power Systems, Vol. 8, No. 3, Aug. 1993, pp 1159-1171.

[194] C.O. Nwankpa and R.M. Hassan, '*A Stochastic based Voltage Collapse Indicator*, IEEE Trans. on Power Systems, Vol. 8, No. 3, Aug. 1993, pp 1187-1194.

[195] M.K. Pal, *Voltage Stability: Analysis Needs, Modelling Requirement and Modelling Adequacy*. Proc. IEE Pt-C, Vol. 140, No. 4, July 1993, pp. 279-286.

[196] M.A. Pai, P.W. Sauer, B.L. Lesieutre and R. Adapa, *Structural Stability in Power Systems - Effect of Load Models*, Athens Power Tech. Conference, Athens Greece. Sept. 1993.

[197] V. Veera Raju and A. Kuppurajulu, *A Closed Loop Controller for Voltage Stability*. Int. J. of Electrical Power and Energy Systems, Vol-15, No. 5, 1993, pp. 283-292.

[198] P.W. Sauer, B.C. Lesieutre and M.A. Pai, *Maximum Loadability and Voltage Stability in Power Systems*, Int. Jr. of Electrical Power and Energy Systems, Vol. 15, No. 3, 1993, pp. 145-154.

[199] C.W. Tan, M. Varghese, P. Varaiya and F. Wu, *Bifurcation and Chaos in Power Systems*. Sadhana: Proceedings in Engineering Sciences of the Indian Academy of Sciences, Bangalore, India, Vol. 18, Part 5, Sept 1993, pp. 761-786.

[200] T.J. Overbye, *Use of Energy Methods for On-Line Assessment of Power System Voltage Security*. IEEE Trans. on Power Systems, Vol. 8, No. 2, May 1993, pp 452-458.

[201] K.N. Srivastava, S.C. Srivastava and P.K. Kalra, *Prediction of Voltage Collapse in an Integrated AC-DC Network using Singular Value Decomposition Concept*. Electric Power System Research, Vol. 28, No. 2, November 1993, pp. 111-122.

[202] H.O. Wang and E.H. Abed, *Control of Nonlinear Phenomena at the Inception of Voltage Collapse*. Proc. 1993 American Control Conference, San Francisco, June 1993, pp. 2071-2075.

[203] V.S. Vankayala and N.D. Rao. Artificial neural networks and their applications to power system a bibliographical survey. *Electrical power system Research*. Vol.28. No.1, pp. 67-79, Oct 1993.

[204] L. Vargas and V.H. Quintana, *Clustering Techniques for Voltage Collapse Detection*. Electric Power System Research, Vol. 26, No. 1, Jan. 1993, pp. 53-59.

[205] C.D. Vournas and N.D. Krassas, *Voltage Stability as Affected by Static Load Characteristics*. Proc. IEE pt-C, Vol. 140, No. 3, May 1993, pp. 221-228.

[206] E.H. Abed, *Bifurcation-Theoretic Issues in the Control of Voltage Collapse*. IMA Volumes in Mathematics and its Applications, Vol. 64, Springer-Verlag, 1994, pp. 1-22.

[207] V. Ajjarapu, Ping Lin Lau and S. Battula, *An Optimal Reactive Power Planning Strategy Against Voltage Collapse*, IEEE Trans. on Power Systems, Vol. 9, No. 2, May. 1994, pp. 906-917.

[208] F. Alvarado, I. Dobson and Y. Hu, *Computation of Closest Bifurcations in Power Systems*, IEEE Trans. on Power Systems, Vol. 9, No. 2, May 1994, pp 918-928.

[209] L. D. Arya and H. K. Verma, *Method for Tracing P-V Curves for Voltage Stability Analysis*, The Journal of The Institution of Engineers(India), Vol. 74, No. 3, Nov. 1994, pp. 174-177.

[210] C.A. Canizares and Stene Hranilovic, *Transcritical and Hopf Bifurcation in AC/DC Systems*, Bulk Power System Voltage Phenomena — III Seminar, NSF/ECC INC, DAVOS, Switzerland, August 22-26, 1994.

[211] C.A. Canizares, Antonio Z. de Souza and Victor H. Quintana, *Improving Continuation Methods for Tracing, Bifurcation Diagrams in Power Systems*, Bulk Power System Voltage Phenomena - III Seminar, NSF/ECC INC, DAVOS, Switzerland, August 22-26, 1994.

[212] *Indices of Prediction of voltage Collapse Including Dynamic Phenomena*, CIGRE Task Force # 38.02.11.

[213] M.L. Crow, *Dynamics of Voltage Instability and Collapse* International Journal of Electrical Power & Energy System(UK) Vol. 16, No. 4, Aug. 1994, pp. 235-242.

[214] F.P. DeMello, *Exploratory Concepts on Control of Variable Series Compensation in Transmission Systems to Improve Damping of Intermachine/System Oscillations*, IEEE Trans. on Power Systems, Vol. 9, No. 1, Feb. 1994, pp. 102-119.

[215] A. Gebreselassie and J.H. Chow, *Investigation of the Effects of Load Models and Generator Voltage Regulators on Voltage Stability*, Int. Jr. of Electrical Power & Energy System, Vol. 16, No. 2, 1994, pp. 83-89.

[216] T. Guo and R.A. Schlueter, *Identification of Genetic Bifurcation and Stability Problems in Power System Differential Algebraic Model*, IEEE Trans. on Power Systems, Vol. 9, No. 2, May 1994, pp. 1032-1044.

[217] D.J. Hill, I.A. Hiskens and D.H. Popovic, *Stability Analysis of Power System Loads with Recovery Dynamics*, International Journal of Electrical Power & Energy

[218] Y.Y. Hong and C.H. Gau, *Voltage Stability Indicator for Identification of the Weakest Bus/Area in Power Systems*, Proc. IEE pt-C, Vol. 141, No. 4, July 1994, pp. 305-309.

[219] B. Jeyasurya, *Artificial Neural Network For Power System Steady-state Voltage Instability Evalution*, Electric Power System Research, Vol. 29, No. 2, march 1994, pp. 85-90.

[220] P. Kundur, *Power System Stability and Control*, the EPRI Power System Engineering Series, McGraw-Hill, New York, 1994.

[221] Y. Mansour, W. Xu, F. Alvardo and C. Rinzin, *SVC Placement Using Critical Modes of Voltage Instability*, IEEE Trans. on Power Systems, Vol-PWRS-9, No.2, May 1994, pp. 757-763.

[222] A.P.S. Meliopoulos, C.S. Chenge and F. Xia, *Performance Evaluation of Static Security Analysis Methods*, IEEE Trans. on Power Systems, Vol-PWRS-9, No.3, August 1994, pp. 1441-1449.

[223] M. Noroozian and G. Andersson, *Damping of Power System Oscillations by use of Controllable Components*, Paper # WM94 064-6-PWRD, IEEE PES 1994, Winter Meeting, New York.

[224] T.J. Overbye, I. Dobson and C.L. DeMarco, *Q-V Curve Interpretations of Energy Measures for Voltage Security*, IEEE Trans. on Power Systems, Vol. 9, No. 1, Feb. 1994, pp. 331-340.

[225] T.J. Overbye, *A Power Flow Measure for Unsolvable Cases*, IEEE Trans. on Power Systems, Vol. 9, No. 3, Aug. 1994, pp. 1359-1365.

[226] T.J. Overbye, *Effects of Load Modelling on Analysis of Power System Voltage Stability*, International Journal of Electrical Power & Energy System(UK) Vol. 16, No. 5, 1994, pp. 329-338.

[227] M.A. Pai, P.W. Sauer, B. Lesieutre and R.K. Ranjan, *Structural Stability in Power Systems*, EPRI final report, TR-103870, April 1994.

[228] V. H. Quintana and L. Vargas, *Voltage Stability as Affected by Discrete Changes in the Topology of Power Networks*, Proc. IEE pt-C, Vol. 141, No. 4, July 1994, pp. 346-352.

[229] R.A. Schlueter and I. Hu, *Types of Voltage Instability and the Associated Modelling for Transient/Mid Term Stability Simulation*, Electric Power System Research, Vol. 29, No. 2, March 1994, pp. 131-146.

[230] K.S. Smith and L. Ran, *Voltage Stability Assesment of Isolated Power Systems with Power Electronic Converters*, Proc. IEE pt-C, Vol. 141, No. 4, July 1994, pp. 310-314.

[231] K.N. Srivastava, *Investigation into Static and Dynamic Aspects of Voltage Stability*, Ph.D. Thesis, Indian Institute of Technology, Kanpur, December 1994.

[232] S. Vallandar and V.C. Ramesh, *A Multi-Agent Technique for Contingency Constrained Optimal Power Flows*, IEEE Trans. on Power Systems, Vol-PWRS-9, No.2, May 1994, pp. 855-861.

[233] C.W. Taylor, *Power System Voltage Stability*, the EPRI Power System Engineering Series, McGraw-Hill, New York, 1994.

[234] L. Vargas and V. H. Quintana, *Dynamical Analysis of Voltage Collapse in Longitudinal Systems*. International Journal of Electrical Power & Energy System(UK) Vol. 16, No. 4, 1994, pp. 221-228.

[235] C.D. Vournas, *Voltage Stability and Controllability Indices for Multimachine Power Systems*. IEEE/PES 1994 Summer Meeting, San Francisco, CA, July 24-28, 1994, Paper no. 94SM 513-2 PWRS.

[236] H.O. Wang, E.H. Abed and A.M.A. Hamdan, *Bifurcation, Chaos and Crises in Voltage Collapse of a Model Power System*, IEEE Trans. on Circuits and Systems—I: Fundamental Theory and Applications, Vol. 41, No. 4, March 1994, pp. 294-302.

[237] W. Xu and Y. Mansour, *Voltage Stability using Generic Dynamic Load Models*. IEEE Trans. on Power Systems, Vol. 9, No. 1, February 1994, pp. 479-493.

[238] M.M. Begovic and Roger Q. Mills, *Load Identification and Voltage Stability Monitoring*. IEEE Trans. on Power Systems, Vol. 10, No. 1, February 1995, pp. 109-116.

[239] C.A. Canizares, *On Bifurcations, Voltage Collapse and Load Modeling*, IEEE Trans. on Power Systems, Vol. 10, No. 1, February 1995, pp. 512-522.

[240] M. H. Haque, *A Fast Method for Determining the Voltage Stability Limit of A Power System*. Electric Power System Research, Vol. 32, No. 1, 1995, pp. 35-43.

[241] Ying Yi Hong and Heng-Yi Wang, *Investigation of The Voltage Stability Region Involving On-Load Tap Changer*. Electric Power System Research, Vol. 32, No. 1, 1995, pp. 45-51.

[242] IEEE Task Force on Load Representation for Dynamic Performance, Bibliograpy on Load Models for Power Flow and Dynamic Performance Simulation, IEEE Trans. on Power Systems, Vol. 10, No. 1, February 1995, pp. 925-931.

[243] IEEE Task Force on Load Representation for Dynamic Performance, Standard Load Models for Power Flow and Dynamic Performance Simulation, IEEE Trans. on Power Systems, Vol. 10, No. 3, August 1995, pp. 1302-1313.

[244] Jayant Kumar and G. B. Sheble, *Clamped State Solution of Artificial Neural Network for Real-Time Economic Dispatch*, IEEE Trans. on Power Systems, Vol. 10, No. 2, May 1995, pp. 925-931.

[245] P.A. Lof, G.Andersson and D.J. Hill, *Voltage Dependent Reactive Power Limits for Voltage Stability Studies*, IEEE Trans. on Power Systems, Vol. 10, No. 1, February 1995, pp. 220-228.

[246] J. Lu, C.W. Liu and J.S. Thorp. *New Methods for Computing a Saddle Node Bifurcation Point for Voltage Stability Analysis*, IEEE Trans. on Power Systems, Vol. 10, No. 2, May 1995, pp. 978-985.

[247] T.J. Overbye, *Computation of a Practical Method to Restore Power Flow Solvability*, IEEE Trans. on Power Systems, Vol. 10, No. 1, February 1995, pp. 280-287.

[248] A.K. Sinha, *Power System Security Assessment using Patterm Recognition and Fuzzy Estimation*, International Journal of Electric Power & Energy Systems, Vol-17, No.1, February 1995, pp. 11-20.

[249] Sri Niwas Singh, *Voltage Security and Loss Minimization Studies in Electric Power Systems*, Ph.D. Thesis, Indian Institute of Technology, Kanpur, April, 1995.

[250] L. wehenkel, *Contingency Severity Assessment for Voltage Security Using Non-Parameteric Regrassion Technique*, IEEE/PES Winter Meeting New York, Jan 29 - February 2, 1995, paper no. 95 WM 162-8 PWRS.

Appendix A

Data for 3-Bus Test System

The 3 bus system is shown in Figure A.1. The system data is taken from ref. [213]. The relevant data are provided in following tables.

Table A.1: Line Data

From bus	To bus	Series impedence		Shunt susceptance B/2(p.u.)
		R(p.u.)	X(p.u.)	
1	2	0.0000	0.1000	0.0500
2	3	0.0000	0.1000	0.0500
3	1	0.0000	0.1000	0.0500

Table A.2: Machine and excitaion system data

parameter	value	parameter	value
H(s)	10	D(p.u)	1.00
$X_d(p.u)$	0.90	$X_{d'}(p.u)$	0.70
$X_q(p.u)$	0.85	$X_{q'}(p.u)$	0.10
$T'_{do}(s)$	8.00	$T'_{qo}(s)$	0.25
$K_A(p.u)$	25.00	$T_A(s)$	0.20
$K_E(p.u)$	1.00	$T_E(s)$	0.35
$K_F(p.u)$	0.05	$T_F(s)$	0.35

Table A.3: Bus Data

Bus No.	Bus Type	Generation(p.u.)		Load(p.u.)		Voltage Magnitude
		Real	Reactive	Real	Reactive	
1	PV	1.25	—	0.00	0.00	1.0300
2	PQ	—	—	2.50	1.00	—
3	Swing	—	—	0.00	0.00	1.0400

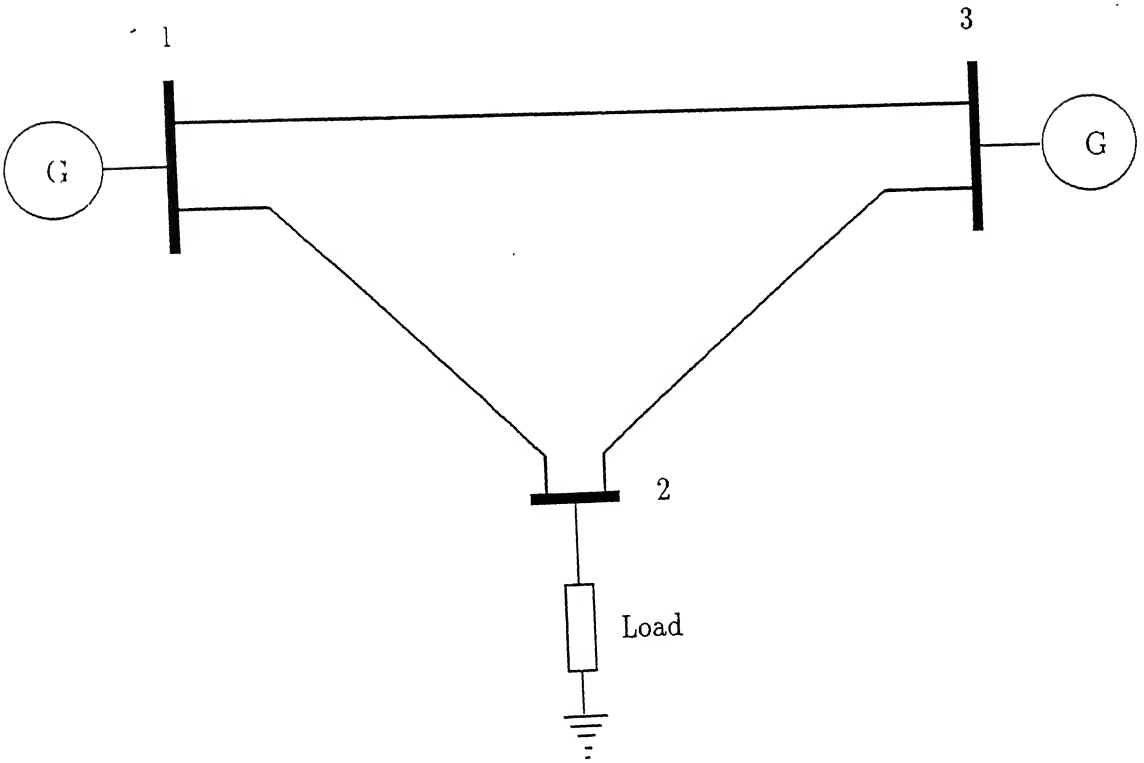

Figure A.1: 3-bus test system

Appendix B

Data for 9 Bus Test System (at 100 MVA base)

The 9 bus system is shown in Fig. B. The system data is taken from ref. [10]. The relevant data are provided in following tables.

Table B.1: Line Data

From bus	To bus	Series impedence		Shunt susceptance B(p.u.)
		R(p.u.)	X(p.u.)	
1	4	0.0000	0.0576	0.0000
4	6	0.0170	0.0920	0.1580
6	9	0.0390	0.1700	0.3580
9	3	0.0000	0.0586	0.0000
9	8	0.0119	0.1008	0.2090
8	7	0.0085	0.0720	0.1490
7	2	0.0000	0.0625	0.0000
7	5	0.0320	0.1610	0.3060
5	4	0.0100	0.0850	0.1760

Table B.2: Machine Data

Parameter	Machine–1	Machine–2	Machine–3
X_d(p.u.)	0.1460	0.8958	1.3125
X'_d(p.u.)	0.0608	0.1198	0.1813
T'_{do}(sec.)	8.96	6.00	5.89
X_q(p.u.)	0.0969	0.8645	1.2578
X'_q(p.u.)	0.0608	0.1198	0.1813
T'_{qo}(sec.)	0.310	0.535	0.600
H(sec.)	23.64	6.40	3.01
D(p.u.)	1.0	1.0	1.0

Table B.3: Bus Data

Bus No.	Bus Type	Generation(p.u.)		Load(p.u.)		Voltage Magnitude
		Real	Reactive	Real	Reactive	
1	Swing	—	—	0.00	0.00	1.0400
2	PV	1.63	—	0.00	0.00	1.0253
3	PV	0.85	—	0.00	0.00	1.0253
4	PQ	0.00	0.00	0.00	0.00	—
5	PQ	0.00	0.00	1.25	0.50	—
6	PQ	0.00	0.00	0.90	0.30	—
7	PQ	0.00	0.00	0.00	0.00	—
8	PQ	0.00	0.00	1.00	0.35	—
9	PQ	0.00	0.00	0.00	0.00	—

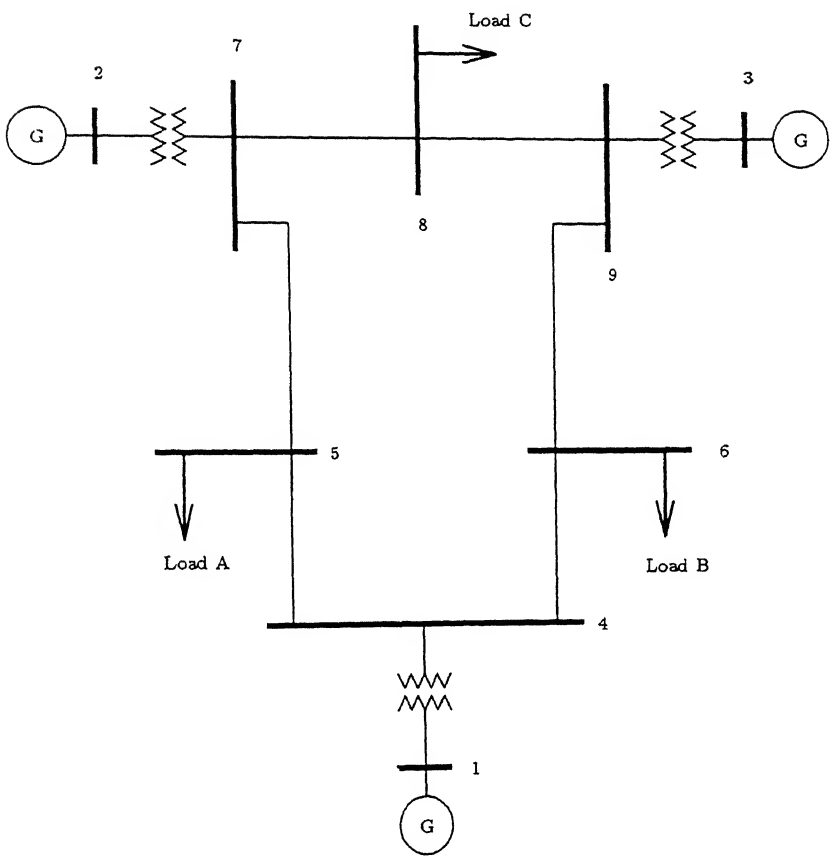

Figure B.1: 9-bus system

Appendix C

Data For IEEE 14-Bus Test System (At 100 MVA Base)

The IEEE 14-bus system is shown in Fig. C.1. The system data is taken from reference [60] and buses renumbered. The relevant data are provided in following tables.

Table C.1: Generator Bus Data

Bus No.	Scheduled real power generation P_G(MW)	Specified Voltage magnitude Vspec. (p.u.)	Load	
			Real (MW)	Reactive (MVAR)
1(slack)	—	1.060	0.00	0.00
2	40.0	1.045	21.70	12.70
3	20.0	1.070	11.20	07.50
4	—	1.010	94.20	19.00
5	—	1.090	0.00	0.00

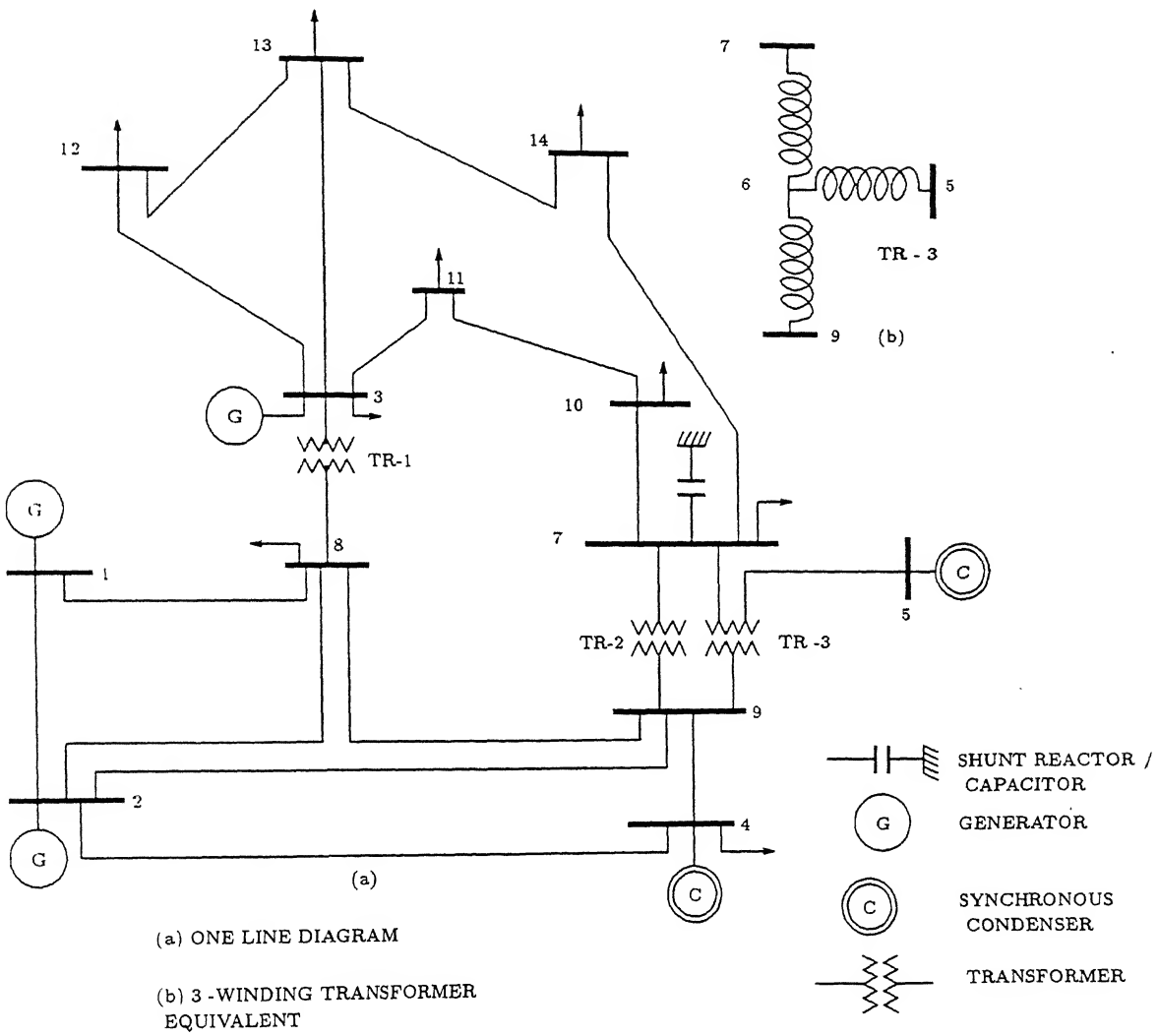

Figure C.1: IEEE 14-bus system

Table C.2: Generator Data

Gen. no.	Real power generation limit		Reactive power generation limit	
	Maximum (MW)	Minimum (MW)	Maximum (MVAR)	Minimum (MVAR)
1	200.0	50.0	100.0	−45.0
2	100.0	20.0	50.0	−40.0
3	100.0	20.0	24.0	−06.0
4	—	—	40.0	0.0
5	—	—	24.0	−06.0

Table C.3: Load Bus Data

Bus No.	Load		External shunt susceptance(p.u.)
	Real (MW)	Reactive (MVAR)	
6	0.0	0.0	0.0
7	29.5	16.6	−0.19
8	7.6	1.6	0.0
9	47.8	−3.9	0.0
10	0.0	5.8	0.0
11	3.5	1.8	0.0
12	6.1	1.6	0.0
13	13.5	5.8	0.0
14	14.9	5.0	0.0

Table C.4: Transformer Data

Line no.	From bus	To bus	Series impedance		Tap settings
			Resistance (p.u.)	Reactance (p.u.)	
1	8	3	0.0000	0.25202	0.962
2	9	6	0.0000	0.20912	0.978
3	9	7	0.0000	0.55618	0.969

Table C.5: Line Data

Line no.	From bus	To bus	Series impedence		Shunt susceptance $\frac{1}{2}$B(p.u.)
			Resistance (p.u.)	Reactance (p.u.)	
4	1	8	0.05403	0.22304	0.0246
5	2	8	0.05695	0.17388	0.0170
6	4	9	0.06701	0.17103	0.0173
7	9	8	0.01335	0.04211	0.0064
8	1	2	0.01938	0.05917	0.0264
9	2	4	0.04699	0.19797	0.0219
10	6	5	0.00000	0.17615	0.0000
11	2	9	0.05811	0.17632	0.0187
12	6	7	0.00000	0.11001	0.0000
13	7	10	0.03181	0.08450	0.0000
14	3	11	0.09498	0.19890	0.0000
15	3	12	0.12291	0.25581	0.0000
16	3	13	0.06615	0.13027	0.0000
17	7	14	0.12711	0.27038	0.0000
18	10	11	0.08205	0.19207	0.0000
18	12	13	0.22092	0.19988	0.0000
20	13	14	0.17093	0.34802	0.0000

Appendix D

Data For IEEE 30-Bus Test System (At 100 MVA Base)

The IEEE 30-bus system is shown in Fig. D.1. The system data is taken from reference [60] and buses renumbered. The relevant data are provided in following tables.

Table D.1: Generator Bus Data

Bus No.	Scheduled real power generation P_G(MW)	Specified Voltage magnitude Vspec. (p.u.)	Load	
			Real (MW)	Reactive (MVAR)
1(slack)	—	1.060	00.00	00.00
2	40.0	1.045	21.70	12.70
3	20.0	1.010	0.00	30.00
4	—	1.082	30.00	0.0
5	—	1.010	9.42	19.00
6	—	1.071	0.0	0.0

Table D.2: Generator Data

Gen. no.	Real generation limit		React. generation limit	
	Maximum (MW)	Minimum (MW)	Maximum (MVAR)	Minimum (MVAR)
1	300.0	50.0	150.0	−100.0
2	150.0	20.0	50.0	−40.0
3	150.0	20.0	40.0	−10.0
4	—	—	24.0	−06.0
5	—	—	40.0	−40.0
6	—	—	24.0	−06.0

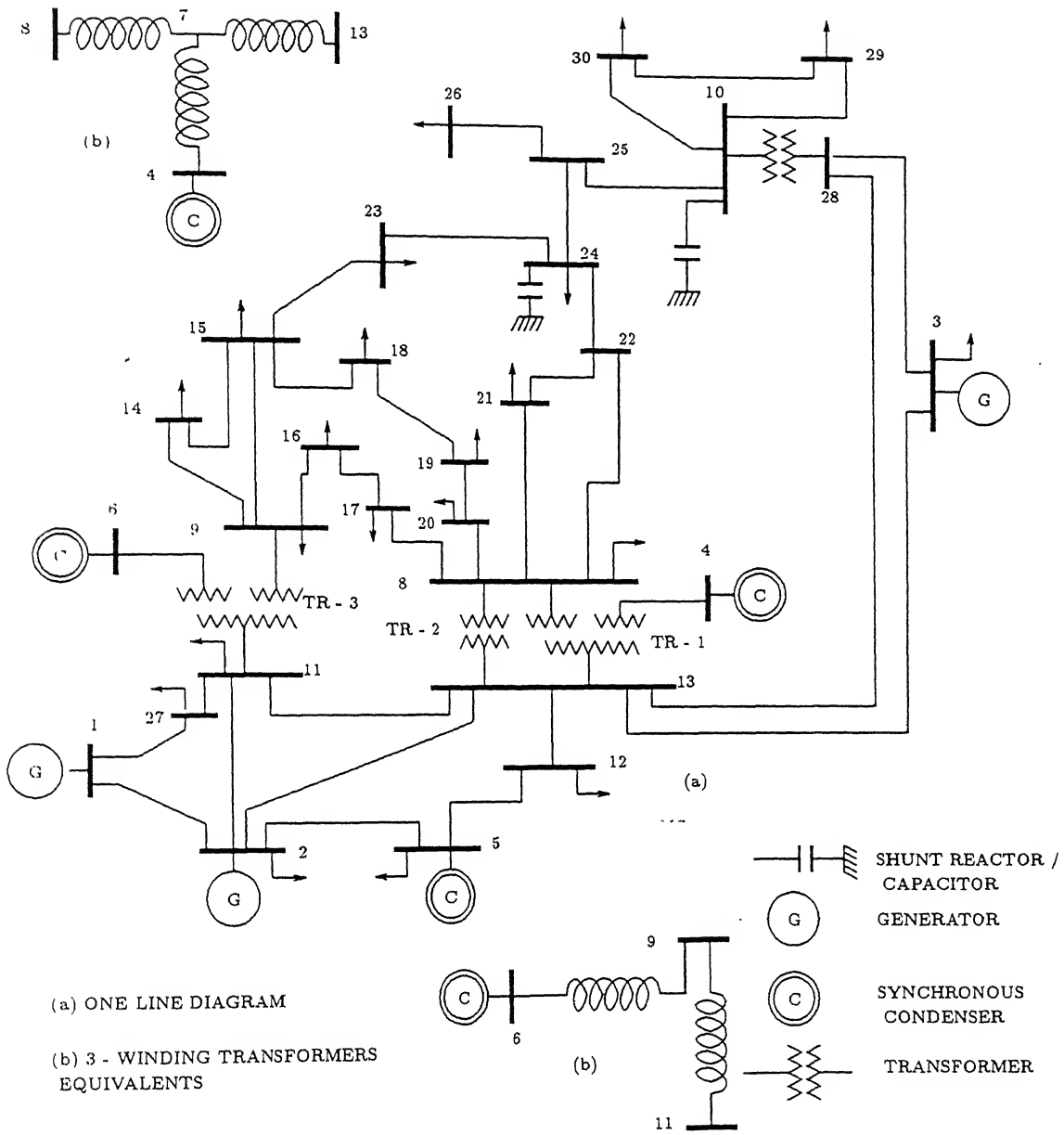

Figure D.1: IEEE 30-bus system

Table D.3: Load Bus Data

Bus No.	Load		External shunt susceptance(p.u.)
	Real(MW)	Reactive(MVAR)	
7	0.0	0.0	0.00
8	5.8	2.0	0.00
9	11.2	7.5	0.00
10	0.0	−0.0	0.19
11	7.6	1.6	0.00
12	22.8	10.9	0.00
13	0.0	0.0	0.00
14	6.2	1.6	0.00
15	8.2	2.5	0.00
16	3.5	1.8	0.00
17	9.0	5.8	0.00
18	3.2	0.9	0.00
19	9.5	3.4	0.00
20	2.2	0.7	0.00
21	17.5	11.2	0.00
22	0.0	0.0	0.00
23	3.2	1.6	0.00
24	8.7	6.7	0.043
25	0.0	0.0	0.00
26	3.5	2.3	0.00
27	2.4	1.2	0.00
28	0.0	0.0	0.00
29	2.4	0.9	0.00
30	10.6	1.9	0.00

Table D.4: Transformer Data

Line no.	From bus	To bus	Series impedance		Tap settings
			Resistance (p.u.)	Reactance (p.u.)	
1	13	07	0.0000	0.2080	0.978
2	13	08	0.0000	0.5560	0.969
3	11	09	0.0000	0.2560	0.962
4	28	10	0.0000	0.3960	0.968

Table D.5: Line Data

Line no.	From bus	To bus	Series impedence		Shunt susceptance
			Resistance (p.u.)	Reactance (p.u.)	$\frac{1}{2}$B(p.u.)
5	2	5	0.0472	0.1983	0.0209
6	2	13	0.0581	0.1763	0.0187
7	11	13	0.0119	0.0414	0.0045
8	5	12	0.0460	0.1160	0.0102
9	13	12	0.0267	0.0820	0.0085
10	13	3	0.0120	0.0420	0.0045
11	1	2	0.0192	0.0575	0.0264
12	1	27	0.0452	0.1852	0.0204
13	7	8	0.0000	0.1100	0.0000
14	2	11	0.0570	0.1737	0.0184
15	9	14	0.1231	0.2559	0.0000
16	9	15	0.0662	0.1304	0.0000
17	9	16	0.0945	0.1987	0.0000
18	14	15	0.2210	0.1997	0.0000
19	16	17	0.0824	0.1923	0.0000
20	15	18	0.1070	0.2185	0.0000
21	18	19	0.0639	0.1292	0.0000
22	19	20	0.0340	0.0680	0.0000
23	8	20	0.0936	0.2090	0.0000
24	8	17	0.0324	0.0845	0.0000
25	8	21	0.0348	0.0749	0.0000
26	8	22	0.0727	0.1499	0.0000
27	21	22	0.0116	0.0236	0.0000
28	15	23	0.1000	0.2020	0.0000
29	22	24	0.1150	0.1790	0.0000
30	23	24	0.1320	0.2700	0.0000
31	24	25	0.1885	0.3292	0.0000
32	25	26	0.2544	0.3800	0.0000
33	25	10	0.1093	0.2087	0.0000
34	27	11	0.0132	0.0379	0.0042
35	10	29	0.2198	0.4153	0.0000
36	10	30	0.3202	0.6027	0.0000
37	29	30	0.2399	0.4533	0.0000
38	3	28	0.0636	0.2000	0.0214
39	13	28	0.0169	0.0599	0.0065
40	9	6	0.0000	0.1400	0.0000
41	7	4	0.0000	0.2080	0.0000

Appendix E

Data For 75-Bus UPSEB Test System (At 100 MVA Base)

The 75-bus UPSEB system is shown in Fig. E.1. The system data is taken from U.P. State Electricity Borad and buses are renumbered. The relevant data are provided in following tables.

Table E.1: Generator Data

Bus No.	Scheduled real power gen. P_G(MW)	Specified Voltage magnitude Vspec. (p.u.)	Real power limits		Reactive power limits	
			Maximum (MW)	Minimum (MW)	maximum (MVAR)	Minimum (MVAR)
1(slack)	—	1.030	900.0	100.0	400.0	0.0
2	260.0	1.030	300.0	100.0	96.0	0.0
3	180.0	1.050	200.0	40.0	83.0	0.0
4	100.0	1.030	170.0	40.0	60.0	0.0
5	180.0	1.050	240.0	00.0	31.0	0.0
6	120.0	1.050	120.0	00.0	20.0	0.0
7	060.0	1.050	100.0	00.0	19.0	0.0
8	080.0	1.050	100.0	20.0	68.0	0.0
9	550.0	1.050	570.0	60.0	250.0	0.0
10	080.0	1.020	120.0	30.0	56.0	0.0
11	109.0	1.020	200.0	40.0	105.0	0.0
12	1800.0	1.050	1800.0	1800.0	344.0	0.0
13	900.0	1.050	900.0	900.0	280.0	0.0
14	150.0	1.030	150.0	150.0	84.0	0.0
15	454.0	1.010	454.0	454.0	35.0	-30.0

Table E.2: Load Bus Data

Bus No.	Load		Line Reactors in(MVAR)
	Real(MW)	Reactive(MVAR)	
16	-58.69	27.56	
17	0.00	0.00	100.0
19	0.00	0.00	50.0
20	156.37	33.93	
22	0.00	0.00	50.0
23	0.00	0.00	100.0
24	227.95	40.53	
25	210.48	43.43	
26	0.00	0.00	163.0
27	306.00	40.70	
28	127.75	28.35	
29	0.00	0.00	100.0
30	226.46	44.24	
32	78.11	11.59	
34	81.70	83.84	
35	0.00	0.00	50.0
36	0.00	0.00	50.0
37	144.28	40.93	
39	85.12	29.46	
41	0.00	0.00	223.0
42	1000.0	0.0	63.0
46	156.32	83.36	
47	74.55	8.77	
48	50.83	13.97	
49	85.72	51.58	
50	202.10	74.94	
51	57.76	0.62	
52	98.27	-18.15	
53	82.63	-0.33	
54	161.95	29.00	
55	274.23	31.08	
56	140.28	34.32	
57	152.78	18.53	
58	94.19	11.29	
59	121.89	11.01	
60	74.20	7.42	
61	106.50	6.58	
62	100.18	18.13	
63	58.01	5.31	

Table E.2 (Contd.) ...

Bus No.	Load		Line Reactors in(MVAR)
	Real(MW)	Reactive(MVAR)	
65	147.84	12.81	
66	31.74	15.18	
67	96.43	10.55	
68	42.87	33.60	
69	55.94	32.53	
70	23.34	2.30	
71	91.73	21.36	
72	52.52	11.76	
73	477.0	00.0	50.0
74	288.0	0.0	283.0
75	-444.0	0.0	

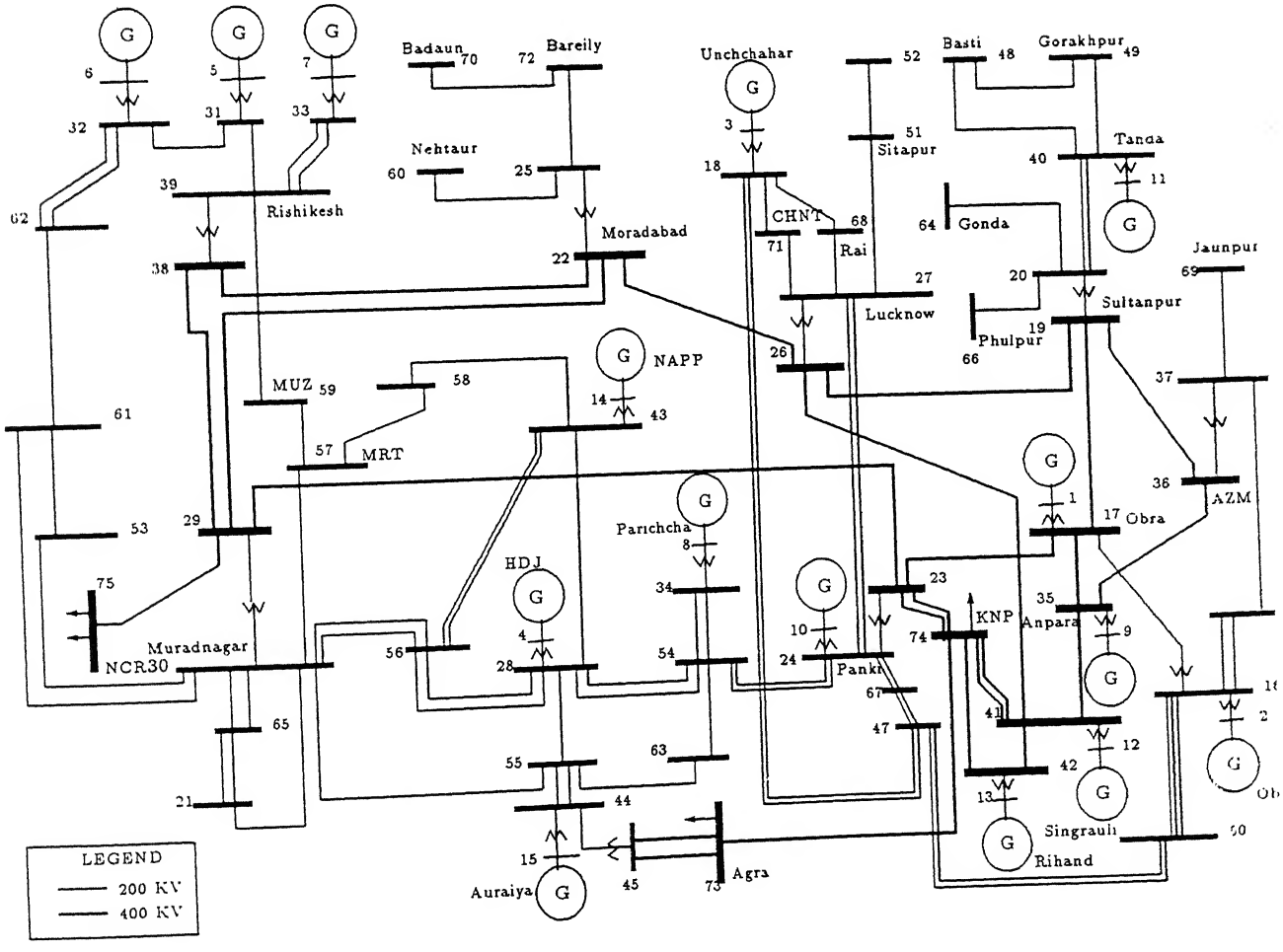

Figure E.1: 75-bus UPSEB system

Table E.3: Transformer Data

Line no.	From bus	To bus	Series impedance		Tap settings
			Resistance (p.u.)	Reactance (p.u.)	
1	17	1	.00073	.01460	1.000
2	16	2	.00123	.02469	1.000
3	18	3	.00000	.02917	1.000
4	28	4	.00306	.06135	1.000
5	31	5	.00235	.04710	1.000
6	32	6	.00514	.10285	1.000
7	33	7	.00549	.10978	1.000
8	34	8	.00000	.04860	1.000
9	35	9	.00049	.01943	1.000
10	24	10	.00243	.04860	1.000
11	40	11	.00770	.02720	1.000
12	41	12	.00016	.00591	1.000
13	42	13	.00030	.01199	1.000
14	43	14	.00000	.02841	1.000
15	44	15	.00000	.02273	1.000
16	19	20	.00130	.05208	1.000
17	19	20	.00130	.05208	1.000
18	17	16	.00065	.02604	1.000
19	22	25	.00130	.05208	1.000
20	22	25	.00130	.05208	1.000
21	23	24	.00130	.05200	1.000
22	23	24	.00130	.05200	1.000
23	26	27	.00130	.05200	1.000
24	26	27	.00130	.05200	1.000
25	29	30	.00129	.05208	1.000
26	29	30	.00129	.05208	1.000
27	29	30	.00129	.05208	1.000
28	36	37	.00130	.05208	1.000
29	36	37	.00130	.05208	1.000
30	38	39	.00130	.05208	1.000
31	45	44	.00112	.04444	1.000
32	45	44	.00112	.04444	1.000

Table E.4: Line Data

Line no.	From bus	To bus	Series impedence		Shunt susceptance
			Resistance (p.u.)	Reactance (p.u.)	$\frac{1}{2}$B (p.u.)
33	16	46	.01620	.07760	.07015
34	16	46	.01620	.07760	.07015
35	16	50	.02979	.14238	.12881
36	16	50	.02979	.14238	.12881
37	16	50	.02979	.14238	.12881
38	17	19	.00468	.04770	.62450
39	17	23	.00785	.07990	1.04738
40	19	26	.00294	.02997	.39206
41	47	50	.01093	.05221	.18892
42	47	67	.00662	.03164	.11451
43	24	27	.00505	.02416	.08730
44	24	54	.02582	.12342	.11164
45	24	54	.02582	.12342	.11164
46	25	43	.01270	.06410	.05220
47	54	28	.01060	.05060	.18320
48	28	43	.00580	.02900	.02370
49	28	56	.00370	.01780	.06440
50	56	30	.00490	.02370	.08590
51	30	57	.00750	.03840	.03110
52	53	30	.00679	.03412	.02782
53	53	61	.00666	.03390	.02672
54	30	61	.01440	.07310	.05850
55	57	58	.00670	.03390	.02670
56	57	59	.00583	.02956	.02346
57	59	39	.01410	.07180	.05700
58	39	31	.01440	.07250	.05900
59	54	63	.00990	.05090	.04010
60	55	63	.00780	.03980	.03140
61	61	62	.01160	.05830	.04750
62	62	32	.01380	.07000	.0563
63	62	32	.01380	.07000	.0563
64	35	36	.00479	.04880	.63614
65	46	37	.01732	.08784	.06973
66	19	36	.00254	.02584	.33798
67	17	35	.00051	.00517	.06760
68	40	48	.00830	.04240	.03340
69	74	41	.00927	.09429	1.23293
70	74	41	.00833	.08478	1.10855
71	26	41	.00823	.08375	1.09503
72	48	49	.00930	.04750	.03740

Table E.4 (Contd.) ...

Line no.	From bus	To bus	Series impedence		Shunt susceptance
			Resistance (p.u.)	Reactance (p.u.)	$\frac{1}{2}$B (p.u.)
73	49	40	.01330	.06680	.05420
74	38	29	.00370	.03762	.48870
75	38	22	.00325	.03307	.43264
76	18	47	.00437	.02552	.09399
77	30	65	.00248	.01186	.04294
78	41	42	.00031	.00310	.04056
79	42	74	.00918	.09306	1.21680
80	23	74	.00015	.00155	.02704
81	24	67	.00124	.00593	.02147
82	18	68	.00336	.01963	.01808
83	18	71	.01344	.07852	.07230
84	27	68	.01344	.07852	.07230
85	27	71	.00336	.01963	.01808
86	43	58	.01315	.06696	.05278
87	43	56	.00499	.02397	.08523
88	55	44	.01996	.09588	.08523
89	55	44	.01996	.09588	.08523
90	73	45	.00121	.01109	.72815
91	29	22	.00260	.02646	.34610
92	21	65	.00083	.00396	.01431
93	34	54	.03540	.17020	.15130
94	34	54	.03540	.17020	.15130
95	39	33	.01410	.07180	.05700
96	39	33	.01410	.07180	.05700
97	31	32	.00050	.00253	.00805
98	20	40	.01160	.05880	.04710
99	20	40	.01160	.05880	.04710
100	21	30	.00695	.03500	.02843
101	28	55	.01998	.10127	.08051
102	35	41	.00031	.00310	.04056
103	37	69	.01212	.06100	.04956
104	25	60	.01660	.08430	.06720
105	51	52	.01550	.07940	.06300
106	20	64	.01830	.09270	.07390
107	70	72	.00878	.04430	.03580
108	20	66	.01325	.06667	.05416
109	29	75	.00051	.00517	.06760
110	26	22	.00650	.06617	.86521
111	23	29	.00806	.08169	1.06808
112	74	73	.00559	.05686	.74354
113	25	72	.01598	.08108	.06436

Curriculum–Vitae

Satish K. Joshi

Reader
Department of Electrical Engineering
Faculty of Technology & Engineering
M.S. University Baroda
GUJARAT- 390001 INDIA

Educational Qualifications

Sl. No.	Examination passed	Board/University /Institution	Years of passing	% of marks	Main Subjects
1	B.E.	MS Univ. Baroda	1981	62.00%	Electrical Engg.
2	M.E.	MS Univ. Baroda	1985	66.80%	Electrical Engg.

Research Papers

(1) *Synergism of Expert System and Artificial Neural Net for Power System Applications*, Proc. of 15th National System Conference, Roorkee March 13-15, 1992, pp 157-162.

(2) *Artificial Neural Netwok Based Load Flow Models*, Proc. of Expert System Applications to Power Systems IV (ESAP'93), Australia, Jan 4-8, 1993, pp 56-61.

(3) *Optimal Power Dispatch: State of Art*, Proc. of All India Seminar on Grid Stability and Load Managment with MW & MVAR control, October 1993, pp. IV:32-41.

(4) *Synergism for an Intelligent System*, Proc. of the Seventh National Power Systems Conference (NSC-93) December 24-26, 1993, pp 358-364.

(5) *Security Analysis Using Fuzzy Logic and Neural Netwok*, Proc. of the International Power Engineering Cofenerce(IPEC-95), Feb. 27-March 1, 1995, pp 642-647.

(6) *Determination of Voltage Control Area Using Entropy Concept*, Proc. of IEE of Japan Power & Energy' 95, pp 143-148.

(7) *Estimation of Closest Hopf Bifurcation in Electric Power System* , communicated in the 12th Power Systems Computing Conference (PSCC'96).

(8) Discussion of IEEE paper # 94WM 064-6 PWRD titled *Damping Of Power System Oscillations by Use of Controllable Components,* IEEE Trans. on Power Delivery, Vol-9, No.4, pp 2046-2054, October 1994.

(9) Discussion of IEEE paper # 93 SM 515-7 PWRS titled *A Generation Rescheduling Method to Increase the Dynamic Security of Power System*, IEEE T-PWRS Vol-10, No.1, pp 68-76, February 1995.

(10) Discussion of IEEE paper # 94 WM 245-1 PWRS titled *Computation of a Practical Method to Restore Power Flow Solvability*, IEEE T-PWRS Vol-10, No.1, pp 280-287, February 1995.

(11) Discussion of IEEE paper # 94 WM 219-6 PWRS titled *Static Security in Power System Operation in Fuzzy Real Load Conditions*, IEEE T-PWRS Vol-10, No.1, pp 77-87, February 1995.

(12) Discussion of IEEE paper # 94 SM 578-5 PWRS titled *On Bifurcation, Voltage Collapse And Load Modeling*, IEEE T-PWRS Vol-10, No.1, pp 512-522, February 1995.

(13) Discussion of IEEE paper # 94 SM 535-5 PWRS titled *Parallel Implementation of Power System Transient Stability Analysis*, IEEE T-PWRS Vol.10, No.3, pp 1226-1233, August 1995.

(14) Discussion of IEEE paper # 94 SM 537-1 PWRS titled *A Hybrid Tool to Assist the Operator in Reactive Power/Voltage Control and Optimization*, IEEE T-PWRS May Vol-10, N0.2. pp 753-759, May 1995.

(15) Discussion of IEEE paper # 94 SM 578-5 PWRS titled *Effects of Load Dynamics on Power System Damping*, submitted to IEEE T-PWRS May Vol-10, N0.2, pp 1022-1028, May 1995.

(16) Discussion of IEEE paper # 94 SM 514-0 PWRS titled *New Methods for Computing a Saddle Node Bifurcation Point for Voltage Stability Analysis*, IEEE T-PWRS May Vol-10, N0.2, pp 978-989, May 1995.
